

# **Spike Timing in Pyramidal Cells of the Dorsal Cochlear Nucleus**

Sarah Elizabeth Street

A dissertation submitted to the faculty of the University of North Carolina at Chapel Hill in partial fulfillment of the requirements for the degree of Doctor of Philosophy in the Department of Cell and Molecular Physiology

Chapel Hill  
2007

Approved by:

Paul B. Manis

Robert Sealock

Robert Rosenberg

Paul Tiesinga

Benjamin Philpot

## **Abstract**

Sarah Street: Spike Timing in Pyramidal Cells of the Dorsal Cochlear Nucleus  
(Under the direction of Paul B. Manis)

The cochlear nucleus is the termination point for all axons of the auditory nerve. In addition to input from the auditory nerve, the dorsal cochlear nucleus (DCN) receives input from other sensory systems. The principal neurons of the DCN, the pyramidal cells, process information from both the auditory and non-auditory inputs and relay this information to the inferior colliculus. While it is known that pyramidal cells can use spike timing to encode some auditory information such as frequency modulation, these neurons are usually described in terms of average rate. This study examines the spike timing characteristics of DCN pyramidal cells.

We first investigated the spike timing characteristics of pyramidal cells by presenting the cells with Gaussian distributed white noise currents. In response to such stimuli, pyramidal cells fired trains of action potentials with precisely timed spikes. In addition, when an inhibitory event, such as an IPSP was added at the midpoint of the stimulus, the spike times became more precise after the IPSP than they were without the inhibitory event.

Intrinsic conductances can shape the output of neurons. One important conductance is a transient outward current known as an A-current. A-currents arise from potassium channels such as Kv1.4, Kv3.4 and the entire Kv4 family. It has been hypothesized that an A-current leads to the build-up response pattern in pyramidal cells, which is characterized by a long latency to the first spike. Using heteropodatoxin-2, a specific blocker of Kv4 channels,

we determined that Kv4 channels are responsible for the long delay to the first spike after a hyperpolarizing pre-pulse. To confirm this result, we also subtracted a model of the A-current using dynamic clamp and observed the same effect.

Finally, the identity of this potassium current was determined using *in situ* hybridization and immunofluorescence. Pyramidal cells were labeled by injecting a retrograde dye into the inferior colliculus. Labeled pyramidal cells expressed Kv4.3 but not Kv4.2 potassium channels. From these results we concluded that Kv4.3 is essential for the characteristic response patterns observed in DCN pyramidal cells.

## **Acknowledgements**

I am indebted to many wonderful people who helped me throughout this undertaking. First, I am grateful to my parents, Joseph and Marjorie Street, who have been supportive and encouraging throughout my life in all of my pursuits and goals. They have been especially supportive of all of my educational goals and have always made it possible for me to have every opportunity for success.

In addition, I must acknowledge and thank my dissertation advisor, Paul B. Manis for his guiding influence, support, and help at all times throughout this project. He has been a friend, a mentor and an exceptional scientific example. My dissertation committee chaired by Robert Sealock and consisting of Robert Rosenberg, Paul Tiesinga and Benjamin Philpot have provided many helpful suggestions and motivating examples that have helped me to bring this work to fruition. I also count each of them among the best teachers I have ever had in my life.

I would like to thank David K. Ryugo at the John Hopkins University for providing the tissue samples used in the immunohistochemistry experiments.

Mark J. Zylka provided helpful guidance and reagents with the molecular biology needed to construct the probes used for the in situ hybridization experiments. In addition to his help with the in situ work, I would also like to extend a heartfelt thank you to my friend and colleague, Janet Hart, at Duke University for helping me construct the plasmid used to make the Kv4.2 in situ hybridization probe.

I would like to thank Lyanne Schlicter at the University of Toronto, for providing me with a full length Kv4.2 clone that was used to construct the probe used in the in situ hybridization studies.

Ann Stuart has been my graduate school mother and has helped me in ways too numerous to mention here. Whether letting me live in her house or proofreading my papers, she has been a genuine friend and teacher from the time I started graduate school at UNC.

Finally, I must acknowledge that if it were not for my great group of friends in Chapel Hill, including Anne Clayton, Amy Lowman, Alisa Muelleck, Alison Neeley, Abby Parcell, and Lisa Jones-Christensen, this process would have not been the enjoyable one that it has been. They have been the best social-support network a woman could ever ask for. A special thanks goes to Alison for formatting my dissertation.

## Table of Contents

<b>List of Figures .....</b>	<b>viii</b>
<b>List of Abbreviations.....</b>	<b>x</b>
<b>Chapter 1: Introduction .....</b>	<b>1</b>
1.1 <i>Overview</i> .....	1
1.1.1    Spike Timing in the Auditory System .....	3
1.2 <i>DCN Anatomy</i> .....	4
1.2.1    Circuitry and Cell Types.....	8
1.3 <i>DCN Physiology</i> .....	12
1.3.1    Neuronal Responses to Sound.....	12
1.3.2    Intrinsic Conductances of Pyramidal Cells .....	19
1.3.3    Other DCN Neurons.....	20
1.3.4    DCN Plasticity.....	21
1.4 <i>DCN Function</i> .....	22
1.4.1    Amplitude Modulation Encoding.....	22
1.4.2    Sound Localization.....	23
1.4.3    Multisensory Integration.....	27
1.4.4    Tinnitus .....	27
1.5 <i>Spike Timing and the Neural Code</i> .....	29
1.6 <i>Transient Potassium Currents</i> .....	31
1.6.1    Molecular characteristics of Transient Potassium Channels .....	31
1.7 <i>Kv4 channel expression patterns</i> .....	34
1.7.1    Kv4 Channel Modulation .....	36
1.7.2    Kv4 channels and neuronal function.....	39
1.8 <i>Summary</i> .....	42
<b>Chapter 2: Action potential timing precision in dorsal cochlear nucleus pyramidal cells.....</b>	<b>43</b>
2.1 <i>Introduction</i> .....	43
2.2 <i>Materials and Methods</i> .....	45
2.3 <i>Results</i> .....	50
2.3.1    Responses of Pyramidal Cells to a White Noise Current Injection .....	50
2.3.2    Sensitivity of SAC to Spectral Structure of the Noise Input .....	61
2.3.3    Dependence of CI on Firing Rate.....	61
2.3.4    Spike Triggered Averages .....	67
2.3.5    Perturbations in the Stimulus Alter Spike Timing .....	70
2.3.6    Population coding.....	75
2.3.7    Pharmacological manipulations of Spike Timing .....	79
2.4 <i>Discussion</i> .....	82
2.4.1    General Characteristics of DCN Pyramidal Cells in Response to Noise.....	82

2.4.2	Inhibition and Spike Timing in the DCN .....	85
2.4.3	Population coding.....	86
<b>Chapter 3: A Member of the Shal Potassium Channel Family Controls the Timing of Action Potentials after Inhibitory Events in DCN Pyramidal Cells .....</b>		<b>88</b>
3.1	<i>Introduction</i> .....	88
3.2	<i>Materials and Methods</i> .....	91
3.3	<i>Results</i> .....	94
3.3.1	rHpTx-2 blocks $I_A$ current in pyramidal cells .....	94
3.3.2	rHpTx-2 alters the build-up response pattern .....	99
3.3.3	Blocking $I_A$ increases action potential width.....	102
3.3.4	$I_A$ alters the timing of spikes after inhibition .....	103
3.3.5	BDS-1 does not block $I_A$ in pyramidal cells.....	104
3.3.6	Subtraction of $I_A$ with Dynamic Clamp .....	108
3.4	<i>Discussion</i> .....	115
3.4.1	Identity of $I_A$ current in DCN pyramidal cells.....	116
3.4.2	Kv4 channels and pyramidal cell processing .....	116
3.4.3	Kv4 Channels and LTP .....	120
<b>Chapter 4: Expression Patterns of Kv4.2 and Kv4.3 in the DCN .....</b>		<b>123</b>
4.1	<i>Introduction</i> .....	123
4.2	<i>Materials and Methods</i> .....	125
4.3	<i>Results</i> .....	131
4.3.1	Kv4.2 <i>In situ</i> hybridization .....	131
4.3.2	Kv4.3 <i>In situ</i> hybridization .....	131
4.3.3	Kv4.2 and Kv4.3 Immunocytochemistry.....	138
4.3.4	Kv3.4 immunocytochemistry .....	149
4.4	<i>Discussion</i> .....	152
4.4.1	<i>In Situ</i> Hybridization Experiments.....	152
4.4.2	Immunocytochemistry .....	153
<b>Chapter 5: Discussion .....</b>		<b>156</b>
5.1	<i>Spike Timing and Potassium Channels in DCN Pyramidal Cells</i> .....	156
5.2	<i>Comparison of DCN Pyramidal Cells to Other Brainstem Neurons</i> .....	157
5.3	<i>Comparison of DCN Pyramidal Cells with Other CNS Neurons</i> .....	162
5.4	<i>Kv4.3 Effects on Dendritic Integration</i> .....	166
5.5	<i>Potential Pathologies</i> .....	169
5.6	<i>Summary</i> .....	170
<b>Bibliography.....</b>		<b>171</b>

## List of Figures

Figure 1.1.....	6
Figure 1.2.....	11
Figure 1.3.....	14
Figure 1.4.....	16
Figure 1.5.....	18
Figure 1.6.....	26
Figure 2.1.....	52
Figure 2.2.....	55
Figure 2.3.....	57
Figure 2.4.....	59
Figure 2.5.....	63
Figure 2.6.....	64
Figure 2.7.....	66
Figure 2.8.....	68
Figure 2.9.....	72
Figure 2.10.....	74
Figure 2.11.....	77
Figure 2.12.....	80
Figure 2.13.....	81
Figure 3.1.....	96
Figure 3.2.....	98
Figure 3.3.....	100

Figure 3.4.....	101
Figure 3.5.....	105
Figure 3.6.....	106
Figure 3.7.....	107
Figure 3.8.....	109
Figure 3.9.....	112
Figure 3.10.....	114
Figure 4.1.....	134
Figure 4.2.....	135
Figure 4.3.....	136
Figure 4.4.....	140
Figure 4.5.....	141
Figure 4.6.....	143
Figure 4.7.....	145
Figure 4.8.....	147
Figure 4.9.....	150

## List of Abbreviations

b-AP	Backpropagating Action Potential
CI	Correlation Index
CN	Cochlear Nucleus
DCN	Dorsal Cochlear Nucleus
FSL	First Spike Latency
PKA	Protein Kinase A
PKC	Protein Kinase C
r-HpTx-2	Recombinant Heteropodatoxin-2
SAC	Shuffled Autocorrelelogram
SD	Standard Deviation
sEPSP	Simulated Excitatory Post-synaptic Potential
sIPSP	Simulated Inhibitory Post-synaptic Potential
VCN	Ventral Cochlear Nucleus

# Chapter 1: Introduction

## 1.1 Overview

Perception of sounds in the environment is an essential survival task for higher organisms. Animals must be able to understand and utilize sound information in order to communicate, find prey, avoid predators, navigate, gain information about the environment, and in some cases, choose a suitable mate. In order to generate perception of incoming sound information, the auditory system differentiates many different aspects of sound such as frequency, location and amplitude. The auditory system does this using a series of nuclei that process and parse out distinct sound information.

The cochlea transduces sound information into electrical impulses that represent all of the important aspects of sound the organism will use to define the environment. The cochlea also initiates the tonotopic organization of the auditory system, which is upheld throughout each ascending auditory nuclei. Because of this tonotopic organization, frequency is encoded at least in part, by a place code.

The auditory nerve carries all information extracted and organized by the cochlea into the brain. The spiral ganglion cells, whose axons make up the auditory nerve, contact the hair cells of the cochlea and are depolarized by glutamate release from the hair cells. Each inner hair cell is contacted by approximately 20 spiral ganglion cells (Liberman 1980). Spiral ganglion cells are spontaneously active and spontaneous rates range from less than 1

Hz all the way to 100 Hz (Kiang 1965). High spontaneous rate fibers have the lowest thresholds while fibers with lower spontaneous activity have higher thresholds (Liberman 1978). Each spiral ganglion cell has a characteristic frequency, which is defined as the sound frequency that elicits an increase in firing rate above the spontaneous rate at the lowest sound pressure level. As the sound pressure level of a pure tone increases, auditory nerve fibers are excited by a broader range of frequencies of tones (Kiang 1965). Auditory nerve fibers characteristically have high firing rates (over 200 Hz) and can phase lock to sound waves up to 4000 Hz (Kiang 1965). The discharge rate is increased by increasing the sound pressure level of the tone and has a maximum value for each auditory nerve fiber. For auditory nerve fibers that do not show phase locking behavior, they respond to pure tones with a primary like response characterized by a sharp increase in firing rate at the onset of the tone, followed by a decrease in firing rate (Popper and Fay 1992). The termination point for all auditory nerve fibers is the cochlear nucleus. Upon entering the cochlear nucleus, the auditory nerve bifurcates into an ascending and descending branch that innervates the ventral and dorsal cochlear nuclei respectively.

The Cochlear Nucleus (CN), located bilaterally at the pontine-medullary junction, receives all of the input of the auditory nerve fibers. The CN is divided into two major parts--the ventral cochlear nucleus (VCN) and the dorsal cochlear nucleus (DCN)--each exhibiting vastly different responses to the sound information carried in the auditory nerve. Bushy cells, the principal cells of the VCN, are contacted by the auditory nerve fibers via the large end bulbs of Held. Bushy cells relay the exact temporal and spectral information contained in the nerve to higher brainstem auditory centers, such as the medial superior olive. On the other hand, the output of the DCN pyramidal cells, the principal cells of the DCN, is

strikingly different from the responses found in the auditory nerve, indicating that the DCN is involved in greater processing and computation. For instance, the DCN has been implicated in head orientation to a sound source (May 2000; Sutherland et al. 1998), and in order to do such a complex task, this nucleus must integrate information from both auditory and non-auditory inputs. However, our understanding of the auditory processing taking place in this nucleus is far from complete. The work presented in this doctoral thesis focuses on the physiological mechanisms employed by the principal cells of the DCN, the pyramidal cells, to encode sound information. Specifically, we investigate the use of spike timing as a method to encode sound information and the cellular mechanisms that enable precise spike timing in DCN pyramidal cells.

### **1.1.1 Spike Timing in the Auditory System**

The precise timing of action potentials in response to inputs has recently been implicated as a method neurons employ to encode information (Mainen and Sejnowski 1995; Softky and Koch 1993). Despite the recent interest in spike timing in other areas of the brain, it has long been known that neurons in the auditory system are responsive to the fine temporal information found in their inputs. For instance, the spiral ganglion cells that constitute the auditory nerve, phase lock to incoming periodic sound information (Rose et al. 1967). Neurons of the medial superior olive act as coincidence detectors in order to localize sound through analysis of microsecond interaural time differences of acoustic stimuli (Goldberg and Brownell 1973).

Neurons in the DCN have not been the target of many studies to determine if they, too, show sensitivity to fine temporal information in their inputs. It is known that they show poor phase locking to pure tone stimuli unlike cells in the VCN (Rhode and Smith 1986). On

the other hand, pyramidal cells are sensitive to temporal information in that they can encode the amplitude modulation of sound (Rhode and Greenberg 1994; Zhao and Liang 1995). Therefore, pyramidal cells are capable of showing some degree of temporal fidelity to complex sounds. Since the DCN is responsible for integrating both auditory and non-auditory inputs, the principal cells of the DCN could utilize this sensitivity to encode information and relay it to the next auditory center by the precise timing of their spikes. Further, since both synaptic input and intrinsic biophysical properties of cells confer the spike patterns observed in each cell, understanding how these properties contribute to spike timing is imperative to understanding how the DCN encodes sound information. In this dissertation I show that the DCN is capable of using spike timing to encode information and this ability is dependent upon some intrinsic conductances. However, to put these observations in context, it is important to first understand the anatomy, physiology, and function of the DCN, and the properties of the intrinsic conductances investigated in this work.

## **1.2 DCN Anatomy**

Embryologically derived from the hindbrain lower rhombic lip (Farago et al. 2006), the DCN is divided into at least three different layers numbered from the most lateral edge to the most medial edge of the nucleus. Layer 1, called the molecular layer, is the most lightly myelinated. Layer 2 houses the principal cells of the DCN, the pyramidal (alternatively called fusiform) cells, and is called the pyramidal cell layer. Layer 3, sometimes made of up of two distinct layers, is the most heavily myelinated layer since the myelinated auditory nerve fibers terminate here (Brawer et al. 1974; Hackney et al. 1990; Kane 1977; Lorente de N6 1981). Cell bodies of neurons are found in every layer of the DCN. For instance, the

pyramidal cells have cell bodies found in layer 2, and two branches of dendrites, apical and basal, which project into the molecular layer and deep layer, respectively (Blackstad et al. 1984; Brawer et al. 1974; Hackney et al. 1990; Oertel and Wu 1989; Osen 1969a). Each sheet, comprising layers 1-4, make up one of the tonotopic sheets, which are oriented in the ventral to dorsal direction. One tonotopic sheet receives input from a very narrow frequency band of sound in the auditory nerve (Osen 1970; Ryan et al. 1982) (see Figure 1.1).

**Figure 1.1**

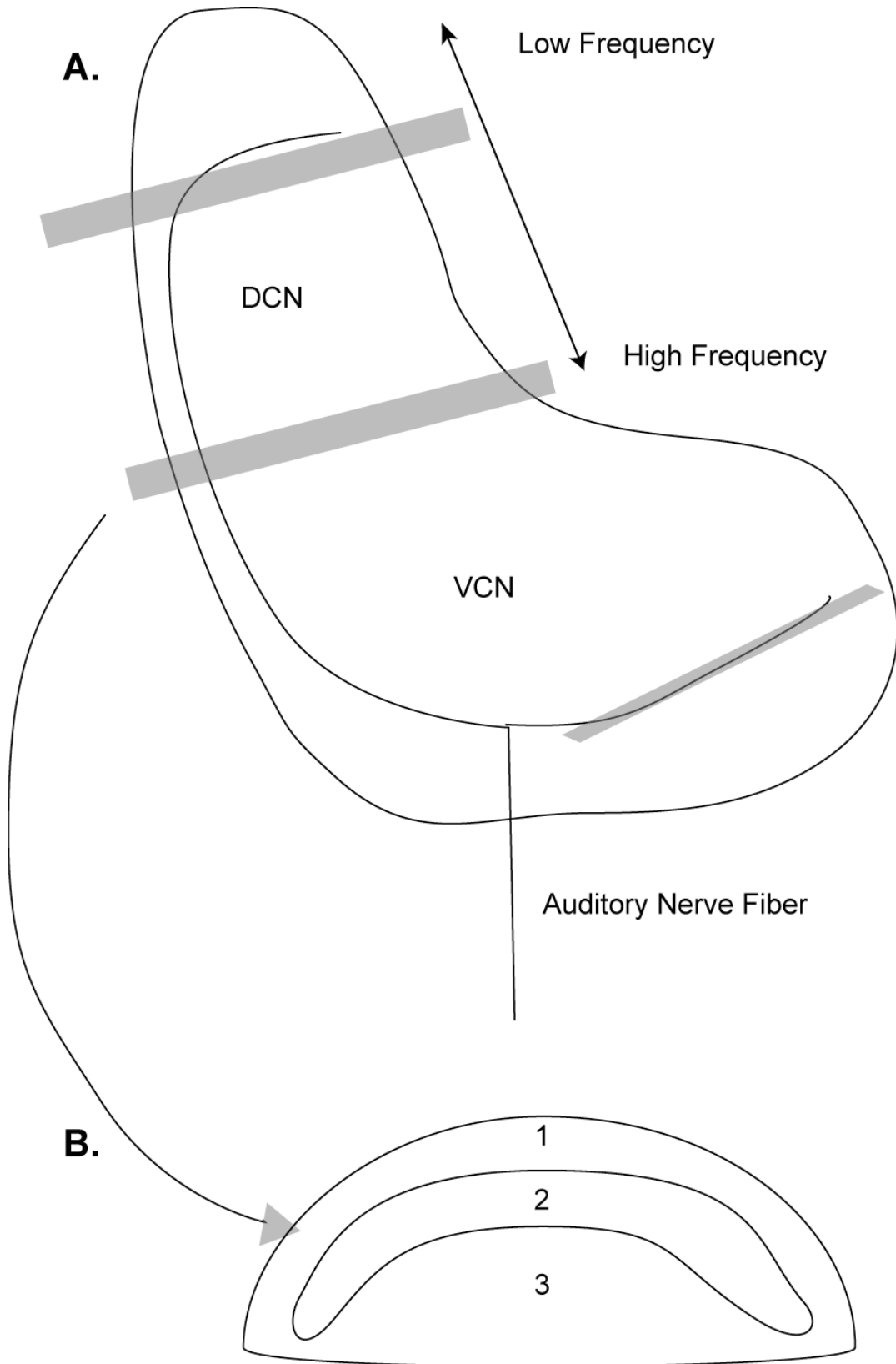


**Figure 1.1** The tonotopic organization of the DCN.

**A.** Schematic of the cochlear nucleus showing the VCN and the DCN and innervation by 1 auditory nerve fiber. The grey rectangles denote tonotopic sheets which represent input from a narrow band of the cochlea.

**B.** One tonotopic sheet of the DCN showing how each tonotopic sheet is organized into layers 1,2 and 3. The auditory nerve fibers terminate in layer 3.

### 1.2.1 Circuitry and Cell Types

Pyramidal cells are the principal neurons of the DCN. They, along with giant cells, are the only cells that project to higher brainstem auditory centers. The pyramidal cells project monosynaptically to the inferior colliculus where the processed information of the DCN is further processed and relayed to the medial geniculate nucleus (Adams 1976; Oliver et al. 1999; Osen 1972; Ryugo and Willard 1985).

The anatomy and synaptic circuitry will be described by orienting the circuitry to the pyramidal cells. The pyramidal cells receive input from both auditory and non-auditory afferents via two separate sets of excitatory synapses. First, auditory information from type I auditory nerve fibers (95% of auditory nerve fibers) terminate in layer 3 on the basal dendrites of pyramidal cells (Lorente de Nó 1981; Manis and Brownell 1983). The type I afferents enter the DCN such that the tonotopic organization established by the cochlea is preserved--each frequency represented by a different tonotopic sheet (see Figure 1.1). Since the basal dendrites of the pyramidal cells are flattened along an isofrequency sheet, each pyramidal cell will receive input from a very limited region of the cochlea (Blackstad et al. 1984). It is estimated that each pyramidal cell receives synaptic input from approximately 12 auditory nerve fibers (Ryugo and May 1993). These synapses are glutamatergic, and AMPA and metabotropic glutamate receptors (mGluR) have been localized to these synapses (Gardner et al. 2001; 1999; Manis and Molitor 1996; Petralia et al. 2000; Rubio and Wenthold 1997; Sanes et al. 1998). The auditory nerve fibers also synapse on glycinergic cells found in the deep layer (called vertical, corn, or multipolar cells; (Lorente de Nó 1981)), which in turn inhibit pyramidal cells (Voigt and Young 1990; 1980; Zhang and Oertel 1993b).

The granule cell system of the CN provides the other principal excitatory input to pyramidal cells. Granule cells are found throughout the CN (Mugnaini et al. 1980b). The granule cells receive input that is both auditory and non-auditory. Some auditory input arises from type II auditory nerve fibers (corresponding to 5% of the auditory nerve fibers) and descending afferents from higher auditory centers (Brown and Ledwith 1990; Kane 1977; Malmierca et al. 1996; Osen 1969a; Schofield and Coomes 2005; Shore and Moore 1998; Weedman and Ryugo 1996). Non-auditory inputs arrive from somatosensory areas, vestibular nuclei and the pons (Babalian 2005; Davis et al. 1996; Shore and Moore 1998; Shore and Zhou 2006; Weinberg and Rustioni 1987; Wright and Ryugo 1996; Young et al. 1995; Zhan et al. 2006). The granule cell axons form parallel fibers that orthogonally cross tonotopic sheets and synapse on the spiny apical dendrites of the pyramidal cells (Hirsch and Oertel 1988b; Manis 1989; Oertel and Wu 1989; Zhang and Oertel 1994). These synapses are also glutamatergic, and have AMPA, NMDA and mGlu receptors postsynaptically (Gardner et al. 2001; 1999; Manis and Molitor 1996; Molitor and Manis 1999; Rubio and Wenthold 1997).

In addition, the granule cells also form excitatory synapses with another inhibitory interneuron of the DCN, the cartwheel cell. Cartwheel cells are similar to Purkinje cells of the cerebellum in that they are very spiny and have robust branching of their dendritic tree into the molecular layer where these dendrites receive synaptic endings of parallel fibers (Manis 1989; Mugnaini et al. 1980b; Oertel and Wu 1989). The cell bodies of cartwheel cells are usually found in layer 1 or layer 2. The cartwheel cells are glycinergic and synapse on the soma of pyramidal cells and other cartwheel cells, and therefore form feed forward inhibitory circuits (Berrebi and Mugnaini 1991; Golding and Oertel 1996; 1997; Manis et al.

1994; Zhang and Oertel 1993a). Recent evidence also indicates that cartwheel-cartwheel interactions can be either depolarizing or hyperpolarizing despite the neurotransmitter being the same (glycine) in both cases (Golding and Oertel 1996; 1997).

Another major class of inhibitory cells in the DCN also receives excitatory input from the parallel fiber of the granule cells; these are the stellate cells. Stellate cells are GABAergic and their cell bodies are found in the molecular layer. It is there that stellate cell axons contact dendrites of both pyramidal and cartwheel cells (Mugnaini 1985; Wouterlood et al. 1984). The circuitry of the DCN (see Figure 1.2) is very complex in that the principal cells of the nucleus receive excitatory and inhibitory synaptic input arising from auditory and non-auditory centers and must integrate this information before sending the processed signal to the inferior colliculus. Exactly how this process is carried out is far from being determined.

**Figure 1.2**

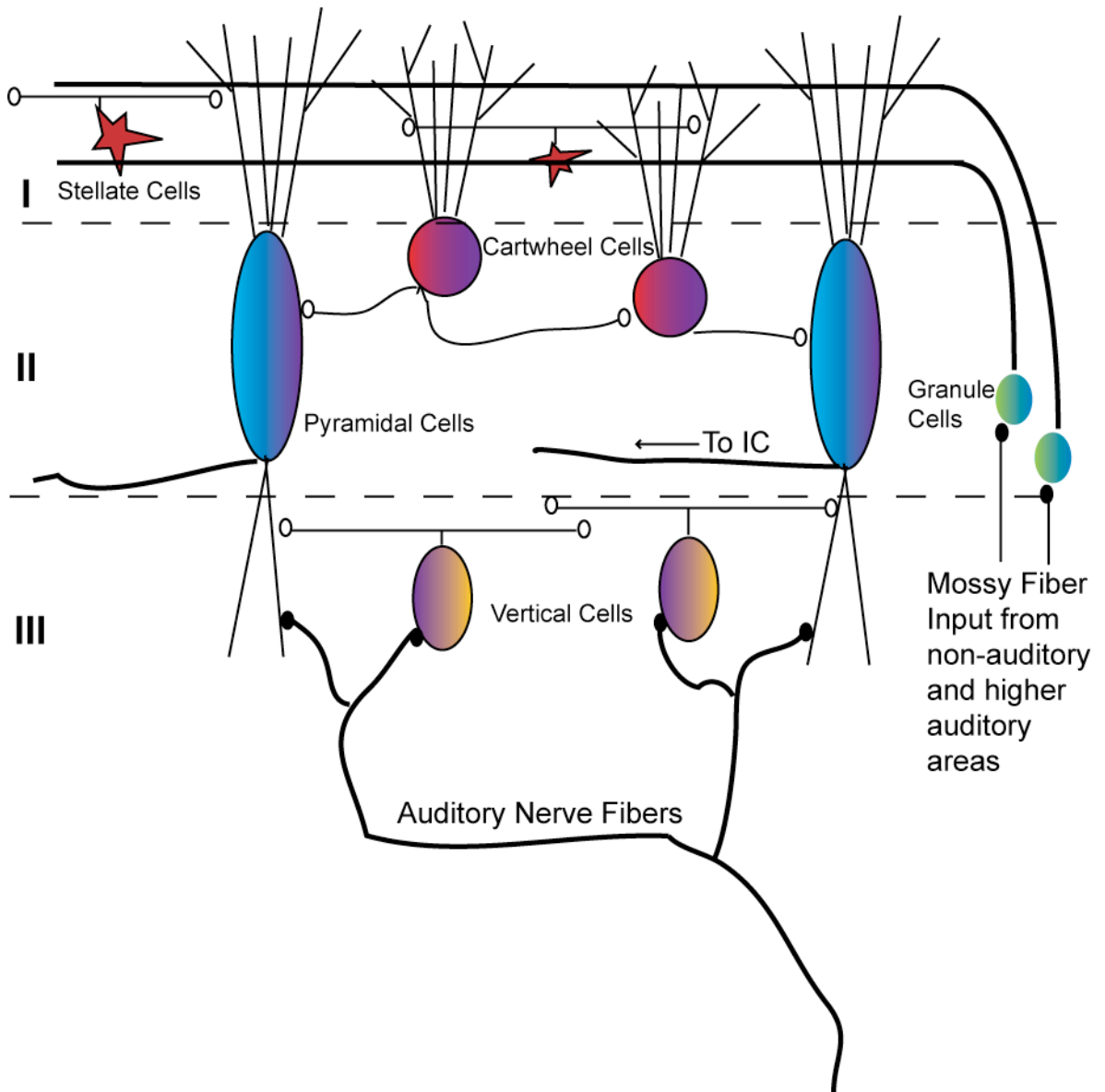


**Figure 1.2** Excitatory synapses are represented by filled circles, inhibitory synapses are represented by open circles.

## **1.3 DCN Physiology**

### **1.3.1 Neuronal Responses to Sound**

Some of the strongest evidence that more complicated integration and processing occurs in the DCN compared to processing in the VCN, comes from response properties of the pyramidal cells to sound stimuli. Whereas the principal cells of the VCN respond to sound in much the same way as the type I auditory nerve fibers, the responses of pyramidal cells are completely different. Several methods of characterizing response patterns of cochlear nucleus neurons have been used.

The simplest auditory stimulus is a tone. When pure tone bursts are given at different frequencies and different sound pressure levels, a frequency-intensity-response map can be generated that is specific for each cell. Principal cells of the VCN and auditory nerve fibers respond to such stimuli with a type I response, characterized by excitation at the lowest sound pressure at the cell's characteristic frequency (CF) and increased excitation across a range of frequencies as the amplitude of sound increases (Evans and Nelson 1973) (Figure 1.3A). DCN pyramidal cells, on the other hand, show the characteristic increase in firing rate at the threshold for their characteristic frequency, but inhibition when tone amplitude increases at the CF. This response pattern is known as a type IV response (Figure 1.3C). As the sound pressure is continuously increased, excitation will be detected for frequencies above the characteristic frequency; this region is known as the upper-excitatory region (Evans and Nelson 1973; Spirou and Young 1991; Young and Brownell 1976). Further, type IV units are excited by broadband noise. Another response pattern found in the DCN is the type II response. This response resembles the type I in that there is continuous excitation as intensity is increased, but type II is characterized by inhibitory sidebands where stimuli at higher and lower frequencies cause inhibition of the cell's response (Rhode 1999) (Figure

1.3B). Type II cells have been identified as the vertical cells and they are responsible for the acoustically-evoked inhibition observed in type IV pyramidal cells (Shofner and Young 1985; Voigt and Young 1990; 1980; Young 1980). Type IV units are excited by broadband noise whereas a type II unit responds very weakly to such stimuli (Nelken et al. 1997; Spirou and Young 1991). Thus, when type II units are not activated, type IV units respond with excitation. Conversely, when type II units are activated, type IV units respond with inhibition. Therefore, synaptic inputs shape the response properties of pyramidal cells.

Not only do the integrated responses to sound differ in the DCN when compared to the VCN or the auditory nerve, but also the temporal discharge patterns of pyramidal cells show the effects of neural integration. VCN principal cells respond to short tone bursts with a “primary-like” response in their peristimulus time histograms (PSTH). A primary-like response is characterized by a short, large increase in firing rate followed immediately by a less intense activated firing rate (Figure 1.4A) (Godfrey et al. 1975). Pyramidal cells, however, fire in “chopper”, “pauser”, or “buildup” patterns (Figure 1.4B-C) (Godfrey et al. 1975; Rhode et al. 1983a). Chopper units show irregular firing. The buildup response is characterized by a long first spike latency (FSL) followed by a steady increase in firing rate (Figure 1.4B). A pauser response contains a fast, precisely timed spike, followed by a long first inter-spike interval (FISI) before the cell resumes a regular firing rate (Figure 1.4C). In addition, these responses also are observed when individual cells are recorded with an intracellular electrode and stimulated by depolarizing currents *in vitro* (Figure 1.5) (Manis 1990). This latter observation shows that synaptic inputs are not solely responsible for the output patterns of pyramidal cells. Intrinsic conductances, without other synaptic input, can also shape response patterns of pyramidal cells as has been reported for other types of neurons (Llinas 1988).

Figure 1.3

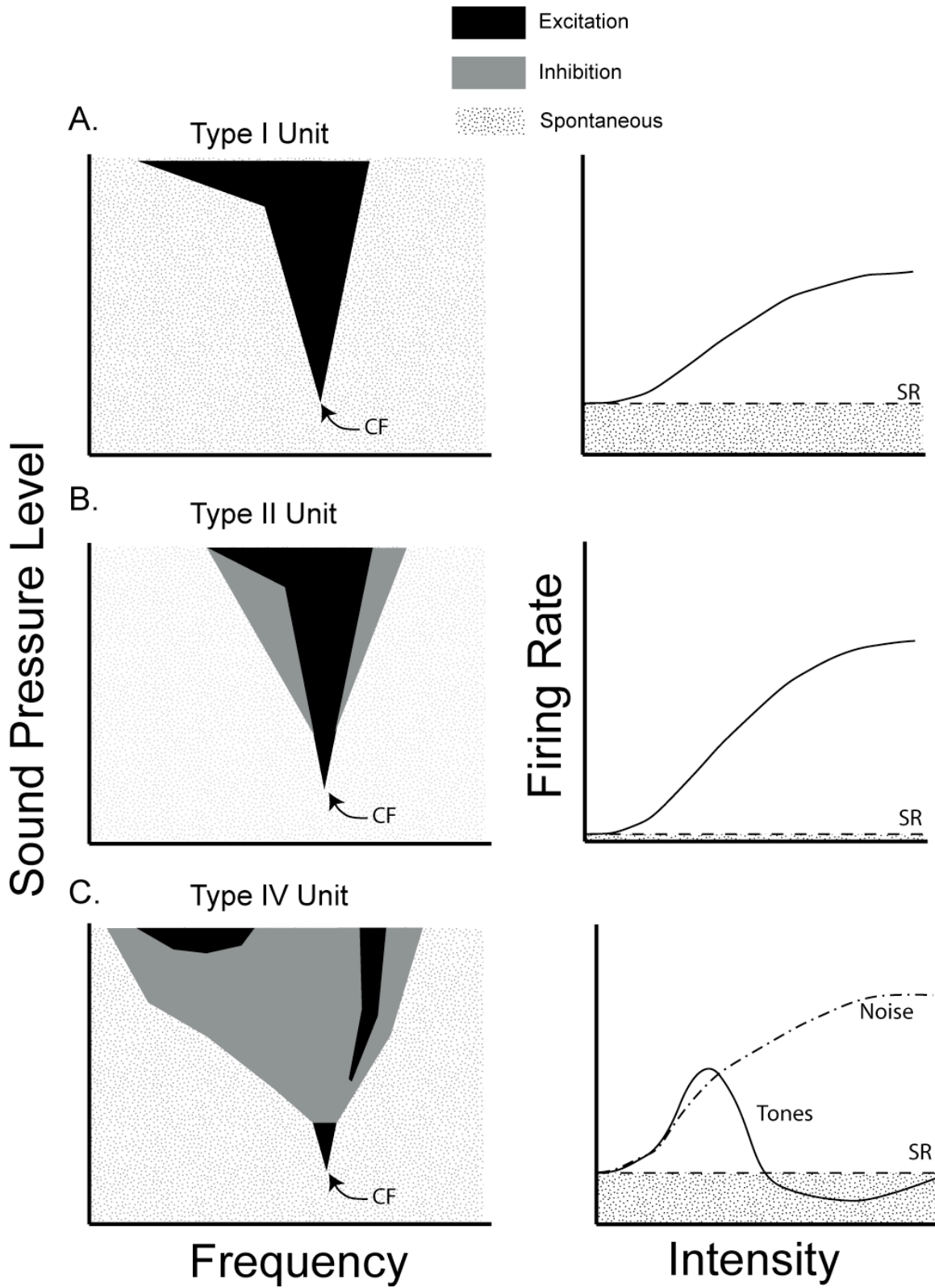


**Figure 1.3** Representation of 3 response patterns found in the cochlear nucleus.

**A.** Type I unit typical of bushy cells in the VCN.

**B.** Type II unit representative of vertical cells in the DCN.

**C.** Type IV unit which shows the complex response of the pyramidal cells of the DCN. Grey denotes combinations of frequency and sound pressure level where the firing rate is lower than the spontaneous rate. Black denotes sound pressure levels and frequency combinations that resulted in the firing rate increasing from spontaneous rate. The spotted background denotes spontaneous rates.

**Figure 1.4**

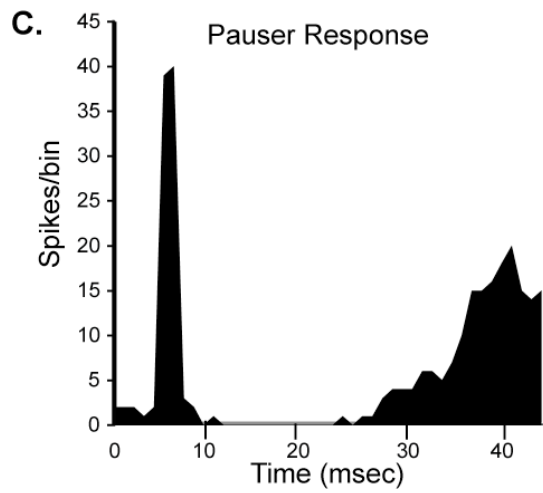
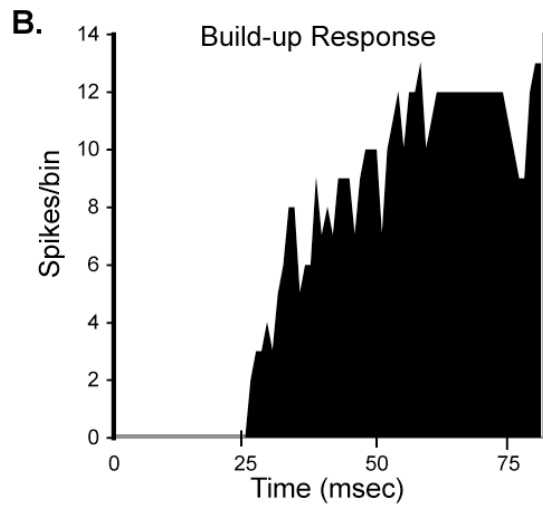
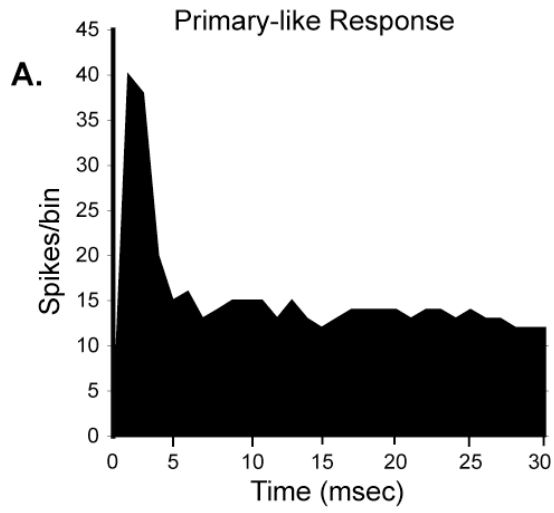


**Figure 1.4** Peri-stimulus time histograms of units in the cochlear nucleus in response to pure tones. The time shown represents the entire time of the stimulus.

**A.** Primary-like response typical of VCN bushy cells and auditory nerve fibers.

**B.** Build-up response patterns typical of DCN pyramidal cells. This pattern is characterized by a long latency to the onset of spiking. **C.** The pauser response pattern typical of DCN pyramidal cells is characterized by the long first inter-spike interval.

**Figure 1.5**

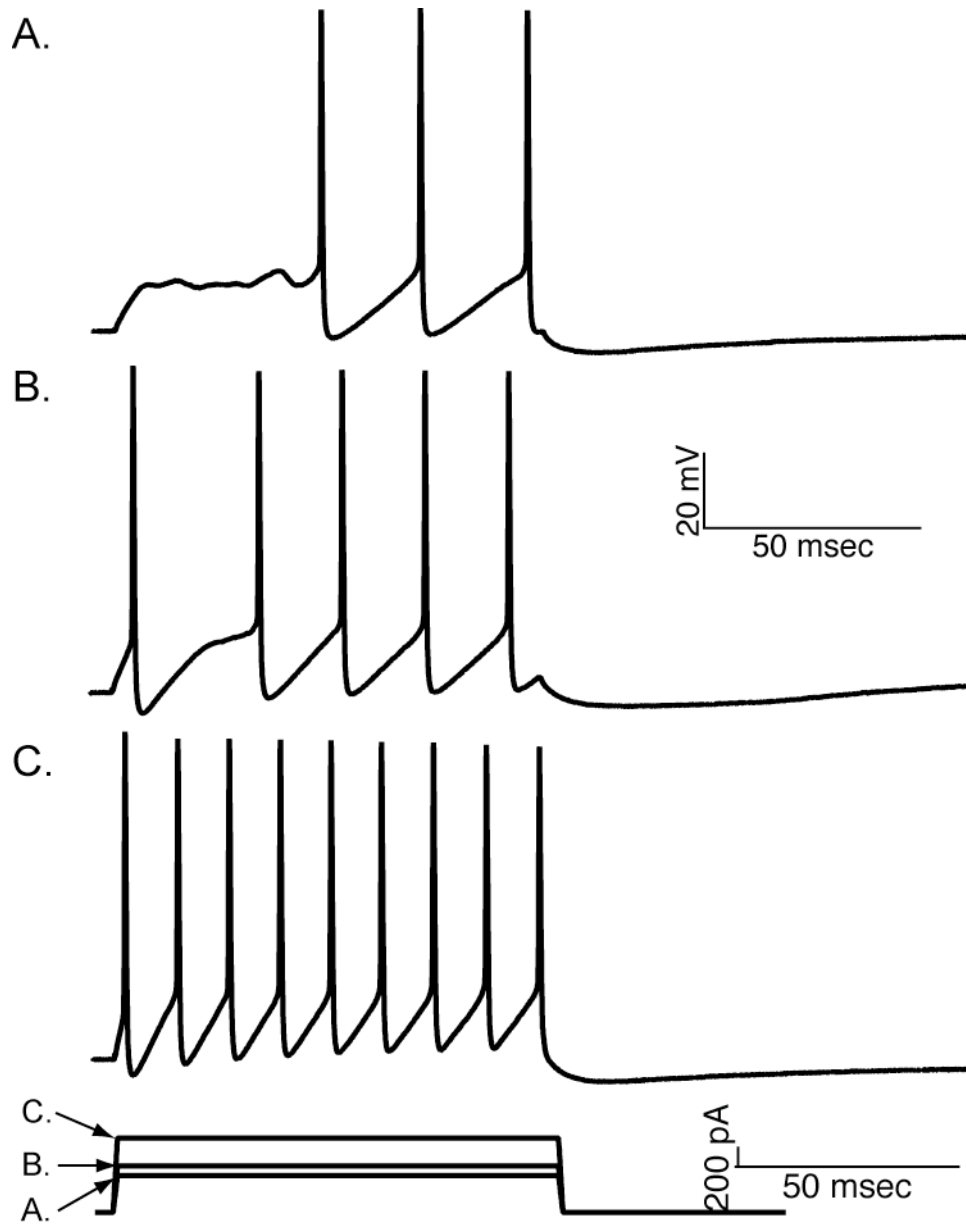


**Figure 1.5** Three different response patterns can be evoked by different depolarizing currents in pyramidal cells in a DCN slice preparation. The response patterns A. Build-up B. Pause and C. Regular were elicited in a single pyramidal cell with the corresponding currents A, B, and C.

### 1.3.2 Intrinsic Conductances of Pyramidal Cells

Pyramidal cells express many intrinsic conductances that shape their discharge patterns. Intrinsic currents respond to changes in the cellular environment, such as membrane voltage, intracellular calcium or intracellular messengers. Therefore, they shape the output patterns of cells based on the history of cellular activity along with synaptic input. Both a rapidly and a slowly inactivating  $K^+$  current have been found in pyramidal cells (Kanold and Manis 1999). It has been hypothesized that the fast inactivating  $K^+$  current causes the long delays before spikes seen in the build up pattern and the pauser pattern of pyramidal cells while the slowly inactivating  $K^+$  current is responsible for repolarization phase of action potentials (Kanold and Manis 2001; 1999). A persistent  $Na^+$  current is partially enabled at rest and is responsible for sub-threshold oscillations observed as the cell membrane potential slowly depolarizes to threshold (Hirsch and Oertel 1988a; Manis 1990; Manis et al. 2003). During this phase, the persistent  $Na^+$  current and the rapidly inactivating  $K^+$  current are both activated and exert opposite effects on membrane potential. The persistent  $Na^+$  current causes the cell to slowly depolarize and shapes the slope membrane potential rise toward threshold, whereas the transient  $K^+$  current opposes the inward current by making the membrane more leaky to current flow out of the cell, pulling the cell towards the  $K^+$  equilibrium potential. The end result of these two conductances working in concert is the long latency to the first spike seen in the pyramidal cell build-up pattern.

Pyramidal cell also express other intrinsic conductances that could influence the timing, shape, and firing pattern of action potentials. A hyperpolarizing activated cation channel causes the membrane potential to slowly depolarize during sustained hyperpolarizations (Manis 1990). It also sets the resting cell membrane potential to a more

positive voltage than when these channels are blocked (Manis lab, unpublished results). Finally,  $\text{Ca}^{2+}$  currents are also found in pyramidal cells. These channels are most likely L-type channels that begin to activate around -50mV and are fully activated around 20-35 mV (Molitor and Manis 1999). It is unlikely that these channels contribute to the timing of action potentials since large depolarizations are needed to activate a substantial amount of conductance. However, these channels would certainly contribute to dendritic integration and synaptic plasticity by strengthening back-propagating action potentials and activating intracellular messengers that are necessary for these phenomenon to occur (Molitor and Manis 2003).

### **1.3.3 Other DCN Neurons**

The many other cells that are found in the DCN have not been as extensively characterized as pyramidal cells. For instance the other projection neuron, the giant cell, is still hard to distinguish from pyramidal cells with our current level of understanding (Smith et al. 2005). Cartwheel cells, the second most characterized cell type, are the only cells in the DCN currently known to display complex spikes in response to depolarizations. These cells exhibit sustained  $\text{Ca}^{2+}$  depolarizations, which give rise to a burst of 2-4 action potentials followed by long after-hyperpolarizations (Manis et al. 1994; Zhang and Oertel 1993a). These burst of action potentials are seen as temporally related IPSPs in pyramidal cells (Mancilla and Manis, 2006). Stellate cells are the other inhibitory interneurons that synapse on apical dendrites of pyramidal cells and to date there is only one recording from a stellate cell reported in the literature (Zhang and Oertel 1993a). This one stellate cell was a regular spiking cell with overshooting action potentials and a two-phase after-hyperpolarization. The same firing pattern was also found in vertical cells recorded in a slice preparation (Zhang and

Oertel 1993b). It is known that vertical cells respond to pure tones with a type II firing pattern (Rhode 1999). Therefore, as discussed previously, it is thought that vertical cells inhibit pyramidal cells in response to pure tones and cause pyramidal cells to respond with mostly inhibition. Granule cells, to this day, remain difficult to record from, but it is thought that they are spontaneously active in slice preparations (Rusznak et al. 1997; Zhang and Oertel 1994).

#### **1.3.4 DCN Plasticity**

The cellular machinery necessary for long-term synaptic changes is found in both the molecular and fusiform layer of the DCN, indicating that the synapses on spiny dendrites of pyramidal cells and cartwheel cells might undergo long-term potentiation and depression in response to synaptic activity. All forms of glutamate receptors including AMPA, NMDA and some metabotropic glutamate receptors are all expressed on apical dendrites of pyramidal cells and the dendrites of cartwheel cells (Gardner et al. 2001; 1999; Manis and Molitor 1996; Molitor and Manis 1997; Rubio and Wenthold 1997). In addition, PKC expression is observed in the molecular and fusiform layers and stimulating PKC with phorbol esters can potentiate synapses found in the molecular layer (Francis et al. 2002). Hence, it is no surprise that post-synaptic LTP and LTD can be evoked at parallel fiber-pyramidal cell synapses and also parallel fiber-cartwheel cell synapses. This form of LTP and LTD requires  $Ca^{2+}$  in both pyramidal cell and cartwheel cells, and it is NMDA-receptor dependent in cartwheel cells (Fujino and Oertel 2003). However, synapses could be only moderately depressed and potentiated without NMDA and mGlu receptors in fusiform cells.

In addition, spike timing dependent synaptic plasticity (sometimes referred to as “Hebbian”) has also been reported at parallel fiber synapses. Action potentials evoked 5

msec after EPSPs caused potentiation of pyramidal cell synapses whereas when action potentials were evoked 5 msec before EPSPs there was depression along the lines of Hebbian rules (Tzounopoulos et al. 2004). However, in this same study it was also reported that the opposite effect occurred in parallel fiber-cartwheel cell synapses and is therefore “anti-hebbian”. Cartwheel cell synapses were depressed when an action potential followed an EPSP and were not potentiated for any temporal pattern of action potential/EPSP. Therefore, the same pattern of synaptic input can cause opposite synaptic changes in pyramidal cells and cartwheel cells. The significance of this is not yet fully understood; however, strengthening pyramidal cell synapse to the same synaptic input that causes depression in a cartwheel cell synapse would even further strengthen the response of the pyramidal cells to parallel fiber synaptic drive, since the the LTD would weaken the feed-forward inhibition by cartwheel cells.

## **1.4 DCN Function**

### **1.4.1 Amplitude Modulation Encoding**

While much is known about the circuitry and the physiology of the DCN, attempts to elucidate the function of the DCN are still unfolding. DCN neurons, unlike neurons of the ventral cochlear nucleus, do not phase lock to the fine structure of sounds. In addition, the response patterns of DCN pyramidal cells are strikingly different from principal cells of the VCN. Therefore, many have proposed vastly different functions for the DCN.

One possibility is that the DCN encodes amplitude modulation of sounds. Amplitude modulation occurs in complex sounds such as speech, music and other forms of vertebrate communication (Frisina 2001). While DCN pyramidal cells do not phase lock to frequency information in pure tones, they do encode sound envelope information contained in

amplitude modulated tones with high fidelity from 400-1200 Hz and up to sound pressure levels of 90dB (Kim et al. 1990; Rhode and Greenberg 1994; Zhao and Liang 1995). Unlike other neurons of the cochlear nucleus, pyramidal cells' ability to encode amplitude modulated sounds actually increases with increasing sound pressure levels and they are able to process this information at all but the lowest signal to noise ratios (Rhode and Greenberg 1994). This observation led to the hypothesis that the DCN was important for detecting behaviorally important sounds in a noisy environment. In the presence of a loud noise, amplitude modulation coding increased in pyramidal cells and in the presence of background noise this ability either stayed the same or decreased minimally. In such environments synchronous firing increased, implicating wideband and lateral inhibition as a potential physiological mechanism (Frisina et al. 1994; Neuert et al. 2004). While these findings suggest that the DCN can detect amplitude modulated sounds with a low signal-to-noise ratio in noisy environments, Joris and Smith found that the responses of pyramidal cells became more non-linear as the sound pressure level increased, and called into question the feasibility of this function for the DCN (Joris and Smith 1998). At the very least, this study revealed the complexity of circuitry and interactions of neurons in the DCN. The exact role of the DCN in encoding amplitude modulation is still undergoing investigation, but it seems certain that sound information contained in the envelope is encoded by spike timing in the DCN. Further, this finding gives credence to our attempts to characterize spike timing behavior of DCN pyramidal cells.

#### **1.4.2 Sound Localization**

Animals must be able to detect the location of the sound source in order to survive. Another proposed function of the DCN is localizing sound in the vertical plane and

integrating multisensory information so that the head can be oriented to the sound source. Lesions of the dorsal acoustic stria, the fiber tract containing pyramidal and giant cell axons leaving the DCN, results in the inability of cats to orient their heads to a sound source (May 2000; Sutherland et al. 1998). This observation has led many to investigate how the DCN integrates sound information with other sensory input.

The DCN is important for localizing sound sources in the vertical plane (Oertel and Young 2004). It accomplishes this task by neuronal sensitivity cued to sensing notches in the spectral energy of sound waves. When a sound wave reaches the ear, it reflects off the irregularly shaped pinna, and the reflections interact to attenuate energy in a small bandwidth of sound known as a spectral notch (Middlebrooks and Green 1991; Rice et al. 1992). As the head moves, or the pinna or sound source changes position, this notch in the sound spectrum will shift in frequency, conferring a feature in the spectral structure that could be detected by neurons tuned to, or sensitive to, spectral notches. This change in the spectrum of sound energy reaching the eardrum with changing source position is known as the head related transfer function (HTRF).

The majority of pyramidal cells are inhibited by noise with spectral notches centered at the neuron's characteristic frequency; however, a small percentage of pyramidal cells do respond with excitation to spectral notches (Nelken and Young 1997; Spirou and Young 1991). These results have also been corroborated in neuronal models (Zheng and Voigt 2006). Because of these and other studies, it was thought that pyramidal cells sensed the notch by inhibition. One recent study demonstrated that pyramidal cells are indeed inhibited by spectral notches centered at the best frequency of the neuron, but went on to demonstrate that pyramidal cells are excited by the rising edge of the notch (Reiss and Young 2005).

Therefore, it is not simply the notch, but the edge of the notch that is encoded by the DCN in order to convey sound localization information.

Many neuronal circuits have been proposed to explain this response. Most agree that the type II inhibitory neurons, the vertical cells, are excited by narrow band stimuli and those cells inhibit the pyramidal (type IV cells) as discussed previously. However, a wideband inhibitor, D-stellate cells of the VCN, are proposed to weakly inhibit pyramidal cells and strongly inhibit the vertical cells (Nelken and Young 1994). Pyramidal cells are usually excited by broadband noise. Vertical cells are strongly inhibited by broadband noise due to the strong inhibition from the wideband inhibitor. Because the vertical cells are strongly inhibited to noise by the wideband inhibitory, the pyramidal cells would be only weakly inhibited to noise with spectral notches at characteristic frequency since the weakly inhibitory wideband inhibitor is responsible for this inhibition (Figure 1.6) (Nelken and Young 1997). While this model adequately explains responses of pyramidal cells to spectral notches, it is insufficient to explain the excitation at rising edge of the spectral notch (Reiss and Young 2005). Reiss and Young hypothesized that another source of inhibition would be necessary to generate excitatory responses to the notch rising edge. The exact source of this inhibition has yet to be ascertained.

**Figure 1.6**

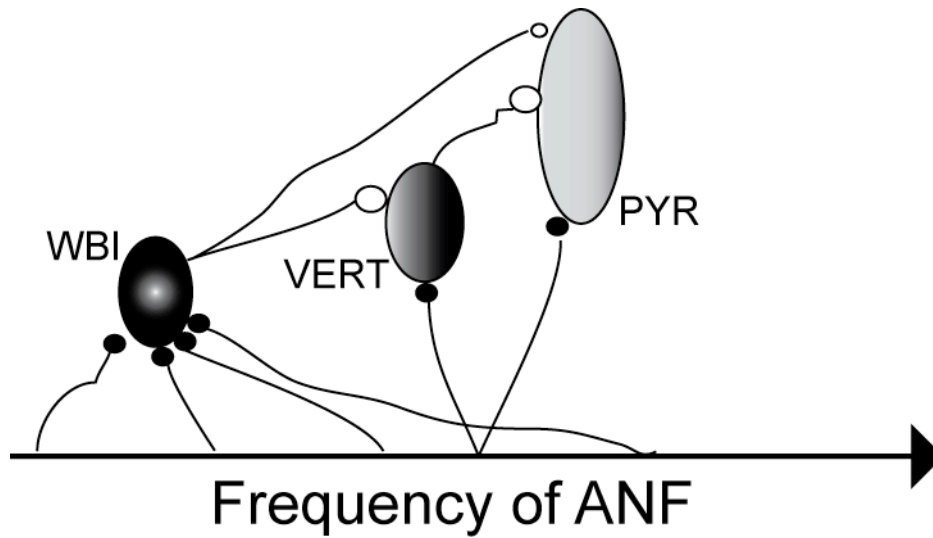


**Figure 1.6** Proposed model that accounts for response patterns recorded in DCN pyramidal cells. Two different inhibitory neurons receive different sound frequency information from auditory nerve fibers (ANF). The wideband inhibitor (WBI) weakly inhibits the pyramidal cell (PYR) and strongly inhibits the vertical cell (VERT). The vertical cell, on the other hand, strongly inhibits the pyramidal cell. The strength of inhibition is symbolized by the size of the circle that represents the synapse. Open circles are inhibitory, black circles are excitatory.

### **1.4.3 Multisensory Integration**

In addition to localizing a sound source by information in the sound wave, the DCN must also process the position of the head and pinna to both perceive the correct position of the sound and aid the animal in orienting to the sound. It is thought that this might be one reason that the DCN receives somatosensory inputs through the granule cell system.

Electrical stimulation of the trigeminal nuclei and the dorsal column alters the output of pyramidal cells. Stimulation of these nuclei result in both inhibitory and excitatory responses when paired with additional auditory stimuli such as broadband noise (Shore 2005; Young et al. 1995). In addition, stretch and vibration of the pinna muscles in cats elicit both excitatory and inhibitory responses in DCN pyramidal cells, whereas light touch and stretching of the skin were ineffective in altering DCN output (Kanold and Young 2001). These results suggest that the movement of the pinna, in particular, is encoded in the DCN, while generalized somatosensory information is not. In addition to the obvious role in processing sound localization, it has also been hypothesized that this multisensory input attenuates self-imposed noise from movement or chewing and also increases the signal to noise ratio of important sounds in the presence background noise (Shore and Zhou 2006). The multisensory input to DCN pyramidal cells has also implicated the DCN in a disorder known as tinnitus, or ringing in the ears, since this disorder is often associated with temporomandibular joint dysfunction.

### **1.4.4 Tinnitus**

Tinnitus is an auditory disorder characterized by phantom sounds, usually buzzing or ringing in the ears. As many as 10-15% of the population experience unremitting tinnitus, many of whom have serious mental and emotional side effects as a result of severe tinnitus

(Heller 2003). The exact causes and mechanisms of the disorder are not understood, but it is clear that such insults as cochlear damage, noise-induced hearing loss, cisplatin and salicylate treatment can all lead to temporary tinnitus. While it is widely accepted that the cochlea is the initiation site of tinnitus, it is uncertain what area generates and maintains long-term tinnitus.

Recently the DCN has been implicated in tinnitus. It is well known that tinnitus can be modulated or exacerbated by perturbations in somatosensation such as temporomandibular joint dysfunction. In addition tinnitus patients can modulate their tinnitus by contracting certain head and neck muscles (Levine et al. 2003; Zhou and Shore 2004). Hence, the DCN could play an important role in the mechanism of tinnitus since it is responsible for integrating both auditory and non-auditory inputs such those from somatosensory nuclei (Kaltenbach et al. 2005; Salvinelli et al. 2003).

Multiple labs have reported increases in spontaneous activity in different animal models by utilizing such insults as intense tone exposure, noise exposure, or cisplatin or salicylate administration (Brozoski et al. 2002; Kaltenbach and Afman 2000; Kaltenbach et al. 2002; Zhang and Kaltenbach 1998). The elevated spontaneous activity was found in the tonotopic area associated with the frequency of the tone used to induce tinnitus (Kaltenbach and Afman 2000). In addition, the increases in DCN activity has been correlated to behavioral evidence of tinnitus in both hamsters and chinchillas (Brozoski et al. 2002; Kaltenbach et al. 2004). Animals that had behavioral evidence of tinnitus also had larger increases in spontaneous activity in the DCN. In addition, animals exposed to intense tones also showed similar DCN activity to that of animals that were presented with a regular intensity tone of the same frequency (Kaltenbach and Afman 2000). A recent surge in

interest in this area of research promises to bring more enlightenment to the DCN's role in tinnitus.

## 1.5 Spike Timing and the Neural Code

The major premise of this work is that DCN pyramidal cells utilize a spike timing code to relay sound information to the IC. It has long been observed that cortical neurons, *in vivo*, fire irregular spike patterns. This observation has since caused many investigators to ask if information can be encoded by the precise times of spikes versus an average rate code (Softky and Koch 1993). Neurons using a spike timing code, would be more efficient in communicating information and therefore, capable of transmitting more information (Softky 1995). This theory has been investigated using many *in vivo*, *in vitro*, and model preparations. Many of the *in vivo* studies have been done in the visual system and show that when time varying visual stimuli are presented to various species, areas of the brain such as the lateral geniculate nucleus, visual cortex and retinal ganglion cells respond with reproducible trains of spikes to repeated stimuli (Berry et al. 1997; Buracas et al. 1998; de Ruyter van Steveninck et al. 1997; Reich et al. 1997). In addition repeating spike patterns have been observed in response to repeated external events that could not be attributed to chance in the frontal cortex of behaving monkeys (Abeles et al. 1993). Behavior was also shown to be responsive to the timing of microstimulation during a learned task (Seidemann et al. 1998).

*In vitro*, cells respond to time varying input by firing trains of action potentials that are both precise (the standard deviation of the spike time) and reliable (probability that a spike will be fired), demonstrating that they are capable of using spike timing to encode information (Mainen and Sejnowski 1995). It has even been demonstrated that precisely

when spikes occur prior to synaptic events can determine to what extent the synapse is potentiated or depressed (Froemke and Dan 2002). Spike-timing dependent plasticity has recently been shown in the DCN and the timing of spikes with the PSP results in different changes at different synapses.

A neuron can act as an integrator, firing action potentials in response to excitatory and inhibitory events that sum to threshold over time, or a coincidence detector that fires action potentials only when the timing of synaptic events is precise enough to elicit an action potential (Konig et al. 1996; Salinas and Sejnowski 2001). In order for neurons to act as coincidence detectors, they must have certain properties such as fast membrane time constants and intrinsic conductances that allow fast post synaptic potentials to elicit an action potential (Fricker and Miles 2000; Grande et al. 2004). Synchronous inputs also allow for rapid depolarization and precise firing of action potentials and such inputs are found in the cortex (Azouz and Gray 2000; Stevens and Zador 1998). All of these properties, along with the timing of synaptic inhibition and intrinsic conductances of the cell, have been implicated in determining spike timing reliability of neurons (Hausser and Clark 1997; Schreiber et al. 2004). To complicate matters the shape of dendritic trees also are known to play a role in firing pattern and spike generation, including the distributions of specific conductances and synaptic inputs (Mainen and Sejnowski 1996; Yuste and Tank 1996). While this area of neuroscience is relatively understudied and underappreciated, we are beginning to understand of how different cells utilize their intrinsic properties and synaptic inputs to encode information in action potentials. Studies such as these are essential to eventually elucidate the neural code.

DCN pyramidal cells are known to phase lock to amplitude modulated tones. It is one of the purposes of this study to determine what role, if any, intrinsic conductances play in conferring precise spike timing behavior in these cells. Pyramidal cells possess some of the channels that have been implicated in synaptic amplification and spike timing. They also receive inhibitory input that is likely to be timed to the excitatory input, and such temporal sequencing has been shown to be important in some forms of coincidence detection. Since these cells are the main source of output of the DCN, and show evidence of signal integration and processing, pyramidal cells could respond to their converging inputs by firing precise timing of spikes to convey information to the IC. Moreover, it is our hypothesis that this is conferred on the cell by both the inherent characteristics of the cells themselves and the local circuitry of the nucleus. In this study we focused on a transient potassium current, which will now be reviewed in detail.

## **1.6 Transient Potassium Currents**

As previously discussed, DCN pyramidal cells contain many intrinsic conductances that shape the neuronal responses to synaptic input. The studies presented in this dissertation primarily focus on the contribution of a transient potassium current to the response patterns observed in DCN pyramidal cells. Like all channels that determine whether or not the cell will fire an action potential and when a cell will fire an action potential, transient potassium currents begin to activate at subthreshold voltages. Therefore, they contribute to dendritic integration of incoming information and the resulting response of the neuron.

### **1.6.1 Molecular characteristics of Transient Potassium Channels**

Potassium channels are undoubtedly the most diverse type of ion-channels. They confer specific properties to cells based on their individual characteristics and expression

patterns. Voltage gated  $K^+$  channels are all characterized by  $\alpha$ -subunits that contain intracellular N- and C-termini, T1 assembly domains, highly homologous selectivity filters and a voltage gate that is found in transmembrane domain S4 (Birnbaum et al. 2004). Each  $\alpha$ -subunit interacts with the T1 domain of 3 other homologous  $\alpha$ -subunits to form a tetramer (Shen and Pfaffinger 1995). The selectivity filter, comprised of the carbonyl oxygens of the amino acid sequence TTXGYGD, is universally conserved among all voltage gated  $K^+$  channels and mutations to this region result in loss of  $K^+$  selectivity (Doyle et al. 1998). Four subfamilies of voltage gated  $K^+$  have been described and the *Drosophila* genes are named Shaker, Shab, Shaw and Shal, which correspond to mammalian homologues Kv1, Kv2, Kv3 and Kv4 respectively.

While Shaker and Shaw channels can give rise to transient currents, the entire Shal subfamily of channels (Kv4.x) are characterized by rapidly activating and inactivating outward currents. Cloning of the three subfamily members, Kv4.1, Kv4.2, and Kv4.3, revealed that these family members are highly homologous in all regions of the protein with the most divergent region being the C-terminus (Baldwin et al. 1991; Tsaur et al. 1997). Kv4.3 is the only member of the family that undergoes alternative splicing in areas other than the brain (Ohya et al. 1997). Kv4.x channels have very a characteristic pharmacology. These channels are resistant to TEA and dendrotoxin, are blocked by 4-AP at mM concentrations, and are blocked by family of peptide toxins called the heteropodatoxins (Birnbaum et al. 2004; Sanguinetti et al. 1997; Zarayskiy et al. 2005). Finally, Kv4.x channels are characterized by rapid, sub-threshold activation, fast inactivation (10's of milliseconds) and quick recovery (50-100 msec) from inactivation and hyperpolarized voltages.

Activation occurs with extremely fast time constants in Kv4 channels. Most reported values are below 5 msec (Jerng et al. 2004). In addition to the nearly instantaneous activation, Kv4 channels begin to activate at membrane potentials between -50 and -40 mV. The half-activation voltage seems to vary with the expression system or neuronal cell type, but most studies report values between 5 and -25mV (Bardoni and Belluzzi 1993; Chen and Johnston 2004; Klee et al. 1995; Wang and Schreurs 2006). In DCN pyramidal cells, this current begins to activate at -45 mV, with a half-activation value of -6.8 mV (Kanold and Manis 1999). This value is in line with other values reported for this family of channels.

Perhaps the most characteristic feature of the Kv4.x channels is the rapid inactivation. This inactivation is often made up of a fast and slow component. Half-inactivation values have been reported to be between -56 and -70 mV with time constants ranging from 8 msec for the fast component of inactivation, all the way to over 100 msec for the slow component (Bardoni and Belluzzi 1993; Chen and Johnston 2004; Jerng et al. 2004; Klee et al. 1995; Wang and Schreurs 2006). A-currents in DCN pyramidal cells are within these ranges with half-inactivation values of -89mV for the fast component and -37 mV for the slow with time constants of 11 msec and 145 msec for the fast and slow components respectively (Kanold and Manis 1999). Unlike other potassium channels which undergo N-type or C-type inactivation, usually from the open state, Kv4.x channels can inactivate directly from the closed or pre-open state (Bähring et al. 2001). This type of inactivation is not completely dependent on N-terminal residues like the typical ball and chain inactivation of other potassium channels. The exact molecular mechanism of inactivation in Kv4.x channels has yet to be elucidated.

Finally, Kv4.x channels are characterized by their voltage-dependent fast recovery from inactivation. In most neurons where  $I_A$  has been characterized, recovery time constants range from 10 to 30 msec at hyperpolarized voltages (Jerng et al. 2004). However, this recovery is highly voltage sensitive. For instance, in cerebellar granule cells,  $\tau$  of recovery from inactivation was reported to be 71 msec at -60 mV but 10 msec at -120 mV (Bardoni and Belluzzi 1993). Therefore, very brief hyperpolarizations can remove a significant amount of inactivation of this current. This feature is important for Kv4.x channels to contribute to dendritic integration.

### **1.7 Kv4 channel expression patterns**

Kv4 channels, mainly Kv4.2 and Kv4.3, are highly expressed in many different areas of the brain and very densely expressed in areas that function in learning and memory such as the hippocampus and the cerebellum (Serodio and Rudy 1998). This study also showed that Kv4.2 and Kv4.3 are expressed in the DCN. Fitzakerley and colleagues later verified this result and reported that Kv4.2 is expressed in cochlear nucleus at higher levels than Kv4.3 and Kv4.1 (Fitzakerley et al. 2000). Kv4.1 is completely absent from the DCN. In addition, they reported that Kv4.2 is found in pyramidal cells of the DCN.

Because of Kv4 channels' putative roles as a regulators of subthreshold events, the subcellular expression patterns of Kv4 channels has been studied in many different neurons. Soon after the cloning of Kv4.2, it was reported that this channels was targeted to the somatodendritic compartment of neurons while another inactivating potassium channel, Kv1.4, was exclusively expressed in axons (Sheng et al. 1992). This observation led the investigators to hypothesize that Kv4 channels are important for dendritic integration of synaptic information. Other studies soon verified that Kv4.2 was indeed targeted to the

dendrites and dendritic spines with the most dense expression levels found at synapses (Alonso and Widmer 1997). The density of Kv4.2 dendritic expression actually increases in proportion to the distance from the soma (Hoffman et al. 1997).

The exact subcellular location of Kv4.2 and Kv4.3 channels is still being evaluated. Two studies have reported that Kv4 channels are expressed in the post-synaptic membrane of GABAergic synapses and found extrasynaptically around excitatory synapses (Burkhalter et al. 2006; Jinno et al. 2005). In contrast, another study done in inhibitory interneurons of the cerebellum found that Kv4.2 and Kv4.3 channels were expressed at uneven distributions in membrane specializations that did not correspond to chemical or electrical synapses (Kollo et al. 2006). These novel membrane specializations were opposed to climbing fibers of the cerebellum. It is unknown what function these clusters of Kv4 channels have in neurons. However, Kv4 channels expressed in dendrites could contribute to many aspects of neuronal information processing and integration.

Kv4 channels contain specific targeting signals that result in their expression close to synapses, which allow for them to shape neuronal responses to synaptic input. Recently, a 16 amino acid dileucine containing motif was demonstrated to be both necessary and sufficient for protein targeting to the soma and dendrites (Rivera et al. 2003). This motif is found in C-termini of Kv4 channels and is highly conserved among all species demonstrating its importance in the proper functioning of these channels. Other amino acid motifs also are important to target Kv4 channels to the membrane. Amino acids 601-604 in the Kv4.2 the C-terminal end are essential for the channel to interact with filamin, an actin crosslinking protein (Wang et al. 1975). This interaction increases the current density of Kv4.2 by trafficking more channels to the cell membrane (Petrecca et al. 2000). In addition to filamin,

Kv4.2 also interacts with PSD-95 through a VSAL motif in the C-terminal region and this interaction also promotes channel surface expression and clustering (Wong et al. 2002). Finally, activity dependent targeting of Kv4.2 channels to the dendritic compartment was reported in cerebellar granule cells (Shibasaki et al. 2004). Kv4.2 remained in the soma of granule cells in culture until the activation of NMDA and AMPA receptors by mossy fibers induced Kv4.2 expression in the dendrites. Kv4 channel targeting to areas proximal to synapses could result in these channels exerting major effects on synaptic input and dendritic integration.

### **1.7.1 Kv4 Channel Modulation**

When Kv4 channels are expressed in heterologous systems, the resulting channel biophysical characteristics do not match those measured in neurons. This observation has led many to ask whether Kv4 channels are the targets of post-translational modifications and interact with other proteins that affect the biophysical properties of the channel. In fact, when Kv4 channel mRNA was injected into oocytes, transient currents could be elicited, but these currents differed from native currents (Serodio et al. 1994). However, when rat brain mRNA that did not result in transient potassium currents when injected alone was co-injected with Kv4 mRNA, the currents more closely resembled native currents. This suggested that additional proteins may interact with the channel in ways that are important for native channel function. Since this time many proteins that interact with and modify Kv4 channels have been discovered.

Kv $\beta$ -subunits are cytoplasmic proteins that can interact with  $\alpha$ -subunits that make up potassium channels. There are 3  $\beta$ -subunits known to modify potassium channel expression and gating characteristics. Upon interaction other potassium channels such as Kv1 and Kv2

subfamilies, the  $\beta$ -subunit causes channels to inactivate more rapidly, even in channels that do not normally inactivate by themselves (Birnbaum et al. 2004). However, when Kv4.3 and Kv $\beta$ -subunits are expressed together in HEK298 cells, more Kv4.3 channels are trafficked to the membrane, but the channels' voltage sensitivity and kinetics are unaffected by the  $\beta$ -subunit (Yang et al. 2001).

Another family of cytoplasmic proteins, the Ca<sup>2+</sup> sensitive K channel interacting proteins (KChIPs), on the other hand, interact with Kv4  $\alpha$ -subunits and alter the kinetics and voltage sensitivity of Kv4 channels. When the N-terminus of Kv4.3 was used as bait in a yeast-two hybrid experiment, 3 proteins, KChIP 1-3, were found to interact with Kv4 channels in cells, increase surface expression of the channel, and change their biophysical properties (An et al. 2000; Shibata et al. 2003). For instance, KChIPs shifted the half-activation voltage from 28.2 mV to -12.1 mV, a value that matches measurements of native channels. However, this interaction did slow the inactivation time constant from 28.2 msec to 104.1 msec and in some cases eliminated it all together (Holmqvist et al. 2002). This value is much slower than reported in most neurons. Despite this, microscopy studies have demonstrated that KChIPs colocalize with Kv4 channels in almost all areas of the brain where Kv4 channels are expressed and are now accepted as being a necessary component of Kv4 channels in neurons and ventricular myocytes (Rhodes et al. 2004; Strassle et al. 2005). The crystal structure of the interaction between these two types of proteins was solved and shows that these proteins interact through the presence of hydrophobic  $\alpha$ -helices on the N-terminal region of the Kv4 channel and the C-terminal region of the KChIP (Scannevin et al. 2004; Zhou et al. 2004). This interaction is calcium dependent and acts to stabilize the tetramer of  $\alpha$ -subunits (Wang et al. 2007). In addition, arachidonic acid has been reported to

inhibit A-currents (Ramakers and Storm 2002) and this effect on Kv4 channels is dependent upon KChIPs (Holmqvist et al. 2001). Therefore, the KChIP interaction with Kv4 channels is essential for the expression of native A-type potassium currents.

Even after the discovery of KChIPs, a remaining puzzle of Kv4 A-type currents remained—fast inactivation. KChIPs co-expressed with Kv4 channels resulted in the opposite effect seen in native cells; these proteins slowed inactivation. However, Nadal and colleagues reported a factor found in cerebellar mRNA could accelerate the inactivation time constant when expressed with Kv4 mRNA (Nadal et al. 2001). This factor was later identified as DPPX (Nadal et al. 2003). DPPX is a transmembrane protein that interacts with the channel transmembrane domains. DPPX results in robust surface expression of Kv4 channels and changes the biophysical properties of the channels. Half-inactivation and half-activation voltages were shifted to more negative values, and the recovery time from inactivation was decreased. These properties are quintessential characteristics of Kv4 channels and are dependent upon the interaction with DPPX.

Finally, multiple putative PKA, PKC, ERK and CAMKII phosphorylation sites have been found on intracellular portions of Kv4 channels (Adams et al. 2000; Anderson et al. 2000). Stimulation of PKA and PKC activation of MAPK results in the half-activation voltage shifting to the right, thereby inhibiting Kv4 channel activity in pyramidal neurons of the hippocampus (Hoffman and Johnston 1998; Yuan et al. 2002; Yuan et al. 2006). However, direct evidence that phosphorylation of Kv4 channels affects the voltage sensitivity has yet to be demonstrated. Two studies have reported that while Kv4 channels are directly phosphorylated by MAPK, any biophysical effect by this modification of Kv4 channels was dependent on KChIPs interacting with the channel (Schrader et al. 2002; Schrader et al.

2006). CAMKII also can directly phosphorylate Kv4 channels, but this modification only results in increased current density due to increased expression on the cell membrane. It does not result in any biophysical changes in channel kinetics or activation (Varga et al. 2004). With such diverse mechanisms to control Kv4 channel expression and physiology, it is not difficult to imagine how this channel can be modulated to change the physiology of the entire neuron.

### **1.7.2 Kv4 channels and neuronal function**

The unique characteristics of Kv4 channels, namely rapid inactivation and sub-threshold activation, confer specialized functions to neurons that express these channels. First, since these channels are expressed in dendrites and begin to activate before an action potential is fired, they could play a very important role in dendritic integration and information processing. For instance, small, brief hyperpolarizations, such as IPSPs, remove inactivation from these channels thereby allowing more of these channels to become activated during depolarizing events such as EPSPs. Because of this feature, these channels can act as a memory of inhibitory input. In fact, in DCN pyramidal cells, the subsequent output patterns of these neurons are affected by brief hyperpolarizations (Kanold and Manis 2005a). Further, the precise spatiotemporal relationship of membrane hyperpolarization and depolarization can change the timing of action potentials. This ability to encode the timing of inhibition has major implications in neurons, like DCN pyramidal cells, that receive relevant inhibitory information in conjunction with excitation.

Kv4 channels not only shape neuronal responses to inhibitory input, but they also can modify the membrane responses to excitatory input as well. Since these channels open at sub-threshold voltages, they provide a current shunt that decreases the amplitude of EPSPs

and confine the depolarization to localized areas of the dendritic tree (Cai et al. 2004; Hoffman et al. 1997). This limits the level of depolarization and prevents action potential threshold from being reached unless large synchronous inputs drive the cell to threshold.

A-currents of Kv4 channels also modify the spike patterns of neurons. Subthreshold activation of Kv4 channels opposes inward currents that depolarize the cell membrane bringing it closer to spike threshold. The result of these opposing currents is a long, slow ramp that increases the time it takes the neuron to reach threshold, the latency to a spike, and the inter-spike interval (Kanold and Manis 2001; 1999; Molineux et al. 2005; Song et al. 1998). To illustrate this point, dopaminergic neurons in the substantia nigra exhibit a linear relationship between the expression of Kv4.3 and action potential frequency (Liss et al. 2001). The amount of Kv4.3 current measured in a cell was inversely proportional to the spontaneous firing rate of the cell demonstrating a specific mechanism for controlling neuronal output. Kv4 channels also modulate the width and repolarization of action potentials. When Kv4 channels are blocked, action potentials are wider and do not repolarize as quickly (Kim et al. 2005; Mitterdorfer and Bean 2002). These effects of Kv4 channels are essential to the specific neuronal function and information processing since they directly affect the output patterns of spikes in response to the spatio-temporal patterns of synaptic input.

Finally, the somatodendritic expression pattern of Kv4 channels, especially at the synapse and in spines of neurons, implicates these channels in synaptic plasticity. Kv4 channels control the height and strength of back-propagating action potentials (b-AP) by opposing inward current. When these channels are in the deinactivated state, they can open with the depolarization associated with the b-AP and weaken this depolarization it as it

propagates through the dendritic tree (Hoffman et al. 1997; Migliore et al. 1999). Normally, b-APs activate  $\text{Ca}^{2+}$  channels that allow the influx of  $\text{Ca}^{2+}$  into dendrites, which initiates a cascade of signaling events that results in strengthening the synapse (Frick et al. 2004). Kv4 channels in dendrites oppose depolarization induced  $\text{Ca}^{2+}$  influx and inhibits the potentiation of synapses (Johnston et al. 2003).

However, EPSPs in localized areas of the dendritic tree can cause Kv4 channels to inactivate since the EPSPs depolarize the membrane. If a b-AP then spreads to this area of the dendrites after the brief depolarization of the EPSP, the Kv4 channels can not activate and  $\text{Ca}^{2+}$  enters the cell and can induce potentiation of the synapses in this specific area of the dendritic tree (Migliore et al. 1999). This mechanism could account for why the temporal relationship of EPSP to action potentials must be within a certain time frame in order for spike-timing dependent plasticity to take place. In fact, when the activation voltage of Kv4 channels is shifted to more hyperpolarized voltages by blocking channel phosphorylation with MAPK inhibitors, induction of long-term potentiation (LTP) is blocked (Watanabe et al. 2002). Therefore, not only can Kv4 channels modulate synaptic strengthening, but modulation of the channels themselves could be important in setting the threshold for such synaptic plasticity. Activation of PKA and PKC by adrenergic and cholinergic agonists results in an increase of b-AP strength (Hoffman and Johnston 1999). Thus, modulation of neurons by other neurotransmitters could change the availability of Kv4 channels and change the conditions that lead to synaptic strengthening. The possibility that a Kv4 channel confers these properties to DCN pyramidal cells is enticing. In this study we hope to provide further evidence that Kv4 channels are essential components of pyramidal cell function.

## 1.8 Summary

DCN pyramidal cells possess many characteristics that could enable them to use precise trains of action potentials to encode the different types of sensory information that converge on them. Since it is already known that these cells can encode some aspects of timing information such as sound envelope modulation, it is our purpose to characterize the spike timing properties and regulatory mechanisms in DCN pyramidal cells. In the second chapter, we report our findings of spike timing characteristics when pyramidal cells are presented with a white noise current stimulus. Using this same stimulus, we also characterized which aspects of the noise current elicit reliable and precise trains of action potentials. HCN and mGluR receptors were also perturbed in order to determine what role, if any, these membrane proteins play in determining spike timing behavior.

Chapter three deals with the role of the transient potassium current in determining spike timing and response patterns. Previous work in our lab has implicated a Kv4 channel in spike timing behavior of pyramidal cells. In this study we use heteropodatoxin-2 and dynamic clamp to elucidate how Kv4 might affect pyramidal cell discharge patterns.

The A-current, not only can alter spike timing characteristics, but it also can confer other important characteristics to neurons. For this purpose, we also investigate the specific identity of the potassium channel that gives rise to the A-current in these cells. The results of this study are presented in chapter four. By understanding the role that the A-current plays in the spike-timing ability of pyramidal cells, we hope to broaden the understanding of how information is encoded and processed by the DCN.

## **Chapter 2: Action potential timing precision in dorsal cochlear nucleus pyramidal cells**

### **2.1 Introduction**

Spike timing and average spike rate are both considered elements of the neural code that represents information about the sensory environment. While neurons can communicate using average rate (Shadlen and Newsome 1998) precise and reproducible spike timing is also frequently observed, raising the likelihood that this firing regime is used to encode information (Abeles et al. 1993; Bair and Koch 1996; Beierholm et al. 2001; Berry et al. 1997; Buonomano 2003; Buracas et al. 1998; de Ruyter van Steveninck et al. 1997; Mainen and Sejnowski 1995; Nowak et al. 1997; Reich et al. 1997). The precision and reliability of action potential timing depends upon the membrane time constant, fluctuations in both excitatory and inhibitory input, the activation of, and noise from, voltage-gated ion channels, and coincident excitation from pre-synaptic neurons (Azouz and Gray 2000; Diesmann et al. 1999; Dorval and White 2005; Fricker and Miles 2000; Gauck and Jaeger 2003; 2000; Grande et al. 2004; Grothe and Sanes 1994; Hausser and Clark 1997; Jaeger and Bower 1999; Schreiber et al. 2004; Sourdet et al. 2003; Svirskis et al. 2003; Svirskis et al. 2002; 2004). Certain neurons in the auditory system have long been known to represent precisely timed information about the acoustic environment by phase-locking in their spike trains (Rose et al. 1967), and this depends on specific combinations of ion channels and synaptic

receptors. However, many other auditory nuclei, such as the dorsal cochlear nucleus (DCN), show little high-frequency phase-locking and so have been most extensively characterized in terms of mean firing rate.

Pyramidal cells in the DCN receive auditory information via the auditory nerve, and non-auditory information that is relayed through a system of granule cells that give rise to parallel fibers, similar to the circuitry found in the cerebellum. Pyramidal cells integrate synaptic input from these excitatory inputs, as well as from at least three types of inhibitory interneurons, and pass this processed information on to the inferior colliculus (for review, see (Oertel and Young 2004)). While the DCN has not previously been thought to utilize precise spike timing because it exhibits poor phase locking to high-frequency, pure tones (Goldberg and Brownell 1973; Rhode and Smith 1986), recent evidence suggests that timing might play an important role in information processing. For example, parallel fiber synapses onto pyramidal cells exhibit spike timing dependent plasticity (Tzounopoulos et al. 2004). The EPSP-spike coincidence window for plasticity in the DCN is on the order of 10 msec, which is notably smaller than the window reported for other regions of the brain. Furthermore, pyramidal cells exhibit sensitivity to temporal information by encoding the envelope of amplitude modulated sounds up to a few hundred Hz (Frisina et al. 1994; Joris and Smith 1998; Kim et al. 1990; Neuert et al. 2005; Zhao and Liang 1995). Together, these observations support the hypothesis that spike timing may be an important code in this nucleus.

Since spike timing may be important in DCN information coding, we sought to characterize the ability of pyramidal cells of the DCN to respond to time-varying stimuli with reproducible spike trains *in vitro*, and to identify features of the stimulus that affect spike

timing. Using Gaussian distributed noise current pulses, to simulate fluctuations in synaptic drive, we were able to determine if time-varying input improves the reproducibility of spike times. The results indicate that pyramidal cells can fire with good precision in response to dynamic stimuli and that firing precision can be affected for several hundred milliseconds by brief hyperpolarizations.

## **2.2 Materials and Methods**

***Slice Preparation.*** Sprague-Dawley rats, post-natal day 10-14, and 21-24 were deeply anesthetized with ketamine (100 mg/kg),-xylazine (10 mg/kg) , decapitated, and the brainstem removed. The brainstem was trimmed to a block of tissue that included the dorsal cochlear nucleus. The block was mounted on agar supports, sliced in the trans-strial plane (250 $\mu$ m) (Blackstad et al. 1984), and stored in an incubation chamber for 1-2 hours at 34°C. All procedures were performed under protocols approved by the Institutional Animal Care and Use Committee of the University of North Carolina. Slices were transferred to the recording chamber, held in place by a net, and perfused with recording solution at 34°C at 3-5mL/min.

***Solutions.*** The dissection and slicing procedure was carried out in a low Ca<sup>2+</sup>/high Mg<sup>2+</sup> solution, which contained the following (in mM), 122 NaCl, 3 KCl, 1.25 KH<sub>2</sub>PO<sub>4</sub>, 25 NaHCO<sub>3</sub>, 20 glucose, 2 myo-inositol, 2 sodium pyruvate, 0.4 ascorbic acid, 0.1 CaCl<sub>2</sub>, and 3.7 MgSO<sub>4</sub>. The slices were incubated and perfused with the same solution, except containing (in mM) 2.5 CaCl<sub>2</sub> and 1.2 MgSO<sub>4</sub>. Solutions were continuously equilibrated with 95%/5% O<sub>2</sub>/CO<sub>2</sub> at 34° to maintain pH at 7.3-7.4, and the osmolarity ranged from 310-320 mOsm. Strychnine (2 $\mu$ M) was added to the bath to block glycinergic inhibition in all experiments. In some experiments, ZD7288 (20 $\mu$ M) was used to block hyperpolarizing-

activated channels (BoSmith et al. 1993). The electrode solution contained the following (in mM), 4 NaCl, 130 potassium gluconate, 0.2 EGTA, 10 HEPES, 2 Mg<sub>2</sub>ATP, 2Mg<sub>2</sub>GTP, and 2 creatine phosphate. AlexaFluor 488 (Na<sup>+</sup> Salt, Molecular Probes, Eugene, OR) was added to the electrode solution (0.1 mM) allowing cells to be visualized and characterized morphologically. All chemicals were obtained from Sigma-Aldrich (St. Louis, MO) with the exception of ZD7288, which was obtained from Tocris Bioscience (Ellisville, MO).

**Recording.** Electrodes were pulled from 1.5 mm diameter KG-33 glass (Garner Glass, Claremont, CA) to a tip diameter of 1-2  $\mu$ m and a final tip resistance of 2-7 M $\Omega$  on a P-2000 Sutter puller. The tips were coated with Sylgard 184 (Dow Corning, Midland, MI) to decrease pipette capacitance. The slices were transferred to the recording chamber on a fixed stage microscope and visualized with a 40X, 0.75 NA or 63X 0.9 NA water immersion objectives using video-enhanced differential interference contrast illumination in infrared light. Pyramidal cells were selected based on shape and visualization of apical and basal dendrites at opposite ends of the cell body. The membrane potential was recorded using standard techniques for whole-cell, tight seal recording in slices with a Multiclamp 700A amplifier (Molecular Devices, Foster City, CA). Data acquisition was carried out under computer control with custom software program written in Matlab (The Mathworks, Natick, MA) using high-speed 12 or 16 bit A-D boards (National Instruments, Austin, TX) with a sampling rate of 50 kHz. All voltages were corrected for a -12 mV electrode-bath junction potential during analysis.

**Stimuli.** Different types of stimuli were applied to the pyramidal cells. The first was a rectangular DC current pulse, shaped using  $\cos^2$  ramps to minimize onset and offset transients. The other was a low-pass (250-1500 Hz) filtered (8-pole Butterworth digital

filter) noise current (peak to peak amplitude of 500 pA unless otherwise noted). The exact amplitude and pattern of synaptic input that pyramidal cells receive is currently unknown. While some in vivo measurements of membrane fluctuations have been made with sharp electrodes, these measurements probably do not accurately reflect the frequency content of the membrane potential nor the relevant amplitudes of the fluctuating and steady-state components due to the low-pass filtering effect of sharp electrodes (Hancock and Voigt 2002; Rhode et al. 1983a). Therefore we chose a Gaussian noise waveform, which theoretically includes all possible combinations of current trajectories that might ever be experienced. However, since there is a limited range of parameters in terms of amplitude and frequency content that will be experienced under normal conditions, our stimulus waveform was selected so as to present an experimentally tractable part of this large parameter space.

Factors that were considered in determining the stimulus included the low-pass filtering effect of the dendrites on the excitatory input that reaches the cell body, and the high frequency barrages of both excitatory input from the auditory nerve (>300 Hz) and inhibitory input of the vertical cells (>300 Hz). We would therefore expect to see frequency content in the membrane potential that included components at least up to 300 Hz. Taken together, these considerations suggest that an appropriate stimulus to test the cell's temporal coding abilities should include both high and low information. The noise was superimposed on the DC pedestal. The average firing rate of the cell was controlled by adjusting the DC pedestal. Experiments examining spike timing used frozen noise in which the same noise token was used for 100 consecutive trials. To determine the spike triggered average of the cells, random noise was generated by changing the noise token in each trial for 50 consecutive trials. A simulated IPSP (sIPSP) or simulated EPSP (sEPSP) consisting of a short train of

three alpha waves [ $I(t) = I_{\max} * a * t * \exp(-a * t)$ ;  $a=0.1 \text{ msec}^{-1}$ ], separated by a 15 msec interevent interval, was added to the stimulus with a delay of 500 msec, allowing us to compare the regularity of firing before and after the sIPSP or sEPSP.

**Analysis.** The digitized current and voltage traces were stored in a Matlab file and were then analyzed using custom Matlab routines. To calculate the reliability and precision of spike timing, we first used a method similar to that of Mainen and Sejnowski (1995). Peristimulus-time histograms were constructed by convolving spike times with a Gaussian function 2 msec wide. *Events* in the response were defined as peaks in the PSTH where the rate was greater than 9 times the mean rate throughout the stimulus. *Reliability* was defined as the fraction of trials that the neuron fired an action potential within an event. The *precision* was defined as the standard deviation of the spike times within events. While this method has been used in previous reports involving spike timing, it requires that the investigator choose the parameters that are needed to build the histogram and calculate the standard deviation of each event. Often, these assumptions led to spikes that were not binned according to the correct event, which in turn led to misleading results.

A second approach with fewer assumption about spike timing precision was to calculate the coefficient of variation for the population (CV-P) of inter-spike intervals (ISI) by the following formula:

$$\{(\mu_{\text{ISI}}/\sigma_{\text{ISI}})-1\}/\sqrt{N}$$

where  $\sigma_{\text{ISI}}$  is the standard deviation of the ISI for all spikes in all 100 trials,  $\mu_{\text{ISI}}$  is the mean of all the ISI for all spikes in all 100 trials, and N is the number of trials (Tiesinga and Sejnowski 2004). This formula gives a number that varies between 0 and 1 where 0 denotes a Poisson process where there are no reproducible spike patterns, and 1 where the spike times

are perfectly reliable and precise. This method is simple and does not require that the investigator decide any parameters needed in the calculation. However, it does not visually show differences in the spike trains.

A third method used to determine the reproducibility of spike trains, we used the shuffled autocorrelogram (SAC) method first described by Joris (Joris 2003; Joris et al. 2006; Louage et al. 2004). For each cell, all non-identical spike trains were paired with each other and the forward time intervals between all spikes of each spike train were used to calculate a cross correlation of the delay between spike times. This histogram is referred to as the SAC. The SAC was normalized by dividing the number of coincidences in each bin (0.1 msec wide) by  $N(N-1)r^2\Delta\tau D$ , where  $N$  is the number of presentations (100),  $r$  is the average firing rate,  $\Delta\tau$  is the choice of bin width and  $D$  is the duration of the stimulus (note that the result is dimensionless). We then fit the normalized value to a Gaussian function to measure the width of the central correlation peak. The height of the Gaussian at 0 delay, the correlation index, (CI; see (Joris et al. 2006)) can then be used to compare the spike timing in response to different stimuli. Since this method is sensitive to changes in mean spike rate during the collection of repeated trials, we used a selection criterion to identify stable recording epochs for comparison. The slope of the firing rate as a function of time was calculated. Any cell that had a mean rate that changed by more than 2 spikes per 1-second trial was discarded. This selection criterion was specifically used for experiments that compared the CI for stimuli that included the sIPSP and the sEPSP. The SAC method does not require *a priori* knowledge of the correlation structure, and thus provides an objective measure of spike timing across trials.

We also calculated the reverse correlation, or spike triggered average (STA) of the current waveform that elicited an action potential. In these experiments we presented the cell with 50 independent noise tokens and then computed the STA for spikes whose preceding ISI was greater than 25 msec. Confidence intervals were calculated according to Bryant and Segundo (1976).

Data analysis was performed with Matlab 7.1 and Igor Pro (5.04). Statistics were calculated using both Matlab 7.1 and Prism 3.0 (GraphPad Software, San Diego, CA). All numerical data are presented as means  $\pm$  standard deviation (SD). Statistical tests of hypotheses used one or two-sided, paired or unpaired (as appropriate) t-tests.

## **2.3 Results**

### **2.3.1 Responses of Pyramidal Cells to a White Noise Current Injection**

We first sought to determine whether pyramidal cells of the DCN are capable of firing reliable and precise trains of action potentials. A total of 45 pyramidal cells with a mean resting membrane potential of  $-63.1 \pm 4.9$  mV and a mean input resistance of  $68.2 \pm 38.4$  M $\Omega$  were identified and recorded for the initial experiments. All cells showed the typical response patterns to depolarizing current pulses including regular, non-adapting trains of spikes, pauser and build-up patterns (Manis 1990). Seventeen cells were confirmed to be pyramidal cells morphologically. We do not include any cells that show bursting action potentials (likely cartwheel cells) in these results.

We tested whether cells were sensitive to the temporal structure of the membrane potential by comparing responses to a flat depolarizing current pulse with responses to stimuli with a superimposed noise. The DC current was chosen so that the cell fired at  $20 \pm 5$  Hz. In response to the DC current (Figure 2.1A), the cells typically respond with a train of

action potentials with regular interspike intervals (ISI). The precise timing of spikes varied between trials. One can easily observe this behavior by examining a raster plot of spike times (Figure 2.1B). The precision of the spike times in response to a flat current injected is high at the beginning of the spike train, but decreases as the stimulus continues.

In contrast, when a Gaussian low-pass filtered (500Hz) noise is superimposed on the DC pedestal (Figure 2.1D), the cell tends to fire spikes at specific times during the stimulus, forming discernable spike time “events” that are visible in the raster plot (Figure 2.1E). The precision of the spike times from the noise current was high throughout the duration of the stimulus. This is also visible in the raster plot and the PSTH (Figure 2.1 E, F).

Figure 2.1

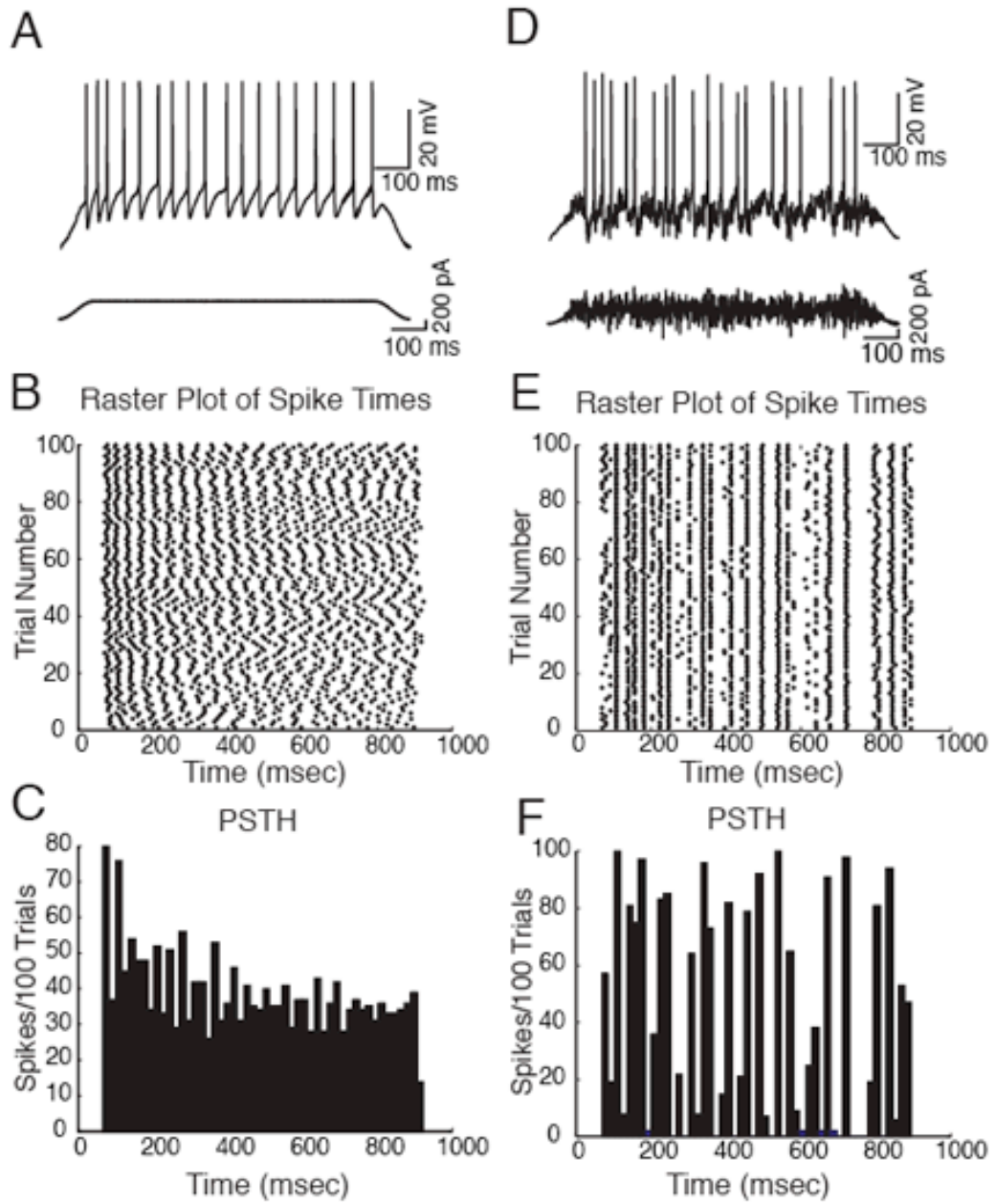


**Figure 2.1.** Spike trains produced by noisy currents show repeatable structure, whereas spike trains produced by flat current steps are not repeatable.

**A.** Raw traces of spike trains resulting from a flat current pulse, showing regular firing. The peak-to-peak current amplitude is 500 pA.

**B.** Raster plots of spike times over 100 trials for the cell shown in A. Although the cell is regular, the spike times are not reproducible with respect to the onset of the stimulus.

**C.** PSTH showing rate adaptation and weak “chopping” due to discharge regularity.

**D.** Response of cell in A to the same current pulse with superimposed noise. The noise for each trial was identical. The firing is less regular.

**E.** Rasterplot, as in B, for noise response. Note that there are discrete events in the firing pattern that are reproducible across trials.

**F.** PSTH for data in E. Clustered spike times produce a PSTH with large moment-to-moment changes in rate. PSTH bin width in C and E is 10 msec

We first used the same analysis method as Mainen and Sejnowski (1995), to calculate the reliability and precision of spike times (see Methods). Reliability is defined as the fraction of times the cell fired a spike during an event and the precision is defined as jitter (standard deviation) of the spike times in each event. Calculation of the reliability and precision from the post-stimulus time histogram (PSTH) is shown in Figure 2.2, panels A and B. Comparing the instantaneous rate to a threshold identifies events in the PSTH. The precision (standard deviation of spikes within an event) and reliability (probability of a spike occurring within an event) is then computed, as shown in the lower plots of Figure 2.2A and B. There is considerable variability in these measures through the duration of the stimulus. However, on average, reliability is greater and precision is better (smaller) when the cell responds to the noise current than to the flat pulse ( $P < 0.0001$ ) (Figure 2.2 C, D). This method of calculation can miss spikes that are part of the event since it is necessary to select both the width of the function and the threshold. The method also assumes that the spike times are clustered into discernable, repeatable events across multiple trials. To overcome these limitations, we applied two other methods. First, we calculated CV-P (see Methods) of the ISI. For responses to flat current pulses, CV-P is very close to 0. In contrast, when the noisy current is presented, and the CV-P is higher ( $P < 0.001$ ) (Figure 2.3). While the CV-P measure yields a larger difference between the two conditions, it fails to reflect the precision of firing.

Figure 2.2

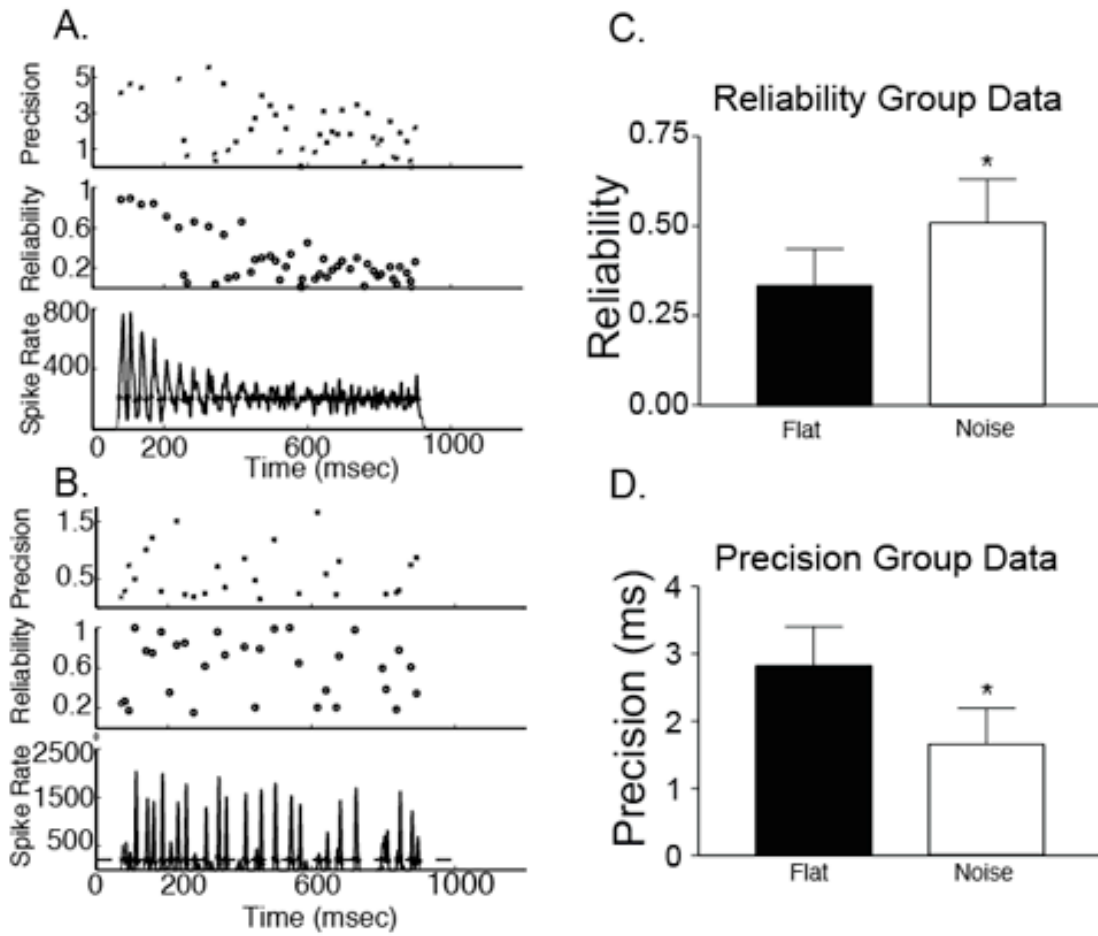


**Figure 2.2** Measurement of spike timing reliability and precision using the Mainen Sejnowski (1995) method.

**A,B**-Calculation of reliability and precision in the same cell as figure 1 for flat (A) and noisy (B) current. The bottom panels show the PSTH (at 0.1 msec bin width) convolved with a Gaussian function with  $\sigma=2$  msec; spike rate given in spikes/second. The middle panels show the reliability value for each event. Reliability decreases over time in response to the flat current pulse, but can continue to be good for the noisy current. The top panels show calculation of spike timing precision (standard deviation of spike times) for each event. Note that the firing is less precise (larger precision index) for the flat current pulse (*Ab* as compared to *Bb*).

**C,D** Pooled data from 45 cells for reliability (C) and precision calculations (D). Reliability and precision are significantly different between flat and noisy current pulses ( $P<0.001$ , paired t-test,  $N = 45$ , reliability mean difference = -0.18; precision mean difference 1.16).

Figure 2.3

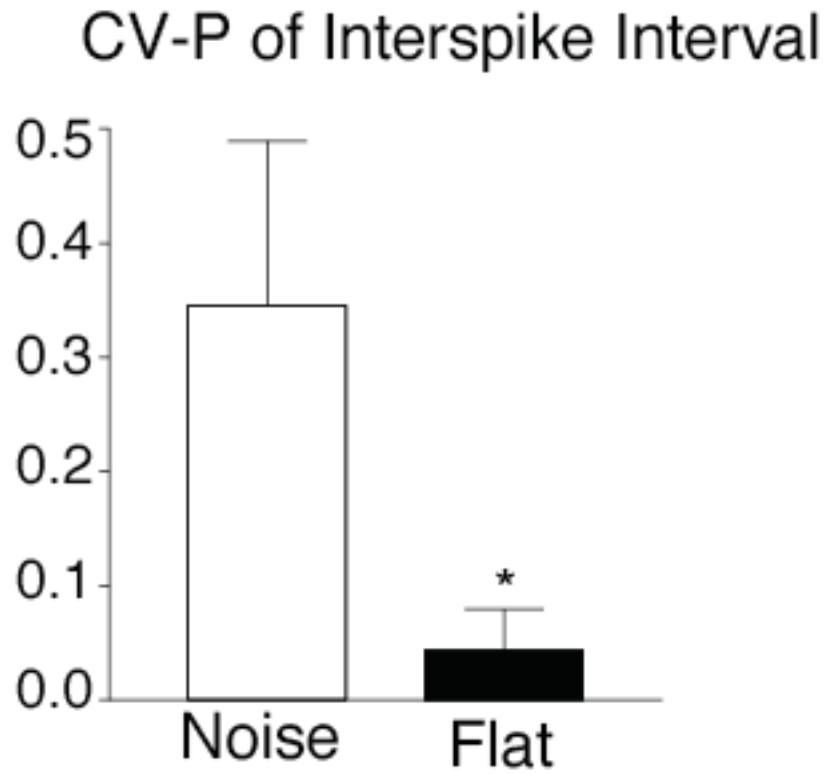


**Figure 2.3** Comparison of CV-P for noise and flat current pulses. CV-P is significantly lower for flat versus noisy currents. ( $P < 0.001$ , paired t-test,  $N = 45$ , mean difference = 0.30).

We therefore applied a third method, the SAC. The SAC makes no assumptions about event times or widths. Instead the SAC shows the delay in spike times between pairs of different trials from the same cell. The SAC uses the difference in spike times between pairs of different trials from the same cell to reveal repeatable temporal structure in the spike train. In response to the flat current pulse, the spike delays are spread out broadly, and have a mean value of 1 (Figure 2.4A). This flat SAC indicates that there is no repeated spike timing structure across trials. However, in response to the noisy current, the delays between spike times in different trials are frequently small, and the SAC shows a large peak around zero delay. The peak can be reasonably fit with a Gaussian function (shown by the line in Figure 2.4A). Across the population of cells, noisy current pulses elicit higher central peaks than flat currents (Figure 2.4B). While our recordings were done in P10-P14 animals, the same result was seen in 5 cells from P20-P24 animals where the peripheral auditory system is fully developed ( $P < 0.01$ , mean difference of CI between each pair = 12.07).

Figure 2.4

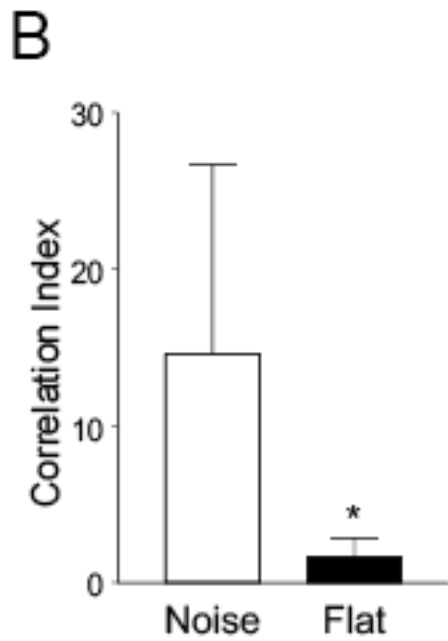
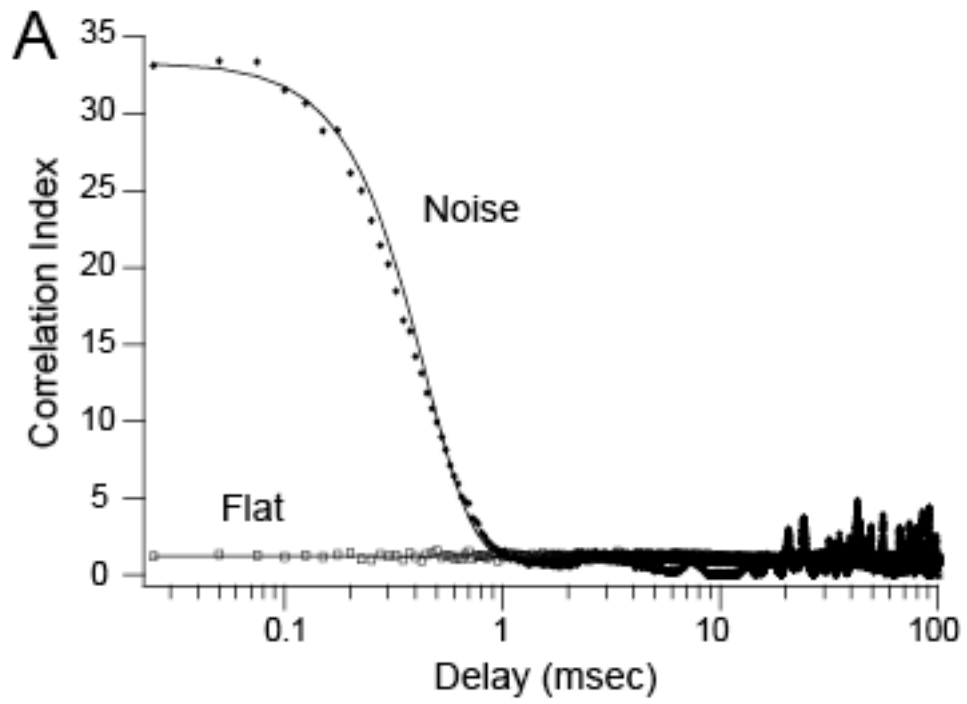


**Figure 2.4** Measurement of spike timing across trials using the shuffled autocorrelation method.

**A** SAC for the same cell as in figure 1 and 2. The open squares denote the delay times for flat currents, and the filled circles denote delay times for the noisy currents. Gaussian fits are shown as lines. The abscissa is on a log scale to emphasize the correlation for delays less than 1 msec. A value of 1 is expected for a random process, or spike timing that is uncorrelated across trials.

**B** Pooled data comparing CI for 45 cells. The noisy CI is significantly larger than the flat CI ( $P < 0.001$ , paired t-test; mean difference=13.0).

### **2.3.2 Sensitivity of SAC to Spectral Structure of the Noise Input**

Pyramidal cells of the DCN have been shown to phase lock to auditory input at low frequencies, and they can encode the frequency and amplitude modulation of acoustic stimuli up to about 500 Hz (Frisina et al. 1994; Kim et al. 1990; Rhode and Greenberg 1994; Zhao and Liang 1995). These observations led us to investigate how the frequency content of the noise current stimulus affected the ability of the pyramidal cells to fire in a repeatable manner. We varied the low-pass cutoff between 250 to 1750 Hz. Varying the noise spectrum did not alter the ability of the cells to respond reliably to the noise (Figure 2.5); although the CI values were variable across cells, there was little evidence for any frequency-dependence. Consequently, we choose to use a low-pass filter frequency of 500 Hz for our subsequent analyses.

### **2.3.3 Dependence of CI on Firing Rate**

It is expected that the reliability might depend on the mean firing rate of a cell. At high firing rates, spike generation is dominated by intrinsic conductances, whereas at low rates, the variability of the membrane potential due to synaptic input or noise is expected to play a larger role. We thus calculated the CI for pyramidal cells firing at low, medium and high rates to a noisy current. The firing rate was manipulated by increasing the DC pedestal on which the noise is superimposed, without increasing the amplitude of the noise itself. In general, the faster the average firing rate, the weaker the correlation between spike times across trials with the same stimulus presented (Figure 2.6A,B). However, note that the precision of spike timing does not change (Figure 2.6B).

As the DC pedestal is changed, the coefficient of variation of the stimulus ( $CV_s$ , measured as the variance divided by the mean amplitude of the stimulus) decreases, and thus

co-varies with increasing firing rate. A smaller  $CV_s$  could, in part, account for the decrease in reproducibility of the spike trains, since the temporally changing component of the stimulus becomes small relative to the average depolarization. We evaluated the relation between  $CV_s$  and the CI (Figure 2.6C). There is a weak, but significant, positive correlation between  $CV_s$  and CI ( $P < 0.005$ ,  $R = 0.341$ ,  $df = 63$ ). To investigate this further, we divided the trials into 3 groups based on the CV of the stimulus, (low,  $0.18 \leq CV_s < 0.28$ ; intermediate,  $0.28 \leq CV_s < 0.38$ ; high,  $CV_s \geq 0.38$ ) and plotted spike rate against CI for each group (Figure 2.6D). Rate was negatively correlated with CI for the intermediate and high CV groups (intermediate:  $R = -0.476$ ,  $P = 0.017$ ,  $df = 22$ ; high:  $R = -0.502$ ,  $P = 0.039$ ,  $df = 17$ ), but CI was relatively independent of rate for the low CV group ( $R = 0.156$ ,  $P = 0.52$ ,  $df = 19$ ). Thus, while decreasing the  $CV_s$  accounts for part of the decrease in reliability with increasing rate, increasing the rate still results in lower numbers of spike times with small delays in the SAC. Even at the higher rates, spike times are determined by the fluctuations in the noise, since the CI values are all well above 1 (Figure 2.6D), whereas the CI for flat current pulses is not different from 1. This indicates that, at least for rates up to 100 Hz, the intrinsic mechanisms do not completely govern the spike times.

Since increasing the average firing rate leads to a decreased CI, we next investigated whether increasing the amplitude of the noise improved spike timing reproducibility. Frozen noise tokens with different amplitude, but the same DC pedestal, were presented to the cells for 50 trials (Figure 2.7A-C). In four out of 5 cells, increasing the noise amplitude results in increased CI of spike times (Figure 2.7D, E). Since the  $CV_s$  increases when the amplitude of the noise component is increased, the time-varying component of the stimulus drives the cell most strongly, and the cell fires in response to the stronger stimulus fluctuations.

**Figure 2.5**

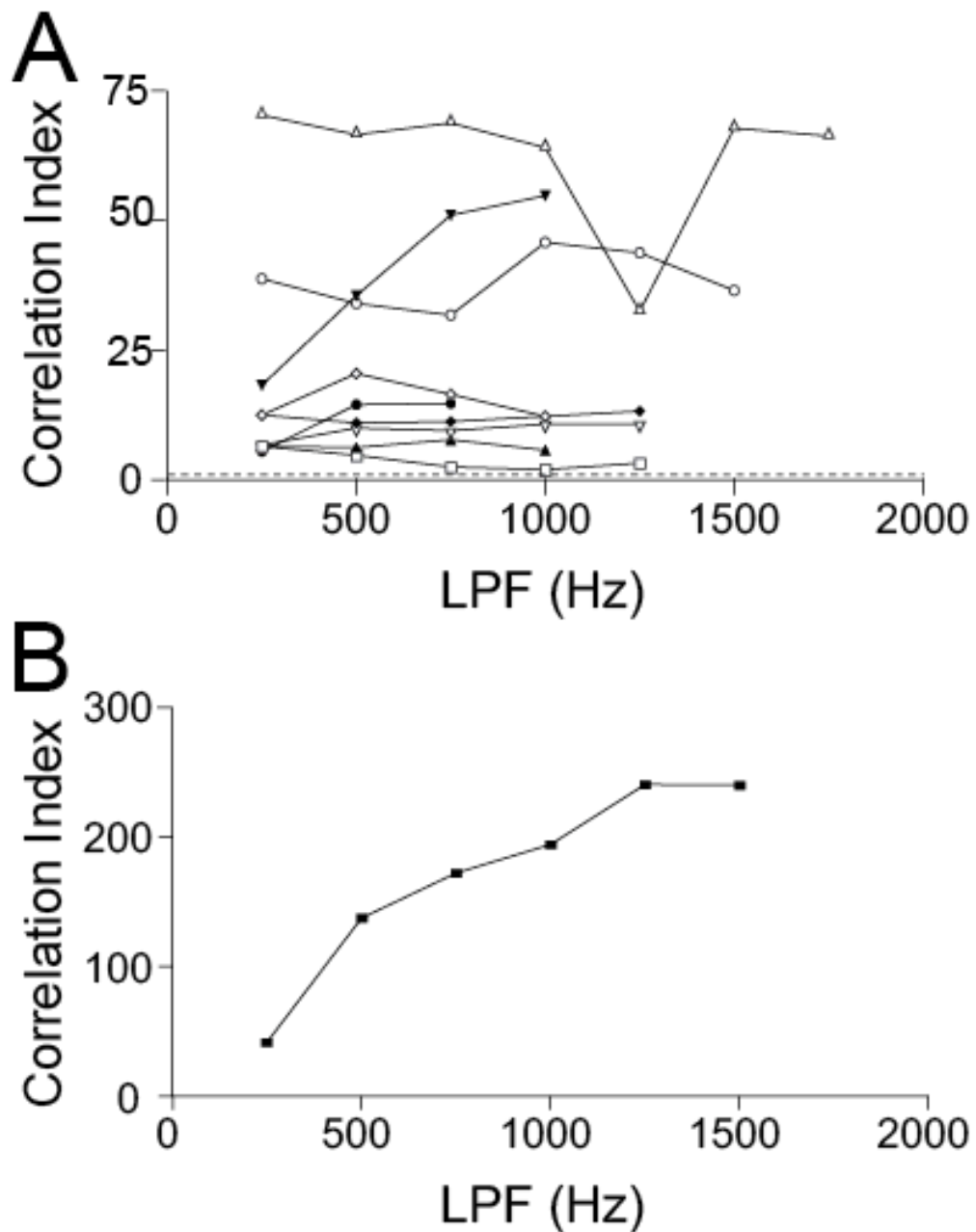


**Figure 2.5** The frequency content of the noisy current does not affect the ability of the cells to fire precisely.

**A, B** CI is plotted as a function of the cutoff frequency of a low-pass filter applied to the noise stimulus. Each line represents a separate cell (N=10; cell in B is on a different ordinate scale).

Figure 2.6

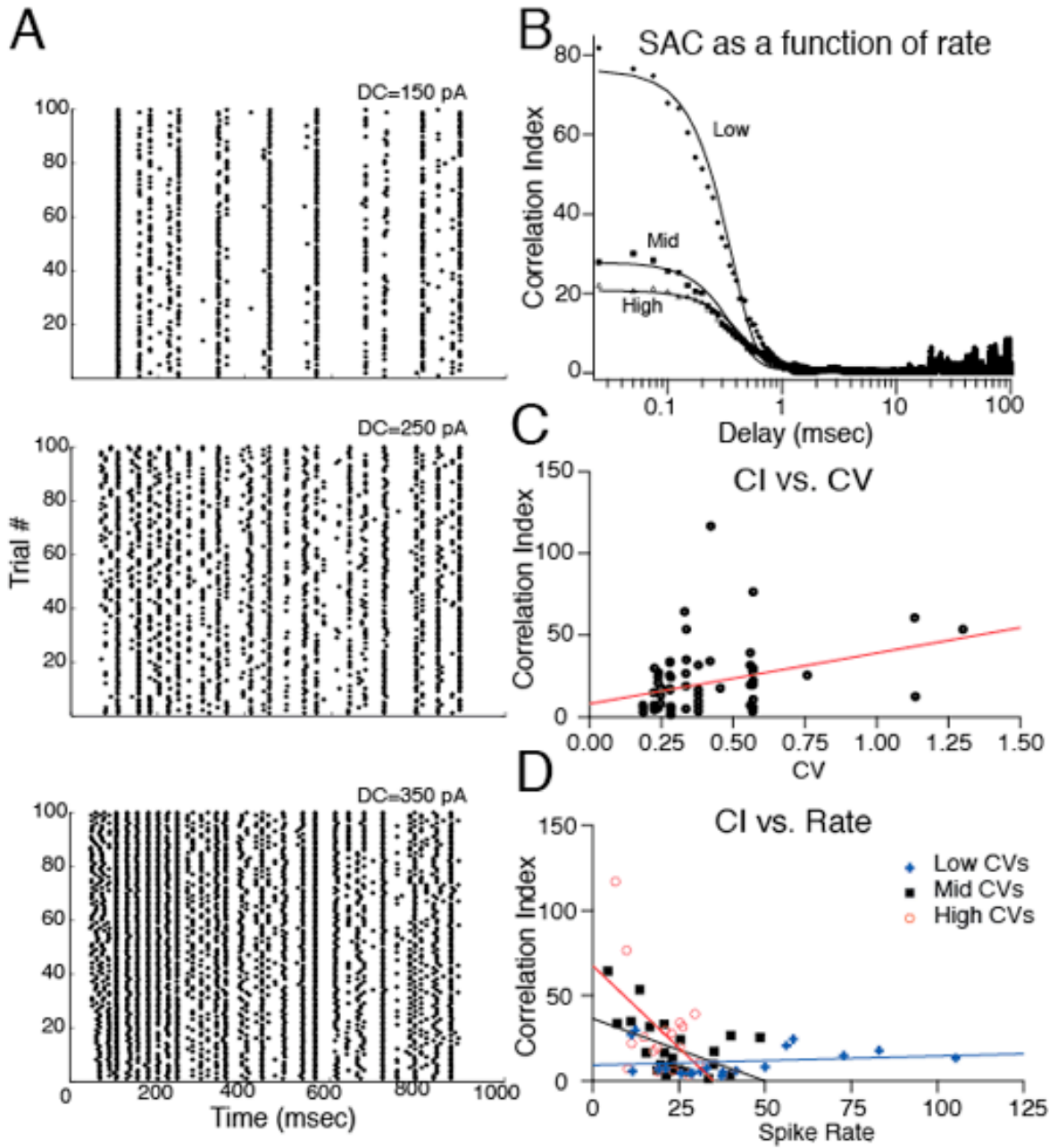


**Figure 2.6** Mean firing rate affects spike timing and reliability.

**A.** Raster plots are shown for a single cell firing at different rates (upper plot is 9.8 spikes/second, middle plot is 16.6 spikes/second, lower plot is 25.4 spikes/second).

**B.** SACs computed from data in A. Filled circles denote delays for low rate, filled squares denote medium rate, and triangles denote high rate. The SACs are fitted by a Gaussian function, as in Figure 4.

**C.** Scatterplot of CI with the stimulus variance,  $CV_s$ , for 26 cells driven at different rates. The CI and  $CV_s$  are positively correlated.

**D** Scatterplot of CI and spike rate, grouped by  $CV_s$ . Low (gray circles); intermediate, (black squares); high, (open circles). The correlation between CI and spike rate was significant for cells where the  $CV_s$  was at high or intermediate ranges ( $R=0.2513$ ,  $P<0.05$  for high;  $R=0.1838$ ,  $P<0.05$  for intermediate).

**Figure 2.7**

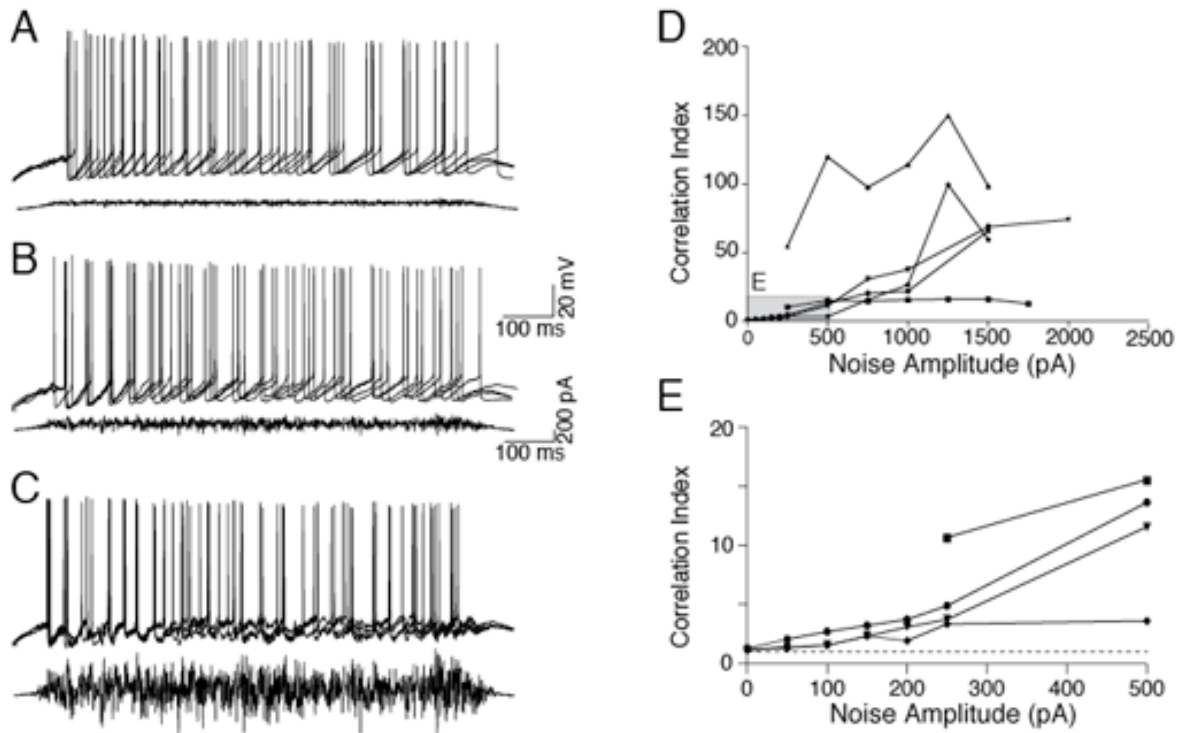


**Figure 2.7** Increasing the noise amplitude increases spike timing precision.

**A-C** Traces from 5 consecutive trials, overlaid to show spikes elicited in response to a noise stimulus with low (A), middle (B), or high (C) amplitude. All data from the same cell.

**D** Increasing the noise amplitude increases the CI. Each line is a separate cell.

**E** The gray box near the origin in D is expanded to show increases with small amounts of noise. Dashed line, CI = 1.

### 2.3.4 Spike Triggered Averages

So far, we have shown that pyramidal cells can respond to time-varying input with reliable and precisely timed spikes. In part, the cells are responding to specific patterns of energy in the stimulus. To identify the time courses of the stimulus events driving the cells, we computed spike-triggered averages by averaging the mean current injected before and after spikes, aligned on spike threshold crossings.

A comparison of STAs is shown in Figure 2.8 for one cell presented with noise low-pass filtered at 250 Hz (thick line), and noise low-pass filtered at 500 Hz (thin line). The two sets of dashed lines show 95% confidence limits for the two sets of noisy current injections. STAs to flat current pulses had no significant deviations from the baseline current (not shown). However, the STA to both the 250 Hz noise and the 500 Hz low-pass filtered noise reveals a broad negative (hyperpolarizing) followed by a sharp positive (depolarizing) current. The main difference between responses to the two different spectra is that the depolarizing current is not as strong or as sharp when the stimulus is filtered at 250 Hz (Figure 2.8A). The hyperpolarizing current is small, but lasts for 10 msec, whereas the depolarizing current is large and lasts for only ~3 msec. There is little difference in the rising slope or shape of the action potentials that result from the different input currents (Figure 2.8B). In most cases, it seems that the cells prefer to be slightly hyperpolarized before a depolarizing current can produce an action potential.

Figure 2.8

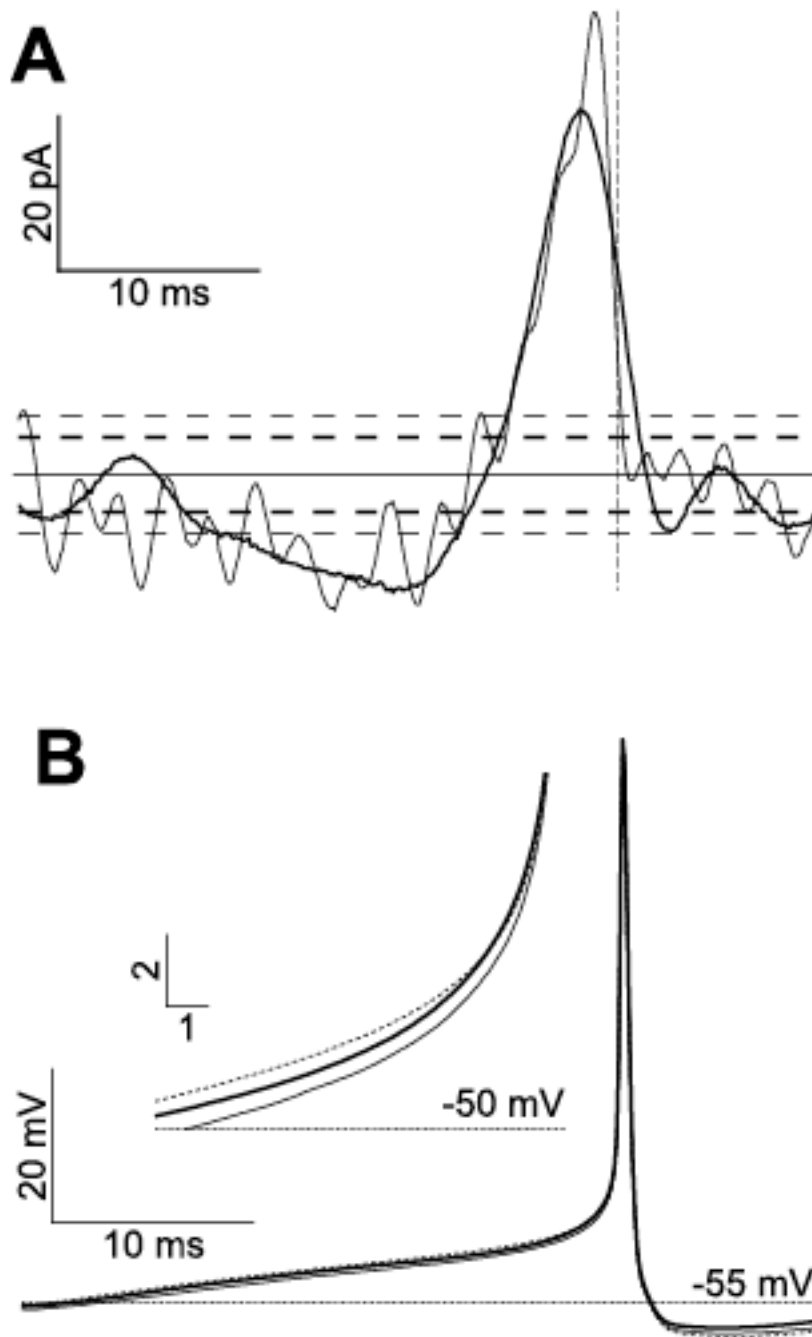


**Figure 2.8** Typical spike triggered average.

**A** The spike triggered average current before and during an action potential is shown for flat current (dots, barely visible), and noisy currents filtered at 250 Hz (thick line), or 500 Hz (thin line). Calculated 95%-5% confidence intervals are shown as dashed lines. The vertical dashed line corresponds to the peak of the action potential.

**B** Action potential shape for flat, 250 Hz, and 500 Hz low-pass filtered noise. There is little variation in action potential shape. The inset shows the small variations in membrane potential leading up to the action potential around threshold. Inset calibration is in ms and mV.

### 2.3.5 Perturbations in the Stimulus Alter Spike Timing

Inhibition is a critical element of sensory coding in the DCN (Oertel and Young 2004). DCN pyramidal cells receive inhibitory input from at least three different types of interneurons: vertical cells, cartwheel cells and stellate cells. We therefore asked how a simulated IPSP (sIPSP) placed in the middle of the noise stimulus would affect spike timing. We hypothesized that superimposing a sIPSP might increase reliability and precision of subsequent action potentials because the STA suggests that these cells prefer to fire when a small hyperpolarizing current precedes a depolarizing current. A sIPSP, consisting of a rapid triplet of alpha waves, was superimposed on the Gaussian noise current 500 msec after the onset of the stimulus (Figure 2.9A,B). We then compare the SACs after the sIPSP.

The SACs revealed that the spike times were more highly correlated after the sIPSP (Figure 2.9C). However, the sIPSP briefly hyperpolarizes the cells, and prevents the noise current from triggering action potentials. After the sIPSP, the first spike is more precise and reliable. The effect continues for at least 300 msec (Figure 2.9B). Summary data for 28 cells is shown in Figure 2.9D-E. For the last 500 msec of the stimulus, the CI is higher when the stimuli contain a sIPSP. The CI of spike times that occur before the sIPSP is similar to that under control conditions indicating that the sIPSP is not affecting the CI at these times. The difference in the CI after a sIPSP is highly significant ( $P < 0.001$ ;  $N = 31$ , paired t-test). In order to determine approximately how long the sIPSP affected the spike times, we compared the CI's of smaller time intervals using a sliding time scale of 100 msec (Figure 2.9E). In the five 100 msec time intervals prior to the sIPSP, there is no difference in CI. However, the CI of the 100 msec interval that includes the spikes from the 450 msec time point to the 550 msec time point (point a in figure 2.9E) was significantly higher compared to the same time

interval without an sIPSP ( $P=0.0003$ ,  $df=25$ , mean difference=-2.088). The effect continued for the next two 100 msec intervals (see points b and c, Figure 2.9E). The CI's for the 550-650 msec interval and 650-750 msec interval were both higher when an sIPSP was present in the stimulus compared to when there was no sIPSP, although the effect was not as pronounced as the 450-550 msec interval (b.  $P=0.022$ ,  $DF=32$ , mean difference=-0.404, c.  $P=0.0104$ ,  $DF=32$ , mean difference=-0.204).

Following the sIPSP, the increase in synchrony could result from the hyperpolarization of the membrane potential, or from any perturbation. We tested the second idea by presenting the frozen noise stimuli superimposed with a sEPSP (Figure 2.10A). The sEPSP produced a brief increase in spike rate, followed by a small hyperpolarization and a delay to the next spike. Spike timing following the sEPSP is more reliable and precise than it would have been without the sEPSP (Figure 2.10B,C), although the increase in CI is not as pronounced with the sEPSP as with the sIPSP ( $P<0.05$ ,  $N=10$ , paired t-test). Therefore, we conclude that a sEPSP is not as effective as a sIPSP in improving the spike timing. In conclusion, small perturbations of the membrane potential, such as a sIPSP, can affect the CI for several hundred msec, and it is most likely that the membrane hyperpolarization engages additional mechanisms that affect subsequent spike timing.

Figure 2.9

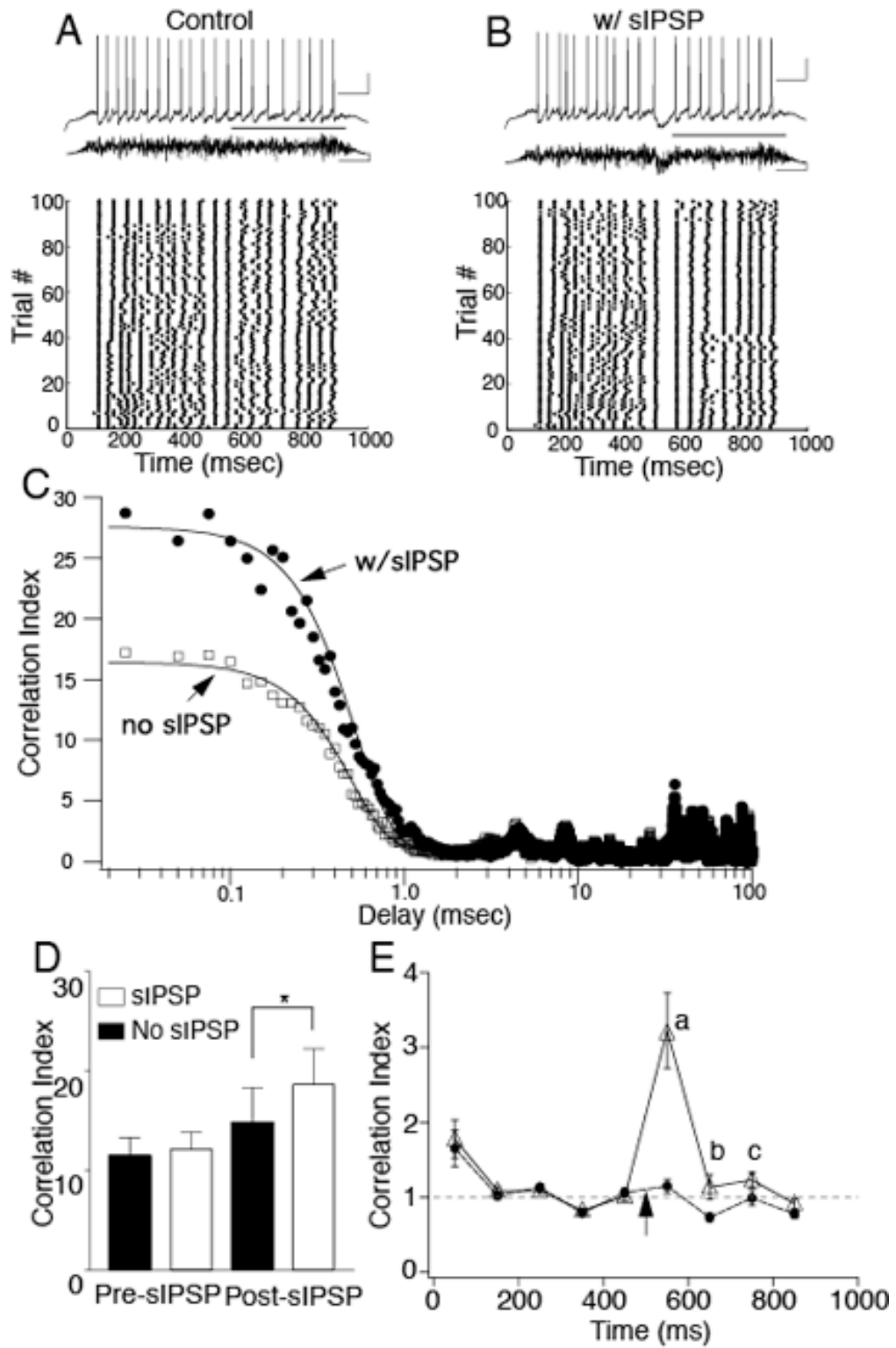


**Figure 2.9** A brief hyperpolarization (simulated IPSP) can improve subsequent spike timing.

**A,B** Single traces and raster plots for spike trains from a single cell when presented with a noise pulse that either did not (A) or did (B) include a sIPSP 500 msec after the start of the pulse. Scale bars: Voltage, 20mV and 100 msec; Current, 200 pA and 100 msec.

**C** SAC computed for spike times during the last 500 msec of the stimulus. Delay values for spike times when the stimulus included a sIPSP are shown by the filled circles. Delay values for spike times when the stimulus did not contain a sIPSP are shown in open squares. The points have been fit with Gaussians (lines). The sIPSP increases spike reliability.

**D** Summary of group data of CI with and without a sIPSP. Pre-IPSP denotes the spike comparison of CI before 2.9E). In the five 100 msec time intervals prior to the sIPSP, times that occurred in the first 500 msec of the stimulus. Post-sIPSP denotes the spike times that occurred in the last 500 msec of the stimulus. CI was significantly greater for spike times that occurred after a sIPSP was imposed upon the stimulus ( $P < 0.001$ ,  $N = 31$ , paired t-test).

**E** CI calculated with a sliding 100-msec time window shows that the largest change occurs in the first 100 msec after an sIPSP (point a), but the CI is still significantly elevated ( $P < 0.001$ ,  $N = 31$ , paired t-test) out to 300 msec after the sIPSP (b,c).

**Figure 2.10**

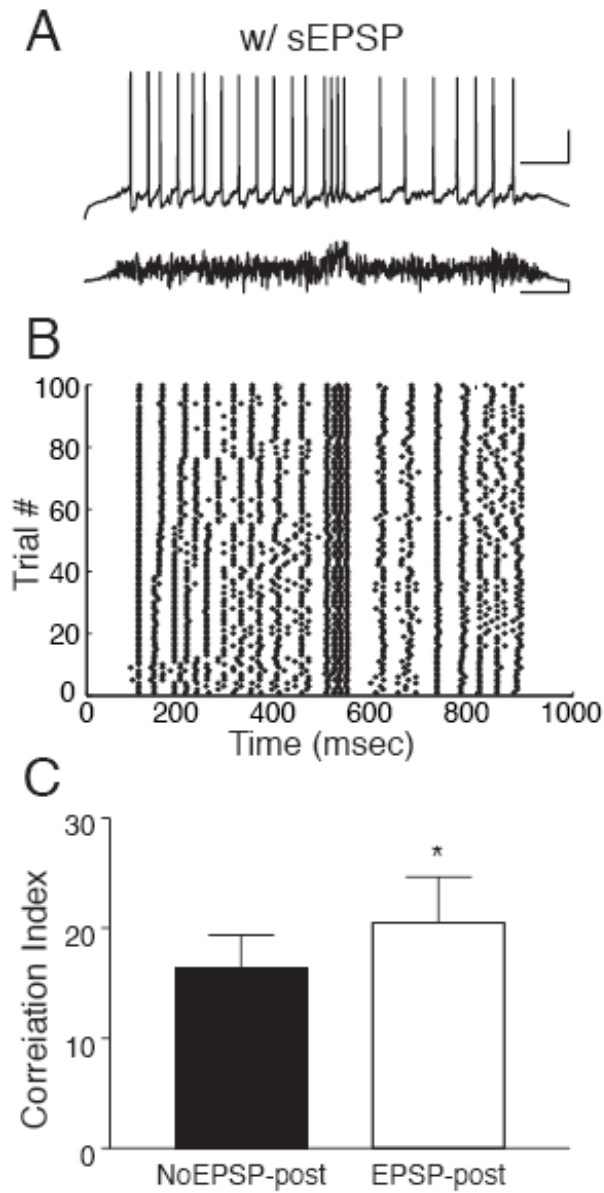


**Figure 2.10** Depolarizing events, such as a simulated sEPSP, can also improve spike timing.

**A** Raw voltage and current traces for a cell stimulated with an sEPSP at 500 msec latency.

**B** Raster plot of spikes for the same cell as in A, where the stimulus contained an sEPSP.

**C** Group data shows that the CI of spike times increased.

### 2.3.6 Population coding

The data shown so far suggest that individual cells can respond with repeatable patterns of activity in response to a frozen stimulus waveform. However, temporal coding also requires the coordinated activity of many neurons at the same time, for example. Since each neuron has different intrinsic excitability due to the differences in the voltage-dependence and density of their ion channels (for example, see (Kanold and Manis 2001; 2005b)), such a temporal code might not be effectively retained across a population of cells receiving similar inputs. To investigate whether synchronous firing can be generated by a common stimulus to a population of cells, we computed the SAC, as a measure of synchrony, across a population of 15 cells collected in 6 independent experiments over a 2-month period, where the same noise token was used for each cell. Such a calculation provides an estimate of the coherent firing that is available across the population of cells. On average, the frozen noise generated a population SAC with a similar shape to that seen in individual cells (Figure 2.11A). The synchrony was good ( $CI=4$ ) and the timing of correlated spikes had a half-width of 0.84 msec. The amplitude of the central peak was smaller than for individual cells, indicating that fewer spikes were correlated between cells than within a single cell. A small secondary peak with a 2-msec half-width also appeared (arrow in Figure 2.11A), suggesting that the spike timing across the population was not quite as temporally precise as in individual cells (Fellous et al. 2004; Reinagel and Reid 2002). The flat current pulse did not result in an elevated central SAC peak, in spite of the regular discharge of all cells. The SAC had the same shape and amplitude even in single trials (Figure 2.11B), raising the possibility that the synchronized firing could convey information about the stimulus with good temporal precision during a single stimulus.

We next examined the synchronization between individual cells by calculating the cross-correlation of spike trains. The peak correlations for both noisy and flat current stimuli are summarized across the 105 possible pair-wise comparisons for the 15 cells in this population in Figure 2.11C. Flat pulses (black line) result in low peak correlation rates that are not significantly different from those obtained with noisy stimuli when one of the spike trains is shuffled to remove temporal correlations (not shown). The noise correlations however show a broad distribution: some cell pairs exhibit relatively high correlations, whereas other pairs show little correlation. Overall, however, the correlated firing rate is at least 2.7 times higher with the noise than with flat pulses. The correlated rate with flat pulses is probably lower than what we estimate, since we chose the maximum correlation value, which is influenced by the statistical variation in the cross-correlation function due to the finite number of spikes available for the computation. Thus, common features in the stimulus can lead to correlated firing among different cells, and the correlations occur in a time window about 2 msec wide.

**Figure 2.11**

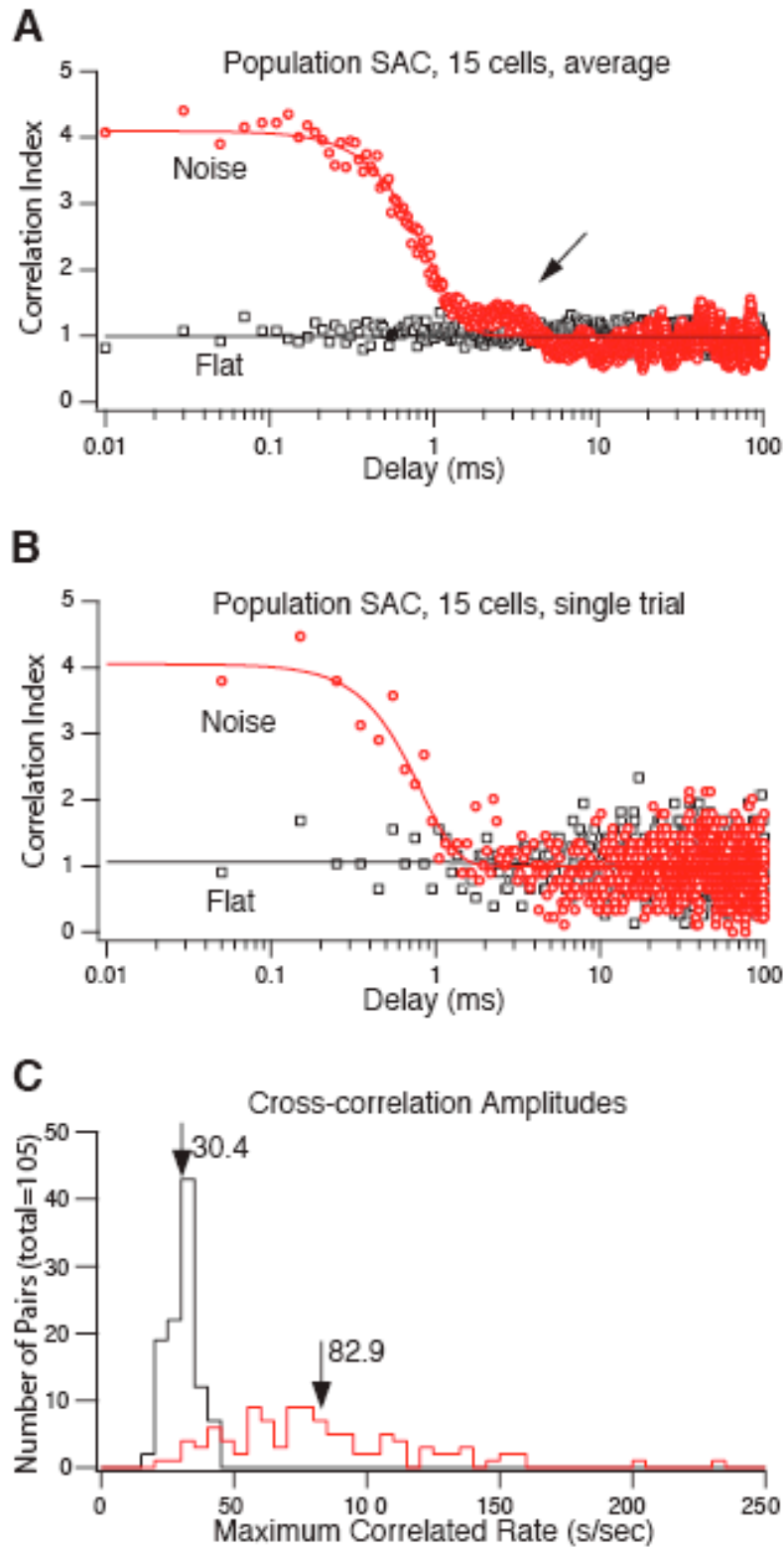


**Figure 2.11** Different cells can synchronize to common features in the stimulus. The SAC was computed across a population of 15 cells recorded from 6 separate preparations in response to the same frozen noise stimulus (Gaussian noise, low-pass filtered at 500 Hz).

**A** A central mound is evident in response to the noise stimulus, indicating that the average rate increases by about four-fold in response to suprathreshold inputs. Note the narrow central peak (half-width, 0.84 msec). Flat current pulses, despite generating regular firing, do not lead to synchronized activity (open squares). Solid lines are fits of a Gaussian function to the data. Average of 100 trials.

**B** SAC for a single 1-second trial shows a similar shape to the average, indicating detectable synchrony in a single trial.

**C** Summary of the peak cross-correlation rates across the 105 possible pair-wise combinations for the 15 cells analyzed in A and B. The black histogram shows the peak correlation rates for flat stimuli; these are not significantly different than the average firing rates of the cell pairs. The red histogram shows the peak correlation rates for noisy stimuli. Arrows indicate the mean rates for the two histograms. The mean correlation rate for noisy stimuli is 2.7 times the flat rate.

### 2.3.7 Pharmacological manipulations of Spike Timing

Pyramidal cells express a hyperpolarization-activated current (Pal et al. 2003). ZD7288 specifically blocks the HCN channels that give rise to  $I_h$  (BoSmith et al. 1993). When we block  $I_h$ , the resting membrane potential hyperpolarizes, making it difficult to match the conditions of the noise current pulse before and after drug administration. In addition, the DC pedestal of the stimulus had to be increased to match the firing rates between the control and drug conditions. In only a few cells were we able to satisfy both requirements (N=5). In these cells, there was no clear effect of blocking  $I_h$  on either the spike times for the entire stimulus, or the spike times after a sIPSP (Figure 2.12). Thus, blocking the hyperpolarizing activated current does not seem to have an effect on spike timing in response to a noise pulse or after a sIPSP.

It has been reported that metabotropic glutamate receptors regulate intrinsic excitability and spike timing (Sourdet et al. 2003). Since DCN pyramidal cells express metabotropic glutamate receptors, we used ACPD to stimulate metabotropic glutamate receptors and then measured the reliability of the spike times according to the Mainen and Sejnowski method. There was no consistent change in the reliability of spike times after ACPD administration (Figure 2.13). Since ACPD did not change reliability, we did not further investigate the effect of metabotropic glutamate receptor stimulation on spike timing. We did not analyze these data with the SAC method.

**Figure 2.12**

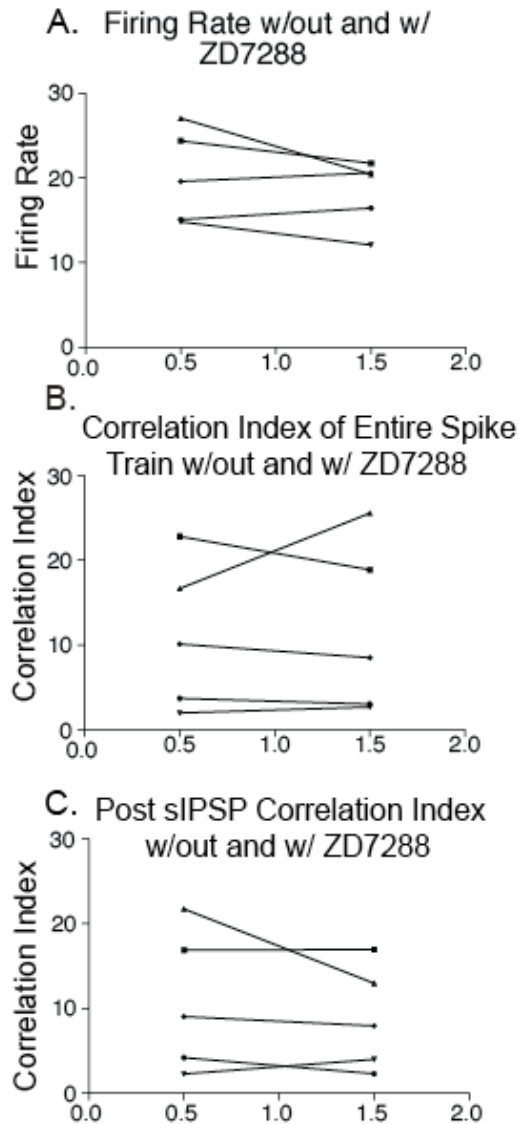


**Figure 2.12** Blocking HCN channels with ZD7288 does not change the timing behavior of spikes.

**A** Plot showing average firing rates for cells when presented with noise current in the presence and absence of ZD7288.

**B** Plot showing CI of spike times in presence and absence of ZD7288 for the entire 1 second noise stimulus.

**C** CI of spike times for the last 500 msec of the stimulus that contained a sIPSP in the presence and absence of ZD7288. None of the results were significant. (N=5).

Figure 2.13

Change in reliability of spike times  
when ACPD is added to the bath

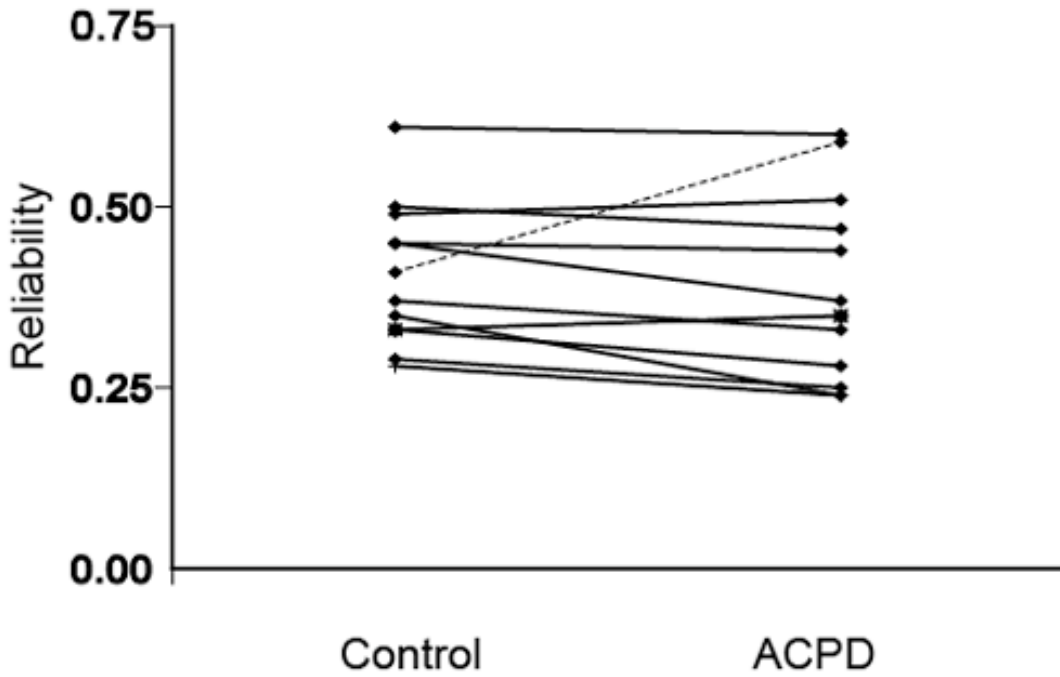


**Figure 2.13** Stimulating metabotropic glutamate receptors with ACPD does not alter spike timing reliability. The reliability of spike times in the presence and absence of ACPD with a paired t-test and were not statistically different.

## 2.4 Discussion

We have shown that DCN pyramidal cells *in vitro* can respond to time-varying stimuli with reliable and precise trains of action potentials. The SAC (Joris 2003; Joris et al. 2006; Louage et al. 2004; Pal et al. 2003), a method that is free of assumptions regarding the timing of spikes in relationship to stimulus events, reveals that pyramidal cells can reliably report temporal events in a stimulus with millisecond precision. Precise spike timing can even be seen across a population of cells with different intrinsic properties. Characteristics of the stimulus such as amplitude and variability alter the reliability of the output spike train, whereas the degree of low-pass filtering does not affect the reliability. Longer hyperpolarizing events, such as a sIPSP embedded in the stimulus, can increase the reliability and precision of firing for up to 300 msec. Blocking  $I_h$  currents and stimulating metabotropic glutamate receptors do not consistently change spike-timing characteristics in pyramidal cells.

### 2.4.1 General Characteristics of DCN Pyramidal Cells in Response to Noise

Many neurons in the auditory system are known for their ability to fire action potentials that occur in a precise temporal relationship to the stimulus (Carr et al. 2001; Oertel 1999; Trussell 1999). Such cells may fire on repeated portions of the waveform with a standard deviation on the order of 115  $\mu$ sec (corresponding to a phase-locking vector strength of 0.8 at 1 kHz); these cells have specialized AMPA receptor subunit and synaptic configurations, and express low-voltage activated potassium conductances. Such specializations are not present in DCN pyramidal cells (Hirsch and Oertel 1988a; Kanold and Manis 1999; Manis 1990; Zhang and Oertel 1994), so it is expected that DCN cells respond similarly to other “generic” neuronal types when presented with time-varying input that

resembles synaptic input (de Ruyter van Steveninck et al. 1997; Mainen and Sejnowski 1995; Nowak et al. 1997). Nonetheless, the STA current waveform in the DCN was the relatively short time scale as compared to cortical neurons. The spike-triggered average current waveform consisted of a small slow hyperpolarizing current followed by a rapidly rising depolarizing current as in other cells. However, in other cells the hyperpolarizing and fast depolarizing phases of the current have been reported to last tens of milliseconds (Mainen and Sejnowski 1995). In DCN pyramidal cells the hyperpolarizing phase lasted about 10 msec, and the depolarization on average had a half-width of 3 msec. This suggests that DCN pyramidal cells integrate synaptic conductances on a relatively short time scale. The sharp depolarization most effectively enables the cell to reach threshold, because the spike threshold is inversely proportional to the slope of the input current (Azouz and Gray 2000). Thus, fast events in the stimulus not only lead to sharp membrane depolarizations, but also decrease the threshold resulting in an increased probability of firing a spike. The brief hyperpolarizing current may help prime the spike generating mechanism by de-inactivating  $\text{Na}^+$  channels and by reducing the resting  $\text{K}^+$  conductance, which together increase the probability of generating an action potential (Svirskis et al. 2002; 2004). Pyramidal cells thus appear to integrate their inputs on a time scale that is in between that of the specialized auditory neurons that show high-frequency phase locking, and the slower neurons of the forebrain.

When we increased the variance in the stimulus (increased  $\text{CV}_s$ ), spike times became more reproducible. The higher amplitudes of the time-varying component increase the magnitude of depolarizing currents. The faster and larger membrane depolarizations permit less time for intrinsic conductances of the cell to oppose the depolarization, and less time for

Na<sup>+</sup> channels to inactivate. These two features lead to a lower spike threshold and higher reliability and precision (Hunter and Milton 2003).

The variance of the synaptic input to DCN pyramidal cells *in vivo* has not been measured. However, even small variations in the input current can evoke reliable spike trains when the stimulus frequency resonates with the intrinsic cell membrane oscillations or with a characteristic firing frequency (Fellous et al. 2001; Haas and White 2002; Hunter et al. 1998). DCN pyramidal cells exhibit subthreshold oscillations that range in frequency from 40 to 100 Hz (Manis et al. 2003). While we did not explore small amplitude stimuli that specifically incorporated enhanced energy within this frequency range, it is possible that these cells could increase their firing reliability when the input resonates with membrane dynamics. We also found that small increases in noise amplitude resulted in increases in the number of spikes that were tightly correlated across trials.

We compared neurons that fired at the same average rates to determine if pyramidal cells fire more reliable trains of action potentials in response to temporally changing input. While pyramidal cells have been reported to phase lock *in vivo* to low-frequency input, at higher frequencies this phenomenon disappears (Rhode and Smith 1986). In addition others have reported that DCN cells phase lock poorly to synchronized repetitive stimulation of the ANFs (Babalian et al. 2003). As the firing rate of a neuron increases, the ISI is less influenced by transient changes in membrane potential and is controlled to a greater extent by the ionic conductances that regulate the refractory period. Consistent with this, when cells were sorted according to the stimulus CV<sub>s</sub>, the precision of spike times decreased with increasing rate. However, the peak rate of the SAC, regardless of CV<sub>s</sub> and rate, is very high compared to stimuli that contain no temporal structure. The CI of the ANF SACs runs in the

range 2-10, even for stimuli that produce strong phase locking (Louage et al. 2004); the temporal coding in DCN cells can easily achieve this same range though with less precision. While reliability and precision does decrease with increasing firing rate, the rates must be well above 100 Hz before the contribution of input current fluctuations ceases to be evident in the spike timing.

#### **2.4.2 Inhibition and Spike Timing in the DCN**

Inhibition's effect on spike timing has received immense attention in recent years. In both the cerebellum and the medial superior olive, inhibition masks integrated, sub-threshold input which results in the cell failing to fire when the input is weak; instead the cell only responds to stronger, coincident synaptic events that elicit more reliable spikes (Gauck and Jaeger 2000; Grothe and Sanes 1994). Inhibition also leads to a delay in spike times in the cerebellum and DCN (Hausser and Clark 1997; Kanold and Manis 2005a), while it shortens the membrane time constant and increases the membrane conductance. Consequently, non-synchronous EPSPs become smaller and briefer, allowing the neuron to act as a more precise coincidence detector (Grande et al. 2004; Jaeger and Bower 1999). The DCN contains at least three types of inhibitory interneurons that share excitatory input with pyramidal cells (Golding and Oertel 1997; Hackney et al. 1990; Oertel and Young 2004). These interneurons can strongly inhibit pyramidal cells in conjunction with activity in ANFs and parallel fibers. Since inhibition is prominent in this nucleus, we imposed a sIPSP to mimic the inhibitory input from the bursting cartwheel cells. This perturbation transiently silenced the cell firing, but resulted in an increased precision of spike timing when the cell resumed activity. The hyperpolarization from the sIPSP most likely perturbs the state of the cell's intrinsic conductances, such as sodium channels and transient potassium currents, and puts the cell

membrane into a regime where it is can reliably fire at the next sharp depolarization.

Cartwheel cells and stellate cells, both of which receive input from parallel fibers, could provide synchronized inhibitory input to pyramidal cells after they are excited by the parallel fibers. This inhibition might prevent pyramidal cells from firing imprecisely-timed spikes to small depolarizing events after the initial excitation from the parallel fibers. This inhibition could also deinactivate membrane conductances so that the cells would be prepared to fire at the next sharp depolarization. In the next chapter we show that a rapidly-inactivating potassium conductance affects the timing precision of the first spike after the sIPSP (see Chapter 3).

### **2.4.3 Population coding**

A surprising result was that correlated spike times could be measured in a population of cells from different animals and slices, in response to the same stimulus (Fellous et al. 2004; Reinagel and Reid 2002). This suggests that a population of pyramidal cells could use a timing-based, population-coding scheme to represent auditory information (Hausser and Clark 1997; Kanold and Manis 2005a). This hypothesis depends on two principal assumptions. First it is assumed that the firing of individual auditory nerve fibers that connect to a group of pyramidal cells shows stimulus-dependent correlations in their firing. Indirect evidence suggests that this is the case, even for high-CF auditory nerve fibers. Responses to repeated stimuli in individual fibers show a significant central peak in their SAC (Louage et al. 2004). In addition, these correlations need to be detected by the pyramidal cells, and the presence of stimulus-dependent central mounds in the cross-correlations of pyramidal cells suggests that this may occur (Voigt and Young 1988). Second, this hypothesis assumes that the pyramidal cells receiving common inputs converge onto individual neurons in the inferior

colliculus in a way that allows the collicular neurons to respond to the correlations in the input; this assumption is necessary for correlated synaptic events across the cell population to be detected and operated on. The convergence patterns between pyramidal cells and their collicular targets are presently not well understood.

Recent studies have demonstrated the existence of long-term synaptic plasticity between parallel fibers and two target neurons in the DCN, the pyramidal and the cartwheel cells (Fujino and Oertel 2003; Tzounopoulos et al. 2004). The timing-dependence of this plasticity is relatively precise: in the pyramidal cells the window is less than 20 milliseconds wide and in cartwheel cells it is less than 5 msec wide. Such a narrow window demands that the firing of the postsynaptic cells to fluctuating synaptic inputs also be temporally precise, and implies that precise spike timing is an integral part of information processing in the DCN, at least as it relates to long-term synaptic plasticity. Our results also demonstrate that precise spike timing can occur in response to dynamic stimulation, and that interactions between inhibition, potassium conductances, and other conductances regulating intrinsic cell excitability can modulate the precision of spike timing over hundreds of milliseconds.

# **Chapter 3: A Member of the Shal Potassium Channel Family Controls the Timing of Action Potentials after Inhibitory Events in DCN Pyramidal Cells**

## **3.1 Introduction**

How central neurons process and encode information depends upon a dynamic interaction of synaptic inputs and intrinsic voltage-gated conductances. Of the many different kinds of ion channels, transient potassium currents ( $I_A$ ) have been shown to shape spike patterns in response to synaptic input of neurons, by regulating dendritic integration as well as spike initiation and latency. The channels that give rise to these currents are characterized by their rapid activation at sub-threshold voltages, and rapid inactivation that is removed only by hyperpolarizing inputs (for review see Birnbaum, et al, 2004). Activation of  $I_A$  can affect many aspects of neuronal physiology including action potential width, action potential frequency, the spread of synaptic depolarization, synaptic plasticity, and action potential repolarization (Cai et al. 2004; Hoffman and Johnston 1999; Hoffman et al. 1997; Kim et al. 2005; Liss et al. 2001; Watanabe et al. 2002). Ion channel proteins that give rise to  $I_A$  currents are the Kv1.4 channel, Kv3.4 channel, and the entire Kv4 family of channels (Birnbaum et al. 2004).

Transient potassium channels have been suggested to play an important role in determining the sensory response patterns of neurons in the dorsal cochlear nucleus (DCN).

Pyramidal cells of the dorsal cochlear nucleus (DCN) receive both auditory information via the auditory nerve and non-auditory information through a system of granule cells (for review see Oertel and Young, 2004). This synaptic input, especially inhibitory input, determines which intrinsic voltage gated-conductances are recruited enabling them to shape pyramidal cell output. Response patterns of pyramidal cells differ remarkably from response patterns of the auditory nerve. While auditory nerve fibers respond to pure tone stimuli with a increase in firing rate that adapts during a sustained tone (Godfrey et al. 1975; Pfeiffer 1966; Rhode and Smith 1986; Rhode et al. 1983b), pyramidal cells often respond to tones with a “build-up” pattern characterized by a long latency to the first spike, or a “pauser” pattern characterized by a long first interspike interval. While these response patterns are in part the result of synaptic interactions (Voigt and Young 1980), both patterns also can be elicited with simple current injection in pyramidal cells in a slice preparation when synaptic input is blocked (Manis 1990). Thus, intrinsic properties of these cells shape their responses to synaptic inputs.

DCN pyramidal cells contain two transient potassium conductances (a fast,  $I_{Af}$  and a slow,  $I_{As}$ ) (Kanold and Manis 1999), that could be responsible for the different discharge patterns, as suggested by computational models (Hewitt and Meddis 1995; Kanold and Manis 2001; 1999; Kim et al. 1994; Kim et al. 2005; Manis 1990). In addition, the voltage dependence of discharge patterns in *in vivo* preparations also supports the importance of  $I_A$  in shaping responses of pyramidal cells (Hancock and Voigt 2002) However, the identity of the channels underlying these conductances is not known. Of those channels that give rise to a transient current, Kv4.2, Kv4.3, and Kv1.4 are expressed in the DCN (Fitzakerley et al. 2000;

Serodio and Rudy 1998). Not only does  $I_A$  potentially affect the pattern of spiking, but it can also affect the timing of spikes in relation to inhibition. When small hyperpolarizations resembling IPSPs are presented to a pyramidal cell, the timing of the first spike following such hyperpolarizations is altered in model pyramidal cells (Kanold and Manis 2005a). With this interaction of small hyperpolarizing currents and  $I_A$ , cells can encode a memory of inhibition since spikes following IPSPs are delayed. Because transient potassium conductances appear to shape the observed output pattern of pyramidal cells, it is important to understand the precise role of  $I_A$  in pyramidal cells information processing.

In this study, we sought to determine whether blocking  $I_A$  produces the same effect in pyramidal cells in a slice preparation as suggested by the pyramidal cell models. We used recombinant heteropodatoxin-2 (rHpTx-2), a peptide toxin that specifically blocks Kv4 channels, which give rise to rapidly inactivating transient potassium currents. RHptx-2 was effective at blocking the transient potassium current (both fast and slow components) in outside-out patches pulled from the somata of pyramidal cells. In addition, in current clamp recordings, it also shortened first spike latency (FSL) in pyramidal cells that were given a hyperpolarizing pre-pulse followed by a depolarizing current step. Subtracting the  $I_{Af}$  from pyramidal cells with dynamic clamp gave similar results to blocking the currents with the toxin, and rescue of  $I_{Af}$  with dynamic clamp after blocking the transient currents with rHpTx2, suggest that the fast component of the transient current is both necessary and sufficient to produce the voltage dependent discharge patterns. These results also suggest that either Kv4.2 or 4.3 is the channel responsible for this current in these cells.

### 3.2 Materials and Methods

**Slice Preparation.** Sprague-Dawley rats, postnatal day 10-14 were deeply anesthetized with ketamine (100 mg/kg),-xylazine (10 mg/kg). Following decapitation the brainstem was removed and trimmed to a block of tissue that included the DCN. The block was mounted on agar supports, sliced in the trans-strial plane (250  $\mu\text{m}$ ) (Blackstad et al. 1984), and stored in an incubation chamber for 1-2 hours at 34° C. All experiments were carried out under protocols approved by the Institutional Animal Care and Use Committed of the University of North Carolina. Slices were transferred to the recording chamber and held in place by a net. The recording solution was perfused at 3-5 mL/ min at 34°C.

**Solutions.** The dissection and slicing procedure was carried out in a low  $\text{Ca}^{2+}$ /high  $\text{Mg}^{2+}$  solution that contained the following (in mM), 122 NaCl, 3 KCl, 1.25  $\text{KH}_2\text{PO}_4$ , 25  $\text{NaHCO}_3$ , 20 glucose, 2 myo-inositol, 2 sodium pyruvate, 0.4 ascorbic acid, 0.1  $\text{CaCl}_2$ , and 3.7  $\text{MgSO}_4$ . Recording solution was the same as above except it contained (in mM) 2.5  $\text{CaCl}_2$  and 1.3  $\text{MgSO}_4$ . Solutions were continuously equilibrated with 95%/5%  $\text{O}_2/\text{CO}_2$  at 34°C to maintain pH at 7.3-7.4. Osmolarity of the solution ranged from 310-320 mOsm. Strychnine (2  $\mu\text{M}$ ) was added to the bath in all experiments to block glycinergic IPSPs. In experiments using recombinant heteropodatoxin-2 (rHpTx-2) and BDS-1, glutamatergic EPSPs were blocked with D-AP-5 (50  $\mu\text{M}$ ) and CNQX (20  $\mu\text{M}$ ). rHpTx-2 was either diluted into the recording solution (100 nM) or puffed onto outside-out patches from a puffer pipette (1  $\mu\text{M}$ ). BSA-1 was diluted in a perfusion pipette at 1 $\mu\text{M}$ . BSA (0.1%) was always added to the solution containing rHpTx or used alone in control experiments.

The electrode solution contained the following (in mM), 4 NaCl, 130 potassium gluconate, 0.2 EGTA, 10 HEPES, 2  $\text{Mg}_2\text{ATP}$ , 2  $\text{Mg}_2\text{GTP}$ , and 2 creatine phosphate. All

chemicals were obtained from Sigma Aldrich (St. Louis, MO) with the exception of AP-5 and CNQX which were obtained from Tocris Bioscience (Ellisville, MO) and rHpTx-2 and BDS-1, which were obtained from Alomone Labs (Jerusalem, Israel)

**Recording.** Electrodes were pulled from 1.5 mm diameter KG-33 glass (Garner Glass, Claremont, CA) to a tip diameter of 1-2  $\mu\text{m}$  and a final tip resistance of 2-7  $\text{M}\Omega$  on a p-2000 Sutter puller. The tips were coated with Sylgard 184 (Dow Corning, Midland, MI) to decrease pipette capacitance. The slices were transferred to the recording chamber on a fixed stage, upright microscope and visualized with a 40X, 0.75 NA or 63X, 0.9 NA water immersion objective using video-enhanced differential interference contrast illumination in infrared light. Pyramidal cells were selected based on shape and spiking patterns. Current clamp recordings in slices and voltage-clamp recordings from outside-out patches were made using standard techniques with a Multiclamp 700A amplifier (Molecular Devices, Foster City, CA). Outside-out patches were pulled from the cell body after obtaining the whole-cell configuration by retracting the electrode from the cell and monitoring the increase in input resistance and decrease in capacitance. rHpTx-2 or BSA was then applied onto the patch by a puffer pipette that was placed upstream in the chamber and in close proximity to the patch pipette. Data acquisition was carried out under computer control with a custom software program written in Matlab (The Mathworks, Natick, MA) using high-speed, 12 or 16 bit A-D boards (National Instruments, Austin, TX) with a sampling rate of 50 kHz. All voltages were corrected for a -12 mV electrode-bath junction potential during analysis.

**Dynamic Clamp.** We implemented the Real-Time Linux Dynamic Clamp system developed by Dorval and colleagues (Dorval et al. 2001). The dynamic clamp was run on a second acquisition computer (Intel Pentium P4, 2.8 GHz) running Linux (Fedora 3.0, RedHat,

Raleigh, NC) and using a 16-bit National Instruments A/D-D/A card (NI6052E), in parallel with the primary acquisition system. The dynamic clamp system operated at 20-40 kHz. To subtract or add the rapidly-inactivating potassium conductance ( $g_{Af}$ ), we implemented the model of Kanold and Manis (2001; 1999), scaled from 22 to 34° C assuming a  $Q_{10}$  of 3 for the channel kinetics.

***Stimuli.*** Noise current stimuli were used in some experiments similar to those we have reported before (see chapter two). Briefly, a rectangular DC current pulse was shaped using  $\cos^2$  ramps to minimize onset and offset transients. This current was then superimposed with a low-pass (500 Hz) filtered (8-pole Butterworth digital filter) noise current. A simulated IPSP (sIPSP) consisting of 3 summed alpha waves [ $I(t)=I_{\max} * \alpha * t * \exp(-\alpha * t)$ ;  $\alpha=0.1 \text{ msec}^{-1}$ ], separated by a 15 msec interval was added to the stimulus with a delay of 500 msec to compare the time of the first spike after the sIPSP with and without the toxin.

***Analysis.*** The digitized current and voltage traces were stored in a Matlab file and were then analyzed using custom Matlab routines. In whole cell experiments, changes in first spike latency (FSL) were used to determine if blocking Kv4 channels changed the discharge patterns of pyramidal cells. The average FSL was calculated by presenting the cell with a hyperpolarizing pre-pulse (either -300pA or -100pA) followed by a depolarizing current pulse for 21 consecutive trials with and without either the toxin or BSA. The mean and standard deviation (SD) of each FSL for each condition within a cell was then compared using a paired t-test to determine statistical significance.

Data analysis was performed with Matlab 7.1. Statistics were calculated using both Matlab 7.1 and Prism 3.0 (GraphPad Software, Sand Diego, CA). All numerical data are

presented as means +/- SD. Statistical tests of hypotheses used one or two-sided, paired or unpaired (as appropriate) t-tests.

### **3.3 Results**

#### **3.3.1 rHpTx-2 blocks $I_A$ current in pyramidal cells**

To determine whether the transient outward current in pyramidal cells could be blocked by rHpTx-2, we pulled somatic outside-out patches from pyramidal cells. We first assessed the amount of current in the outside-out patches by stepping the patches to 40mV for 300 msec. Each depolarizing voltage step was presented twice. In the first trial, the 40 mV step was preceded by a conditioning hyperpolarizing pre-pulse to -100 mV for 300 msec. In the second trial, the step was preceded by a conditioning pre-pulse to -30mV for 300 msec. The first conditioning pre-pulse was given to remove any inactivation of the channels that give rise to  $I_A$  (Figure 3.1A). The -30 mV pre-pulse inactivated the rapidly inactivating transient potassium channels so that the only current elicited during the depolarizing step was the non-inactivating or slowly-inactivating potassium current. Each series of voltage steps was given 4 times, and the currents were averaged across trials. We then subtracted the current elicited with the conditioning pre-pulse of -30mV from the hyperpolarizing conditioning pre-pulse to estimate the inactivating potassium current (Figure 3.1B black trace).

Next, a perfusion pipette filled with recording solution, 1 $\mu$ M rHpTx-2 and 0.1%BSA was placed near to the patch of membrane and pressure was gently added to the pipette to puff the toxin onto the outside-out patch. Transient outward currents were decreased in the presence of the toxin (Figure 3.1B red trace).

Currents can slowly run down in outside-out patches. Therefore we did a control experiment with only 0.1% BSA in the perfusion pipette to ensure that the decrease in current was solely due to the presence of the toxin. Only small decreases in the current was observed when BSA was puffed onto the patches, revealing that the decrease in current was due to rHpTx-2 blocking channels (Figure 3.1C).

To compare the effect of the toxin to the effect of BSA we fit both the subtracted current and the non-subtracted current with a double exponential fit to measure the amplitude of both inactivating components of the outward current (figure 3.1A, dashed white lines). For all patches that could be fit with a double exponential function, the mean fast decay constant was 31.4 msec with a SD of 14.25 msec (N=24). The slow decay time constants had a mean of 250.1 msec and a SD of 166.0 msec (n=24). By constraining the values obtained for the fast and slow time constants in the control traces, we then fit the currents in the outside-out patches after the rHpTx-2 was applied to determine the new current amplitudes with the channel blocked (Figure 3.1B). We then calculated a ratio of the post-treatment maximum amplitude of current to the pre-treatment current and compared the mean values with a t-test. The average current for patches receiving toxin was 61% of the original current. This was significantly different than those patches that received BSA instead of the toxin ( $P=0.012$ , mean difference 0.33,  $df=17$ ) (Figure 3.2). However, there was also an effect of the toxin on the slowly inactivating current. We compared the amplitudes of the slow components of the non-subtracted current traces before and after the toxin was applied. The toxin also blocked a fraction of the slowly inactivating current (Figure 3.2) ( $P=.01$ , mean difference 0.43 ,  $df=12$  ).

Figure 3.1

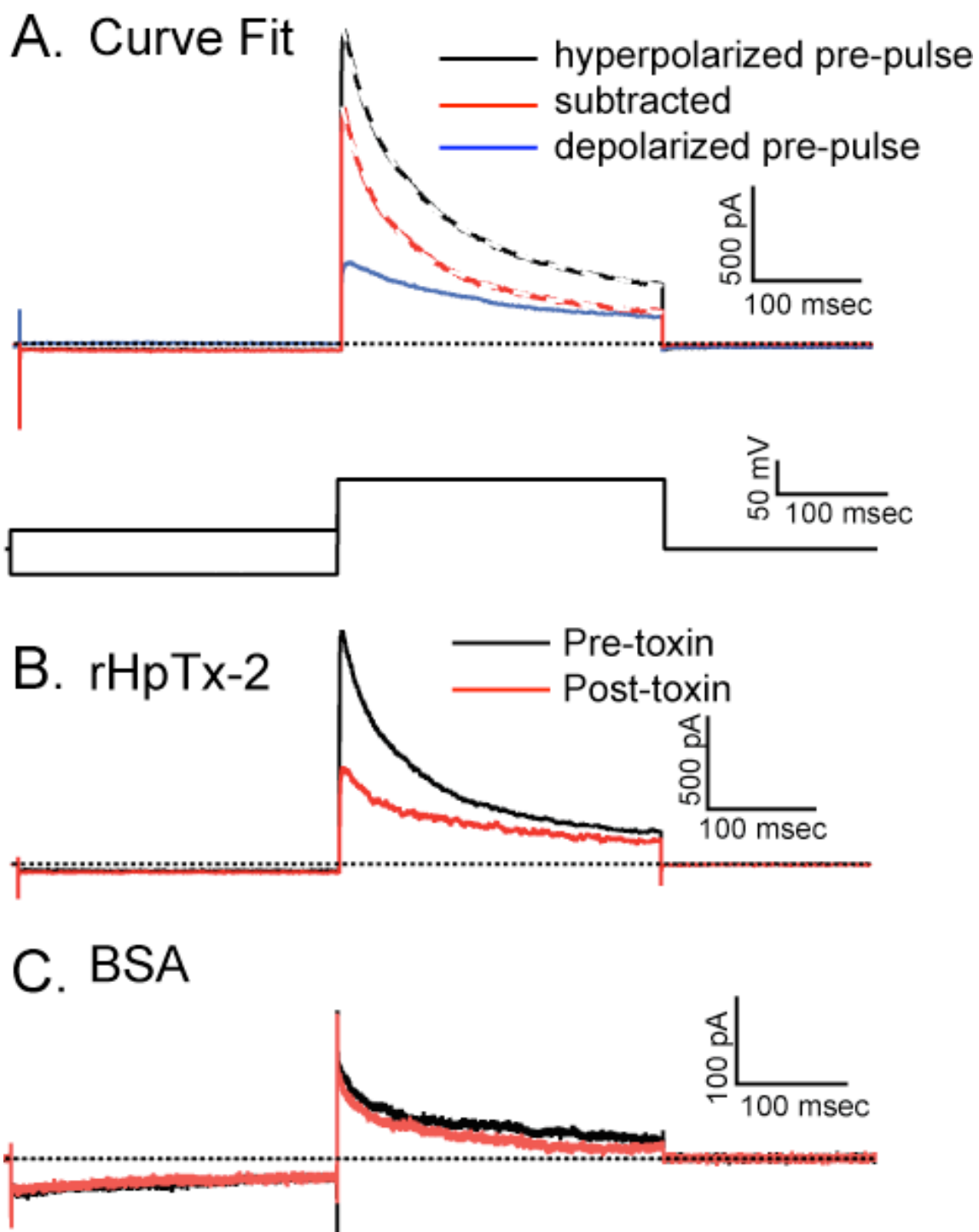


**Figure 3.1** r-Heteropodatoxin blocks outward current in somatic outside-out patches pulled from pyramidal cells.

**A** Outward currents in outside-out patches evoked by depolarizing voltage steps. The black trace is the current measured in one outside-out patch when a -100mV hyperpolarizing prepulse was given to remove inactivation of the rapidly inactivating potassium current. The blue trace is the current measured when the -30 mV prepulse was given to inactivate the rapidly inactivating potassium channel. The red trace is the result of subtracting the blue trace from the black trace to isolate the rapidly inactivating current. The dashed lines denote double exponential fits of the currents.

**B** Subtracted outward currents in one outside-out patch evoked by a depolarizing voltage step either in the absence (black trace) or presence of rHpTx-2 (red trace)

**C** Subtracted outward currents in one outside out patch either in the absence (black trace) or presence of BSA (red trace).

Figure 3.2

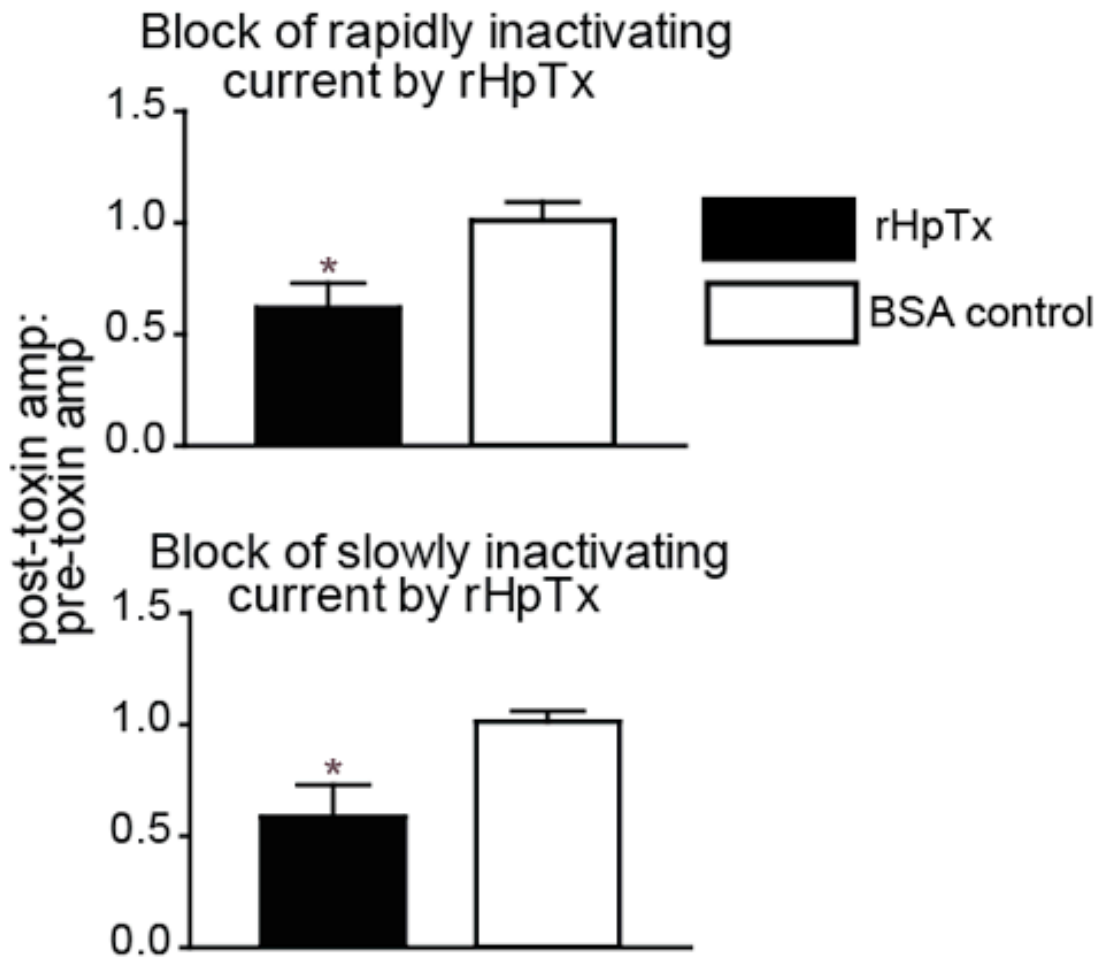


**Figure 3.2** Group data comparing the amplitudes of double exponential fits of the fast and slow components of the currents. Comparison was done by calculating a ratio of post toxin/BSA:pre toxin BSA current amplitudes and statistical significance was assessed by a t-test. Both groups are statistically different ( $P < 0.01$ )

### 3.3.2 rHpTx-2 alters the build-up response pattern

We have previously proposed that  $I_A$  solely determines the latency to the first spike that is observed when a hyperpolarizing current pulse precedes a depolarizing current pulse (Kanold and Manis 2001; 1999; Manis 1990). To ascertain whether  $I_A$  controls the timing of the first spike latency in intact DCN slices, we added 100 nM rHpTx-2 to the recording solution and tested the response of the cells to current steps.

To elicit action potentials whose latency is predicted to depend on the availability of the  $I_{Af}$ , we presented a depolarizing current step that was preceded by a hyperpolarizing current pulses that ranged from -500 pA to 250 pA for 100 msec to the cells. As the channels inactivated with more depolarized pre-pulse current, the FSL decreased. This effect can be seen when FSL is plotted as a function of pre-pulse membrane potential (Figure 3.3 Ab, Bb, black lines).

When we added rHpTx-2 to the bath solution to block  $I_A$ , the FSL of the depolarizing current step was decreased (Figure 3.3 A,B red traces). In some cells the FSL became quite short and, in addition, the firing rate increased (Figure 3.3B). In other cells only the FSL decreased, without a concomitant change in firing rate (Figure 3.3A). However, for all hyperpolarizing pre-pulse voltages, the FSL was decreased (Figure 3.3 Ab and Bb, red line). To certify that the change was due to the specific effect of rHpTx-2 rather than non-specific effects from the BSA or changes in the cell during the duration of the experiment, we also carried out control experiments where rHpTx-2 was eliminated from the bath and only BSA was added. In these experiments there was no effect on FSL (Figure 3.4A).

**Figure 3.3**

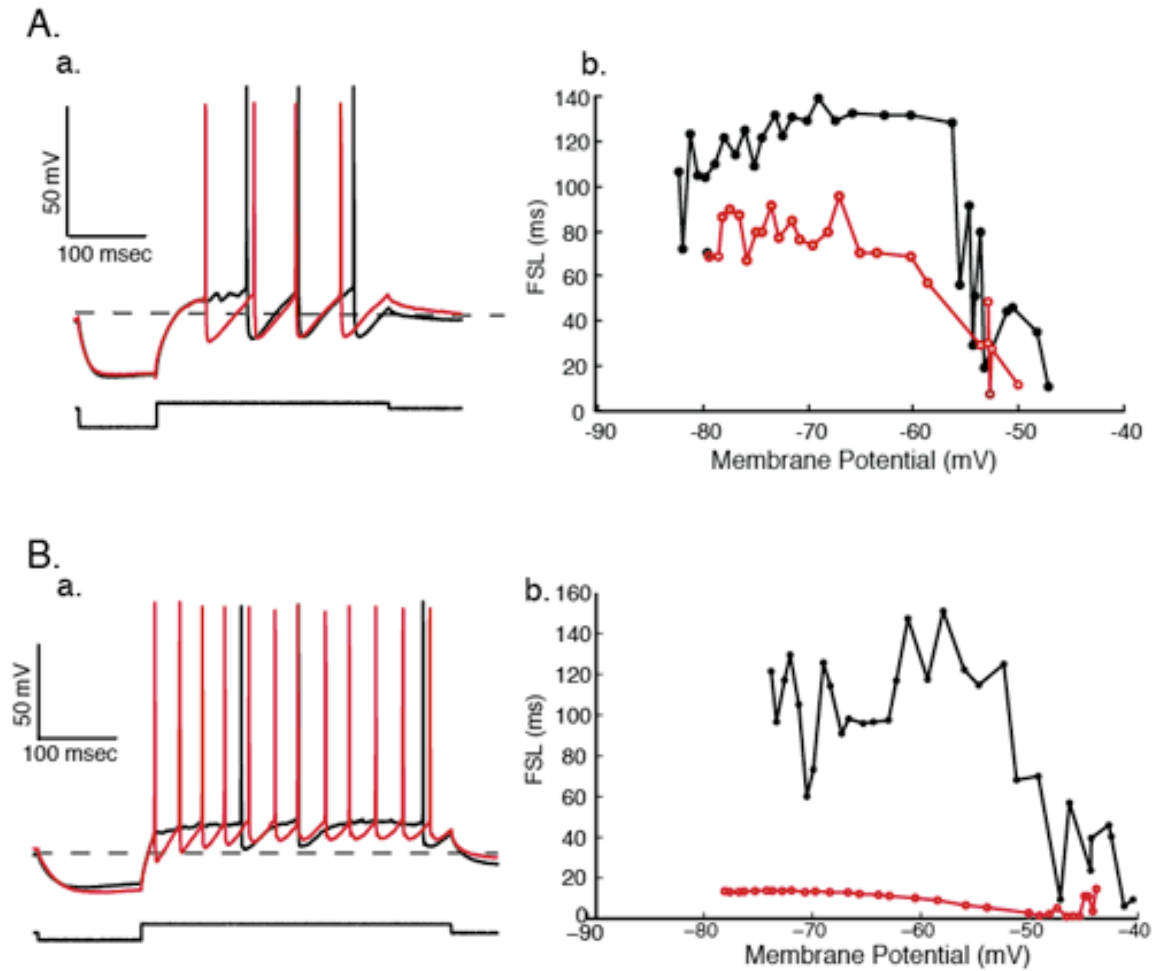


**Figure 3.3** rHpTx-2 reduces the FSL when a hyperpolarizing pre-pulse is presented to the cell prior to a depolarizing current pulse.

**A** Example of a single cell response before (black trace) and after (red trace) application of 100 nM rHpTx-2. a. A single trace depicting a typical cell before (black trace) and after (red trace) rHpTx-2 was added to the bath solution. b. A graph showing the membrane potential during a hyperpolarizing pre-pulse that was sequence from -500 pA to 250 pA by 50 pA steps, and the resulting FSL.

**B** Same as in A except this cell shows a complete reduction of FSL when rHpTx-2 was applied to the bath.

**Figure 3.4**

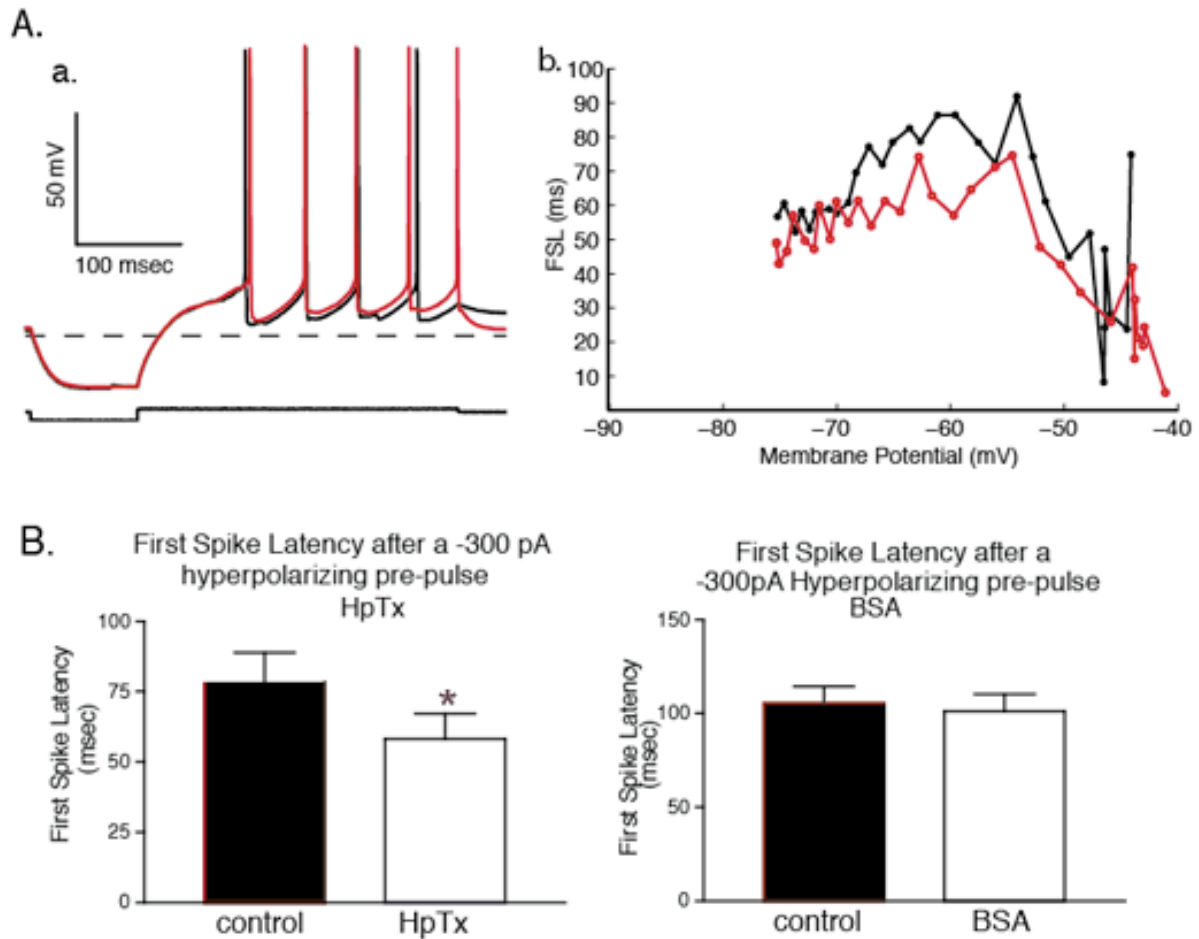


**Figure 3.4** BSA does not cause a shift in FSL when applied to DCN pyramidal cells but rHpTx does cause a shift.

**A** Example of a typical cell's response to a hyperpolarizing pre-pulse when only 1% BSA was added (red trace) to the bath solution.

**B** Comparison of the FSL before and after either the rHpTx-2 or BSA was added to the bath. 21 trials of the same stimulus that included a -300 pA pre-pulse followed by a depolarizing current pulse were presented to the cells before and after rHpTx-2 (a) or BSA (b) was added to the bath. The mean and SD of the FSL were calculated for each cell and each condition and then compared using a paired t-test to determine statistical significance. The difference in FSL is statistically significant for the cells that received rHpTx-2 ( $P < 0.01$ ).

To compare the effect of blocking Kv4 channels with rHpTx-2, we presented the cell with 21 trials of a -300pA hyperpolarizing current pulse followed by a depolarizing current pulse and calculated the mean and SD of the FSL with and without the toxin. We then compared these values with a paired t-test to determine statistical significance. In the presence of rHpTx-2, the FSL was decreased ( $P=0.01$ , mean difference=20.21msec,  $n=12$ ) (Figure 3.4B). Adding BSA alone had no effect on the FSL ( $P=.1192$ , mean difference=4.3 msec,  $n=11$ ) (Figure 3.4B). The results were the same when a -100pA pre-pulse was used (data not shown).

### **3.3.3 Blocking $I_A$ increases action potential width**

Not only does  $I_A$  control the FSL, it has also been reported to control action potential width (Kim et al. 2005). Changing the width of the action potential alters the amount of calcium that enters the cell during an action potential; the wider the action potential, the more calcium (Hoffman and Johnston 1999; Hoffman et al. 1997; Johnston et al. 1999; Mitterdorfer and Bean 2002). Since calcium signaling is important in many types of synaptic plasticity, regulating action potential width might be one mechanism by which  $I_A$  influences synaptic plasticity. We therefore compared the width of action potentials elicited by a depolarizing current pulse in pyramidal cells, before and after rHpTx-2 exposure.

To calculate action potential width, we measured action potential height for each spike. We then measured the length of time it took for the action potential to rise from its half-height to the peak. This value became the first half-width or half-width A (HWA) and indicates the depolarizing phase of the action potential (rise time). The second half-width was then the time it took for the membrane potential to return from the action potential peak to the same voltage on the repolarizing phase. This time is denoted as half-width B (HWB).

Adding these two values together gives the total half-width (THW). With rHpTx-2 added to the bath, the action potential width increased (Figure 3.5). As expected, the greatest increase was in the repolarizing phase of the action potential or HWB ( $P < 0.01$ ). However, the THW was also increased significantly ( $P < 0.05$ ). Therefore, either the fast or slow component of  $I_A$  plays a role in the repolarization phase of the action potential. Without this current, the action potential is wider.

### **3.3.4 $I_A$ alters the timing of spikes after inhibition**

Inhibition engages Kv4 channels by removing inactivation, thereby enabling the channels to open upon subsequent depolarization. When model pyramidal cells are tested with small IPSP-like pulses, the timing of spikes is affected for more than 100 msec, but when  $I_A$  is removed from the model, this effect disappears (Kanold and Manis 2005a). We have also recently shown that DCN pyramidal cells can fire reproducible trains of action potentials when presented with time varying noise currents, and inhibition can increase the reproducibility of spikes for as long as 300 msec after a sIPSP is present in the stimulus (see Chapter Two). We therefore decided to test whether transient potassium currents alter the precision of spike times after a sIPSP presented during a noise current pulse stimulus.

The cells were presented with a noise current pulse (max amplitude 500 pA peak to peak) that had a sIPSP imposed on the waveform at 500 msec. The same stimulus was presented for a total of 100 trials so that the reproducibility of spike times over many trials of the same stimulus could be assessed. The sIPSP typically caused the cells to cease firing (Figure 3.6A). The first spike after the sIPSP is more precise than spikes that come later in the spike train. Blocking Kv4 channels with rHpTx-2 improved the reliability of the spike occurring immediately following the sIPSP (Figure 3.6B). The first spike after the sIPSP in

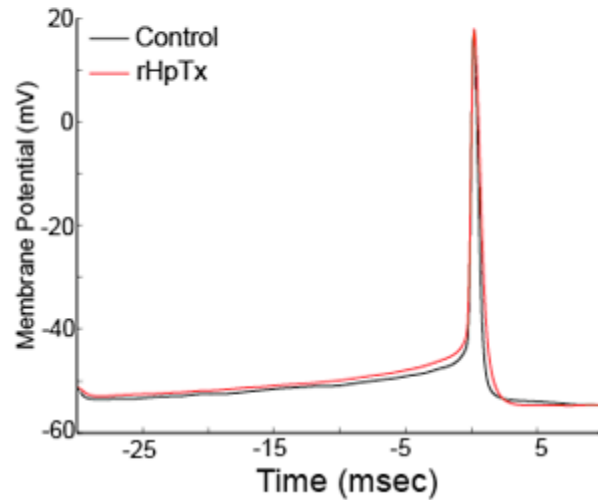
the presence of the toxin is more likely to occur on an earlier depolarizing event, instead of being delayed until a later event. To compare this effect, we calculated the standard deviation of the first spike time with and without the toxin. The standard deviation of the first spike after the sIPSP was improved when the channels were blocked with rHpTx-2 (paired one-tailed t-test  $P=0.027$ , mean difference = 5.386 msec,  $N=7$ ) (Figure 3.6C). Before the rHpTx-2 was added, some of the first spikes after the sIPSP were delayed by tens of milliseconds causing the reliability of the first spike to be low. However, after the rHpTx-2 was added to the bath, the first spike after the sIPSP arrived at the same time, corresponding to the same event, in most of the trials. Only the timing of the first spike after the sIPSP improved after blocking  $I_A$ . The precision of spike times for the entire 500 msec after the sIPSP was not affected by rHpTx-2 (data not shown).

### **3.3.5 BDS-1 does not block $I_A$ in pyramidal cells**

Other Kv channels can also give rise to  $I_A$  currents. For example, Kv 3.4 channels have rapid inactivation, although they activate at more depolarized voltages than Kv4 channels (Baldwin et al. 1991; Jerng et al. 2004). We used BDS-1 to selectively block Kv3.4 channels to determine if other Kv channels made up a portion of the rapidly inactivating current. In 5 pyramidal cell somatic outside-out patches, BDS-1 was ineffective in blocking the rapidly-inactivating current. One example patch is shown in Figure 3.7. Since the kinetics and pharmacology of the rapidly-inactivating current in pyramidal cells does not match that of Kv3.4 (Kanold and Manis 1999), we did not further investigate this channel in pyramidal cells.

**Figure 3.5**

**A.** Blocking Kv4.x channels increases AP half-width



**B.**

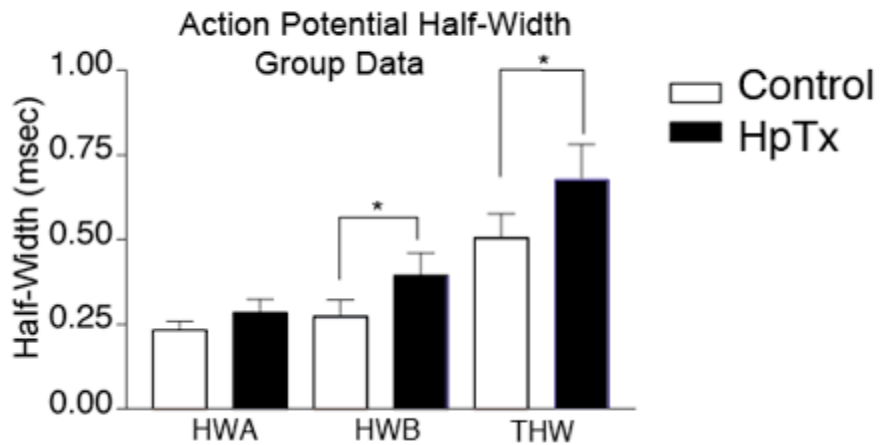


**Figure 3.5** Blocking Kv4 channels with rHpTx-2 increases the width of the action potential.

**A** The average waveform of action potentials evoked with a depolarizing current pulse. When rHpTx-2 was added, the action potential width was increased.

**B** Group data showing increase in action potential half-width. The length of the repolarization phase was increased (HWB) which also significantly increased the total length of the action potential (THW) ( $P < 0.05$ )

**Figure 3.6**

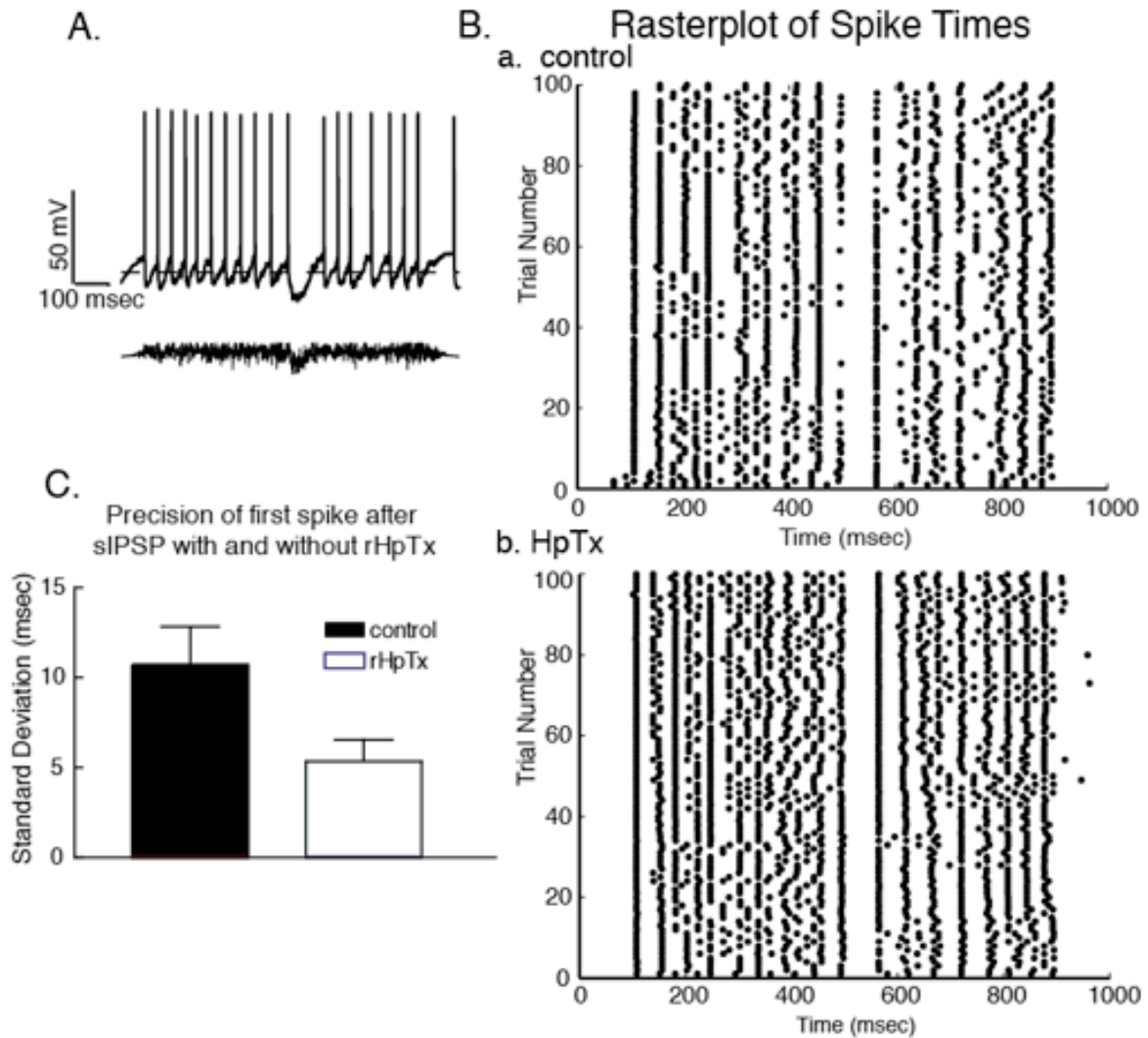


**Figure 3.6** rHpTx-2 increases the reliability of the first spike time when a sIPSP is superimposed on a noise current stimulus.

**A** An example of the noise current stimulus with a superimposed sIPSP at t=500 msec and the resulting spike train.

**B** Rasterplot of spike times for a typical cell when the cell was presented with the stimulus in A before (a) or after (b) rHpTx-2 was applied to the cell. **C.** Comparison of the standard deviation of the first spike time after the sIPSP before and after rHpTx-2 application. rHpTx-2 was able to improve the reliability of the first spike time ( $P < 0.05$ , paired one-sided t-test).

**Figure 3.7**

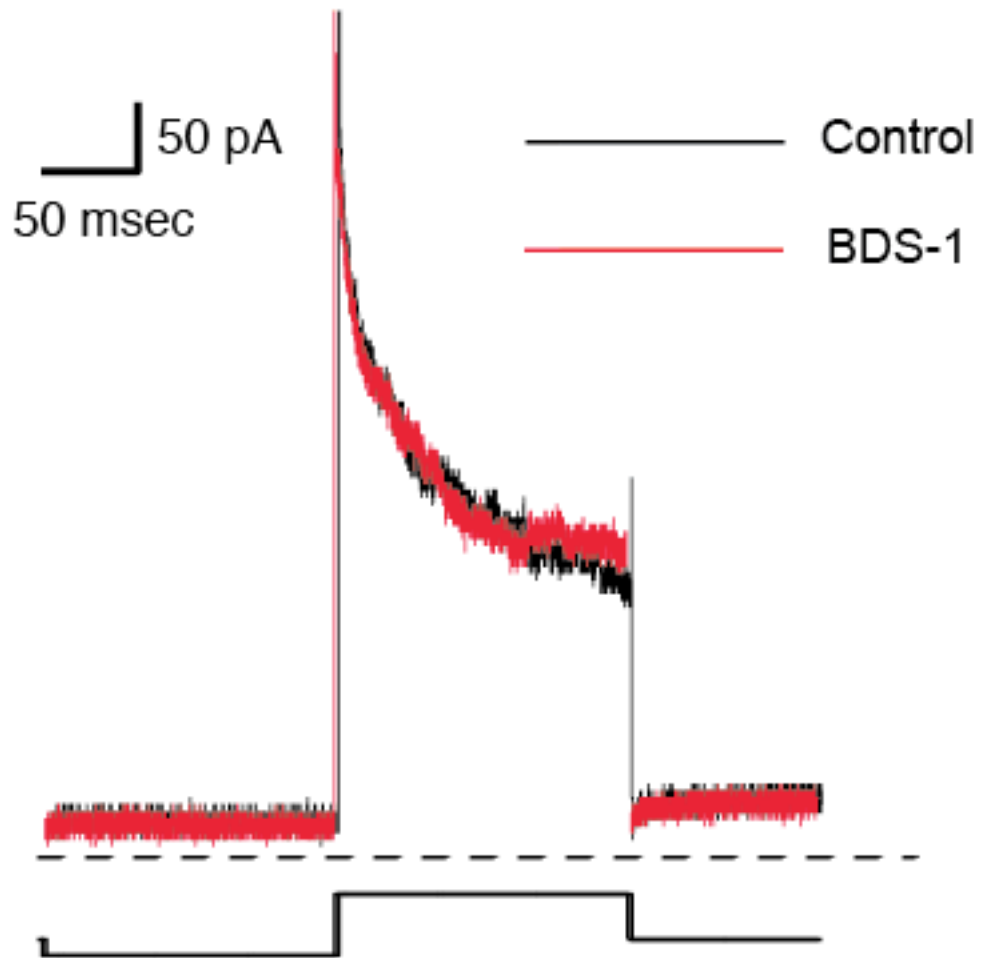


**Figure 3.7** BDS-1 does not block  $I_A$  in outside-out patches pulled from pyramidal cell somata. Outside-out patches were pulled from pyramidal cell somata and  $I_A$  was stimulated by a depolarizing current pulse preceded by a hyperpolarizing current pulse to remove inactivation (black trace). When BDS-1 was puffed onto the patch by a perfusion pipette, there was no difference in the current (red trace).

### 3.3.6 Subtraction of $I_A$ with Dynamic Clamp

While the data above suggests that the rapidly inactivating current indeed plays a role in first spike latency, the potential non-specific effects of the rHpTx-2, including those on spike shape and on the slowly inactivating current, make it uncertain what role  $I_{Af}$  plays relative to  $I_{As}$ . To address this, we performed two experiments. In the first, we used dynamic clamp to subtract the current generated by the rapidly-inactivating potassium channel from the current injected into the cell by subtracting the amount of conductance of the  $I_{Af}$  channels ( $g_{Af}$ ) from the cell. By subtracting the modeled current in dynamic clamp, we can determine if the modeled current is the same as that blocked with the toxin. We implemented the model developed by Kanold and Manis (2001, 1999) in our dynamic clamp system.

To estimate the current generated by  $I_{Af}$  in each pyramidal cell, we titrated the conductance of the channel until the FSL in a train of action potentials elicited by a depolarization was unaffected by pre-hyperpolarization (Figure 3.8A-B). Subtracting more  $g_{Af}$  with the dynamic clamp decreased the FSL in proportion to how much conductance was subtracted. For all cells there was some value of  $g_{Af}$  that could be subtracted from the cell with dynamic clamp that would completely abolish the FSL. Full reduction of the FSL and elimination of the prehyperpolarization effect required between 150 nS and 700 nS (average value for 9 cells was 601.1 nS, sd=171.1 nS). Subtraction of  $I_{Af}$  with dynamic clamp gave similar results to blocking Kv4 channels with rHpTx-2. The FSL decreased with higher values of  $g_{Af}$  subtracted from the cell. While a maximum value of  $g_{Af}$  could always be subtracted to dissipate all the effects of the prehyperpolarization, smaller subtracted values of  $g_{Af}$  caused the FSL to decrease incrementally.

Figure 3.8

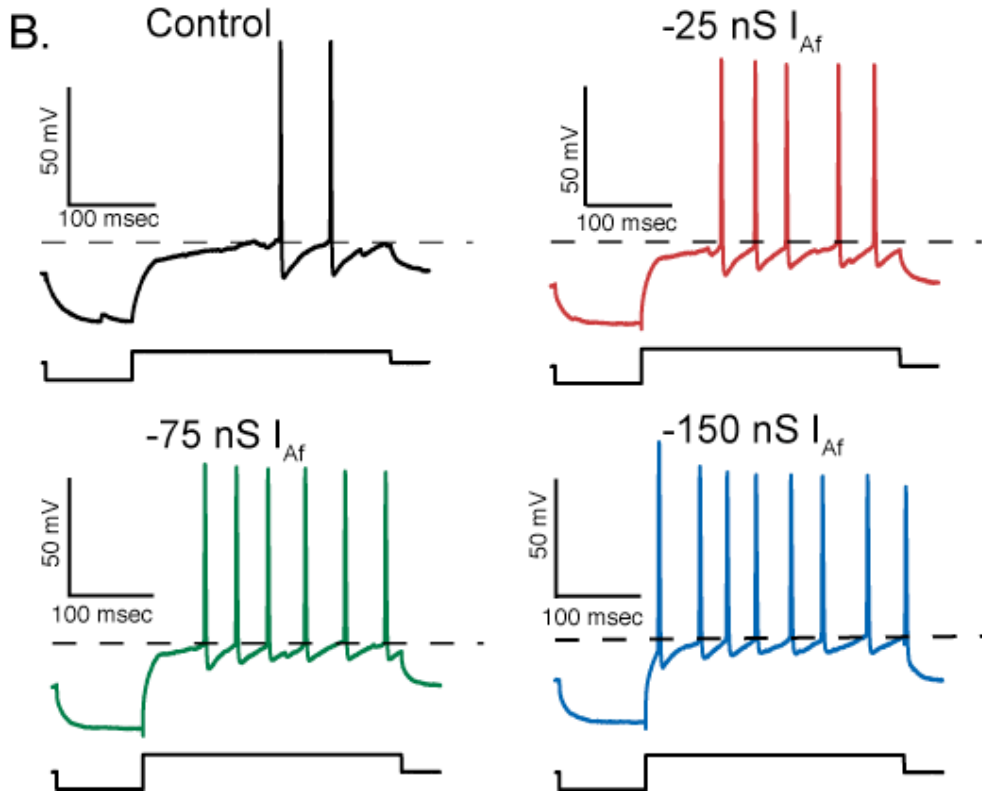
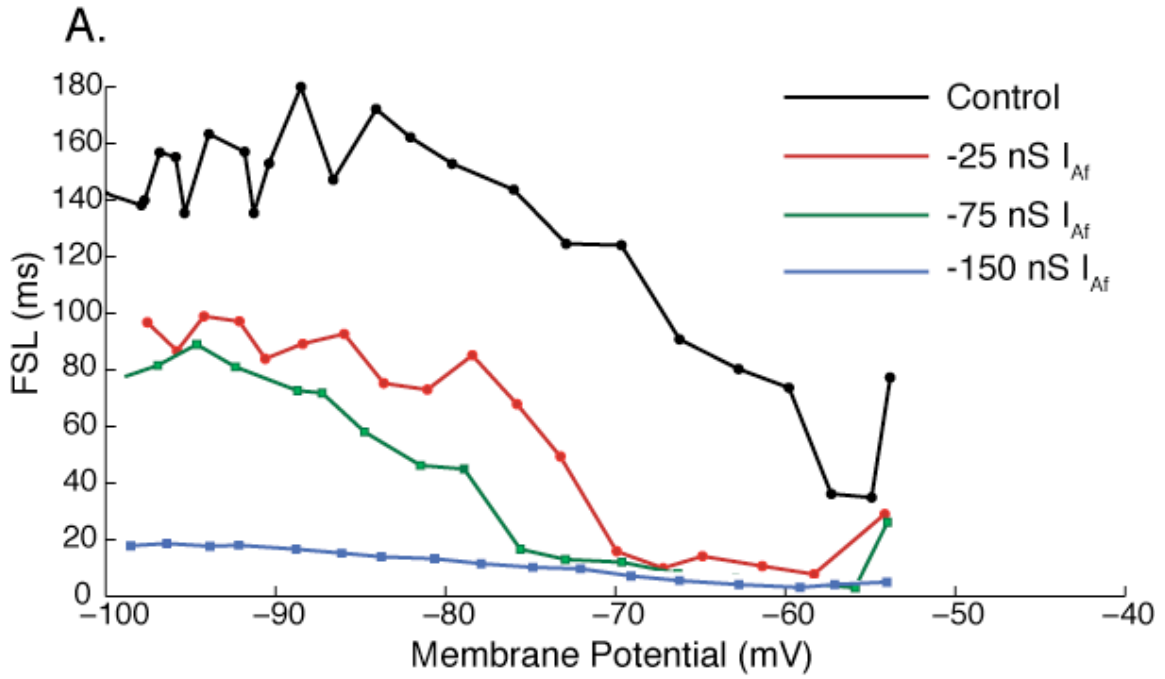


**Figure 3.8** Subtracting  $I_{Af}$  with dynamic clamp reduces the FSL in a similar fashion to rHpTx-2 application.

**A** Plot depicting the FSL in response to the membrane potential during a hyperpolarizing pre-pulse. The hyperpolarizing pre-pulse was sequence -500pA to 250pA in 50 pA steps and the membrane potential at each step was plotted against the FSL. Each line shows the FSL that results when increasing levels of  $g_{Af}$  were subtracted from the cell.

**B** An example of a -300 pA pre-pulse and the resulting spike train at different levels of subtracted  $g_{Af}$ . The colors of the voltage traces correspond to the colors of the lines in A.

We then used the value for  $g_{Af}$  that effectively abolished the FSL after the hyperpolarizing pre-pulse to determine if subtracting  $I_{Af}$  with dynamic clamp also improved the precision of the first spike after a sIPSP in a noise current pulse. Indeed, subtracting modeled current during a noise stimulus significantly decreases the standard deviation of the first spike time after the sIPSP (Figure 3.9A-B), similar to the effects of rHpTx-2. The cells fired spikes more frequently on the first depolarizing event after the sIPSP. This result was similar the effect elicited with rHpTx-2, in that the standard deviation of the first spike is decreased significantly (Figure 3.9C) ( $P < 0.05$ ,  $DF = 7$ , mean difference = 4.09), while the precision of the subsequent spike is unaffected. This result is expected because the current rapidly inactivates (within 80 msec), so the effect is short-lived. Thus,  $I_{Af}$  only affects the spike timing precision transiently, and  $I_{Af}$  alone is necessary for this effect.

Figure 3.9

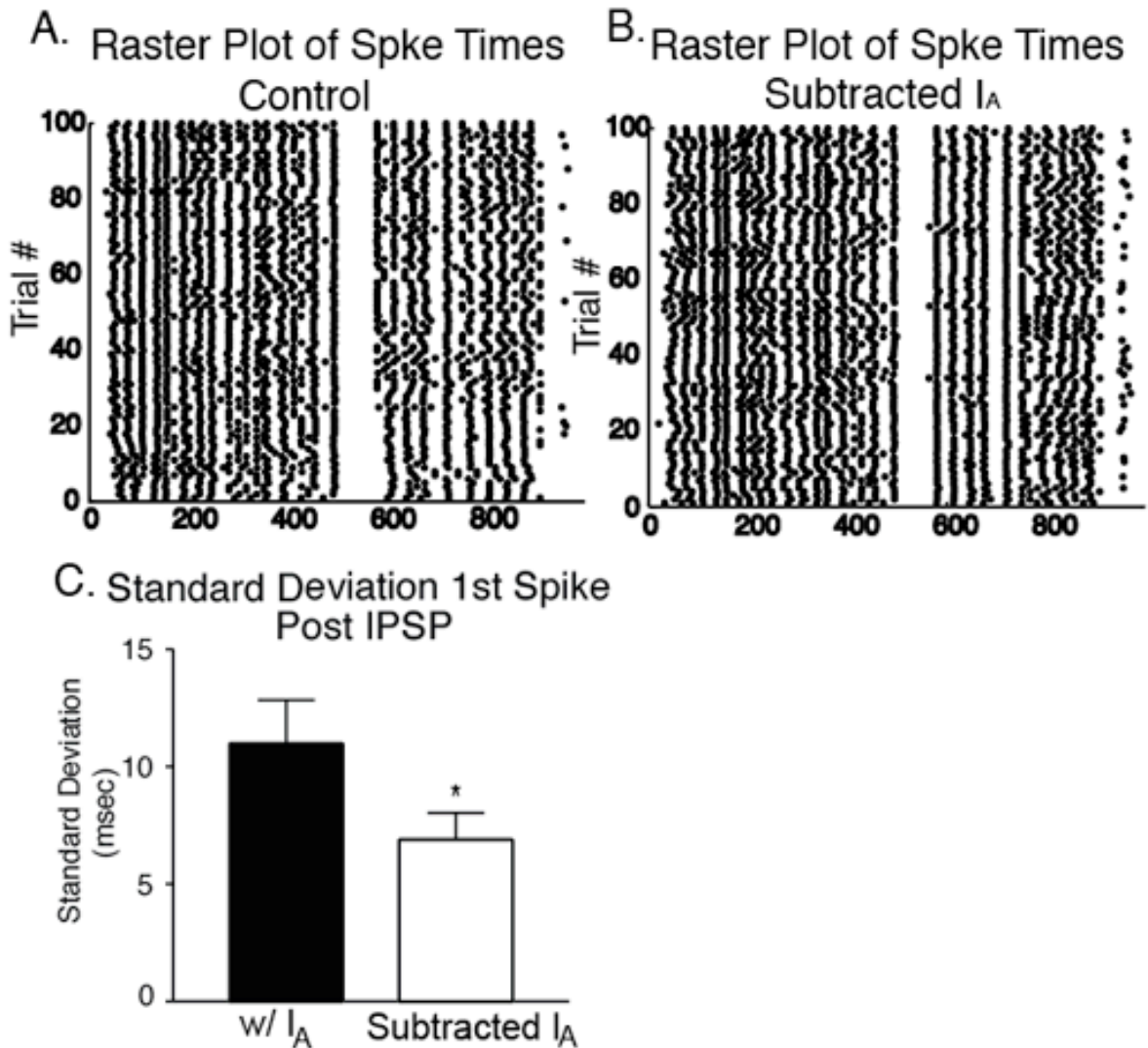


**Figure 3.9** Subtracting  $I_{Af}$  improves the precision of the first spike time when a sIPSP is superimposed on a noise current pulse.

**A-B** Rasterplot of spike times in spike trains of a typical cell when a noise current pulse that contains a sIPSP at 500 msec is presented to the cell in the presence (A) or absence (B) of  $I_{Af}$ .

**C** Comparison of the standard deviation of the first spike time after the sIPSP. The increase in precision with subtracted  $I_{Af}$  was statistically significant when compared with a one-sided, t-test ( $P < 0.01$ ).

In the second set of experiments, we tested whether  $I_{Af}$  was sufficient to generate the delay in spike times, by using  $I_{Af}$  introduced by dynamic clamp to rescue the block of Kv4 channels by rHpTx-2. We first applied the hyperpolarizing pre-pulse step protocol to pyramidal cells to measure FSL as a function of pre-pulse membrane voltage. We then added rHpTx-2 to the bath and again measured the FSL after a hyperpolarizing pre-pulse. In 3 out of 11 cells, rHpTx-2 had no effect on the FSL. In the remaining 8 cells, rHpTx-2 either partially decreased the FSL (4 cells) or completely abolished the FSL (4 cells). We then added the  $I_{Af}$  current back to the cell with dynamic clamp to attempt to rescue the block of Kv4 channels. The FSL could be restored to control or near control values in all 8 cells that were affected by rHpTx-2 (Figure 3.10A). By adding  $g_{Af}$  of 300 to 450 nS, the ability to produce long FSL was rescued, and the FSL could return to pre-toxin values (Figure 3.10B). We also observed that the rHpTx-2, as in previous experiments, increased the firing rates of the cells. Adding back the modeled current with dynamic clamp, however, did not restore the firing rate to pre-toxin levels. Thus, while it is likely that the model of the transient potassium current and the current that is blocked with rHpTx-2 represent the same current, since removing them from pyramidal cells results decreased FSL, there is a component of the current blocked by the rHpTx-2 that cannot be compensated for by the model  $g_{Af}$  in dynamic clamp. This probably corresponds to the slow current ( $g_{Af}$ ; Kanold and Manis, 1999). In conclusion, by blocking the native current with a toxin specific for Kv4 channels, and then restoring  $I_{Af}$  alone to the cell with dynamic clamp, we were able show that  $I_{Af}$  alone is both necessary and sufficient for the generation of long FSL in DCN pyramidal cells.

**Figure 3.10**

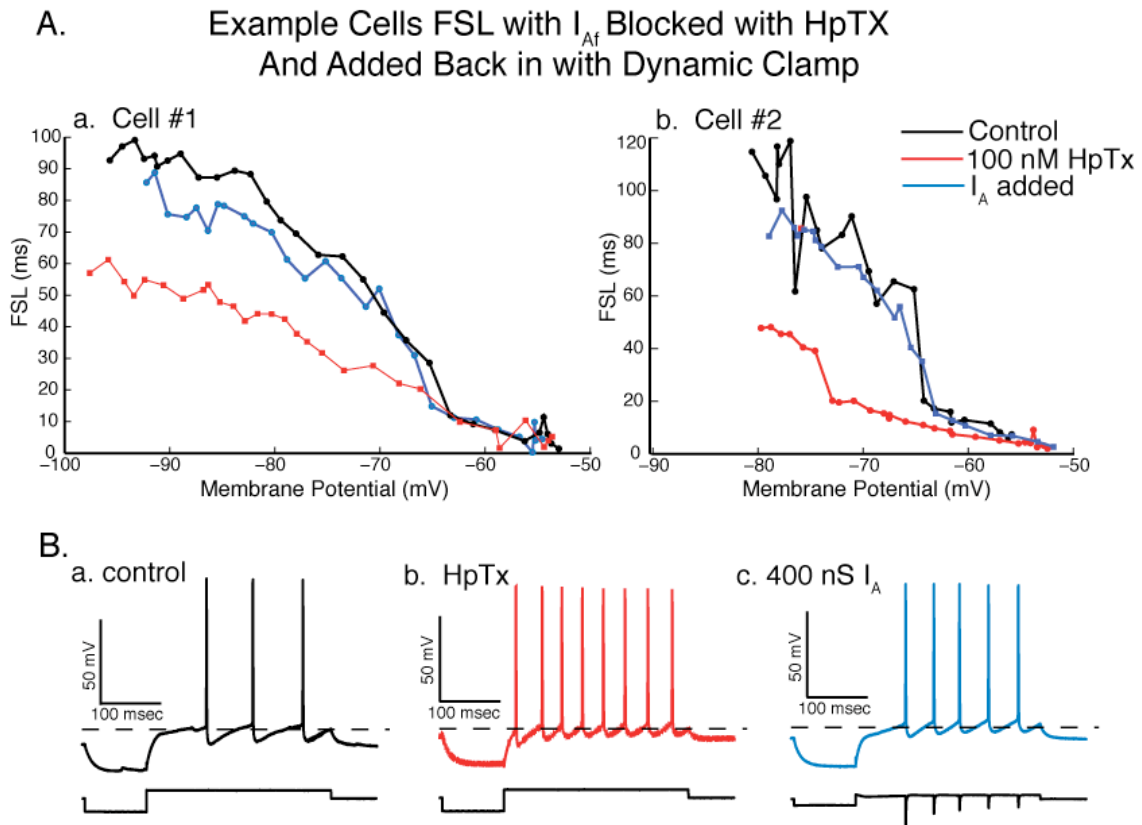


**Figure 3.10** Effects of blocking  $I_{Af}$  with HpTx can be rescued by adding the current back with the dynamic clamp model.

**A** The FSL was plotted as a function of the membrane potential during a sequence of hyperpolarizing pre-pulses ranging from  $-500\text{pA}$  to  $250\text{pA}$  in  $50\text{pA}$  steps (black line). When  $100\text{ nM rHpTx-2}$  was added, the values for FSL were decreased (red line). This effect could be reversed by adding the rapidly inactivating current back with the dynamic clamp (blue line). **a** and **b** are two examples of typical cells with different values ( $a=250\text{ nS}$   $b=400\text{ nS}$ ) of  $g_{KIF}$  added to the cell.

**B** Voltage traces for the cell **Ab** under the different conditions with a  $-300\text{ pA}$  pre-pulse.

### 3.4 Discussion

A low-threshold, rapidly inactivating potassium current is thought to bring about voltage-dependent discharge patterns in pyramidal cells, such as the build-up and pauser responses. We have shown that a toxin, rHpTx-2, blocks this potassium current in outside-out patches pulled from pyramidal cell somata. The build-up pattern, characterized by a long delay to the first spike, was the focus of this study. In previous studies we have shown that the length of the time delay to the first spike is dependent upon the activation of the  $I_A$  current (Kanold and Manis 2001; 1999; Manis 1990). However, these results were predicted using a model of a pyramidal cell. In this study we confirmed that  $I_A$  is responsible for the FSL after a pre-hyperpolarization by using rHpTx-2 to pharmacologically block Kv4 channels in rat brain slices. We then implemented the model of  $I_A$  in dynamic clamp and verified that by subtracting this current from pyramidal cells in slices, we could replicate the FSL decrease we observed when rHpTx-2 blocked the current. Further, after we blocked the channel responsible for this current with rHpTx2, we could rescue the decrease in FSL by adding the modeled  $I_A$  back to the cell with dynamic clamp.

It was shown in Chapter Two that the timing precision of action potentials in response to a noise current stimulus can be improved by adding a simulated IPSP to the stimulus. The precision of the first spike that follows the sIPSP is further improved when  $I_A$  is blocked with rHpTx-2. Removing  $I_A$  from pyramidal cells with dynamic clamp also results in the same improvement in first spike precision. Together, these results suggest that rHpTx-2 blocks the same channel that gives rise to the modeled  $I_A$  current that we have used in previous studies.

### **3.4.1 Identity of $I_A$ current in DCN pyramidal cells**

The heteropodatoxins are peptides that have been shown to selectively block the Kv4 family of potassium channels (Sanguinetti et al. 1997; Wang and Schreurs 2006; Zarayskiy et al. 2005) and rHpTx-2 has been used successfully to block transient potassium currents in neurons and ventricular myocytes (Liss et al. 2001; Wang and Schreurs 2006). While the exact cellular distribution of these channels in the DCN remains unknown, Kv4.2 and Kv4.3 mRNA are both expressed in the DCN (Fitzakerley et al. 2000; Serodio and Rudy 1998). In addition, we have shown that the channel that gives rise to the transient potassium current in DCN cells is blocked by millimolar 4-AP, while being relatively resistant to TEA, and this profile is characteristic of the Kv4 channels (Kanold and Manis 1999). Thus, it seems most likely that the identity of the channel that gives rise to  $I_A$  is Kv4.2 or Kv4.3. Another possible protein for the channel is Kv3.4. Kv3.4 can be eliminated as a possibility since our data shows  $I_A$  in pyramidal cells is insensitive to BDS 1. Kv1.4 can be ruled out because Kv1.4 is not sensitive to rHpTx-2 (Zarayskiy et al. 2005) and the kinetics of Kv1.4 channels are slower than the kinetics of the channel expressed in pyramidal cells (Kanold and Manis 1999).

Since removing the current in dynamic clamp gives the same result as blocking the current with the toxin, and adding the current with dynamic clamp rescues the effect of blocking the channel with rHpTx-2, it is probable that the modeled current from previous studies is identical to the current blocked by rHpTx2. Thus, it is most likely that Kv4.2 or Kv4.3 is the channel that gives rise to the  $I_A$  current in DCN pyramidal cells.

### **3.4.2 Kv4 channels and pyramidal cell information processing**

Kv4 channels have been implicated in the regulation of many neuronal functions such as action potential width, dendritic excitability, action potential back-propagation and

response patterns (Frick et al. 2004; Hoffman et al. 1997; Johnston et al. 2003; Johnston et al. 1999; Liss et al. 2001; Watanabe et al. 2002). Cells that express these channels are affected not only to sub-threshold, depolarizing input, but also to inhibitory input since Kv4 channels recover from inactivation at hyperpolarized voltages. Berman and Maler coined the phrase “conditional inhibition” to describe how inhibition deinactivates Kv4 channels thereby enabling them to activate on subsequent depolarizing input to oppose inward current. The net result would be a spike timing delay that is correlated to the previous membrane voltage (Berman and Maler 1998). Pyramidal cells display this type of voltage-sensitive response pattern and we have shown here that it is dependent on the activation of a Kv4 channel.

Pyramidal cells make up the major output of the DCN. In an addition, pyramidal cells must integrate information from multiple sensory inputs before relaying this information to higher brainstem centers (Oertel and Young 2004). Kv4 channels could play a very important role in integrating this information by priming the cell membrane to pay attention to certain types of input and respond with certain patterns of output. For instance, because of the Kv4 channel, pyramidal cells are not only sensitive to superthreshold, depolarizing inputs, but also to subthreshold and even inhibitory input. In pyramidal cells in slices, intact animals and in our model pyramidal cell, prehyperpolarization leads to a long latency to the first spike (Hancock and Voigt 2002; Kanold and Manis 2001; 1999; Manis 1990). Thus, inhibitory inputs that are timed to excitatory inputs would affect the response spike pattern in pyramidal cells. Pyramidal cells receive inhibitory input from at least three types of inhibitory interneurons, all of which are excited by the same input that excites pyramidal cells. This means that the inhibitory input to pyramidal cells is likely to be temporally correlated with the excitatory input. Therefore Kv4 channels might play an

important shaping the output pattern of spikes in response to certain patterns of excitatory and inhibitory input to the pyramidal cells. Since blocking Kv4 channels with rHpTx-2, removing  $I_A$  with dynamic clamp in pyramidal cells in slices, and removing  $g_A$  from model pyramidal cells all result in decreasing the FSL after a hyperpolarizing pre-pulse, it seems likely that Kv4 channels are the major contributor to this response pattern.

Further, inhibition is important in determining both output patterns of spikes and the precise timing of spikes (Dodla et al. 2006). DCN pyramidal cells are dominated by inhibition both in their response patterns and in their synaptic inputs. For instance, type IV units, thought to be pyramidal cells, are only excited at low sound pressure levels at frequencies very near to characteristic frequency (Evans and Nelson 1973; Voigt and Young 1980). As stated previously, pyramidal cells receive at least three types of inhibitory input from interneurons (Zhang and Oertel 1994). Therefore, intrinsic channels that are active at hyperpolarized and subthreshold membrane potentials will have an important effect on how the cell shapes and responds to synaptic input. The data presented in this study show that pyramidal cells express at least one channel that fits this description and the availability of this channel changes pyramidal cell response patterns. First, the build-up response is dependent upon Kv4 channels. In addition, the precise timing of spikes after a sIPSP changes when Kv4 channels are blocked. Presumably both of these changes in spike timing occur because the membrane is more excitable since the outward conductance that is usually open is now blocked. However, pyramidal cells express other types of channels that are also active at sub-threshold voltages, such as a persistent sodium current, that would also affect threshold and the timing of spikes (Manis et al. 2003). These other conductances were not

studied in any of these experiments and their contribution to spike patterns cannot be ruled out.

DCN pyramidal cells carry out the important function of integrating multiple types of sensory information that are received through two separate dendritic trees. Kv4 channels control the spread of dendritic depolarizations throughout the dendritic tree and also the strength of orthograde dendritic propagations in hippocampal pyramidal neurons (Cai et al. 2004; Hoffman and Johnston 1999). Thus, Kv4 channels could play a role in determining the relative strength of incoming sensory information in the different dendritic trees of pyramidal cells. If Kv4 dampens synaptic input from one type of sensory input, the resulting response of the pyramidal cell could be different. Kv4 channels that are deinactivated by inhibition prior to depolarizing synaptic input would also slow down the rate of depolarization in response to the excitatory input. Action potential threshold is dependent on the slope of the membrane depolarization leading up to a spike (Azouz and Gray 2000). Thus, the presence of Kv4 would affect membrane threshold and the timing of the action potential. Our data suggest that this effect is true in pyramidal cells (see chapter two). When a sIPSP was imposed on a noise stimulus, the timing first spike after the sIPSP was sometimes delayed, possibly because the cell membrane depolarization was not fast or large enough to reach threshold and fire a spike. This delay decreased the reliability in the timing of the first spike; sometimes the cell did fire a spike in response to the event in the stimulus and sometimes it did not. However when Kv4 was blocked, the number of spikes that exhibited this delay were decreased or abolished and reliability was increased. Therefore, the recruitment and availability of Kv4 channels could tune the cells so that they respond only to strong depolarizing events. Smaller and weaker depolarizations would be opposed by the

outward current through open Kv4 channels. In addition, the cell would not depolarize quickly and the threshold would increase further decreasing the possibility that a spike would fire if Kv4 channels were open. In this way, pyramidal cells might act as coincidence detectors by responding only strong or synchronous excitatory input.

However, it is not simply the size of inhibition that affects the recruitment of Kv4 channels. The timing of the inhibition is also crucial in determining the output of the cell (Kanold and Manis 2005a). If inhibitory events are too far removed from excitatory events in time, then Kv4 channel recruitment will not be as robust. Therefore, the precise timing of inhibitory and excitatory input will affect if and when a pyramidal cell fires. In this regime, strong or synchronous input may not be necessary if the timing of inhibition and excitation is configured in a way that minimizes the effect of Kv4. Thus the availability of Kv4 channels can greatly influence how information is processed and encoded in pyramidal cells.

Finally, Kv4 channels are subject to many kinds of post-translational modifications and regulation by other proteins such as DPPX and KChIPs (reviewed in Birnbaum et al. 2002). Depending on the state of the cell, Kv4 channels can have different voltage sensitivities or levels of expression. Many of these post-translational modifications change how the cell responds to input (Hoffman and Johnston 1999). These post-translational modifications confer another way pyramidal cells can set themselves to respond to certain patterns or strengths of input. This capability would be essential for cells that carry out the role of integrating multiple sensory inputs like a pyramidal cell.

### **3.4.3 Kv4 Channels and LTP**

Kv4 channels, because of their subthreshold activation, control the strength of dendritic depolarizations, which are important in initiating synaptic changes such as long

term potentiation. When Kv4 channels open at subthreshold voltages, they dampen excitatory events such as EPSPs and back propagating action potentials (Cai et al. 2004; Hoffman and Johnston 1998; Hoffman et al. 1997). In addition Kv4 determines the width of action potentials (Birnbaum et al. 2004; Kanold and Manis 2001). Calcium entry into dendritic spines and shafts is also decreased as dendritic depolarizations are dampened and action potentials are narrowed (Johnston et al. 2003; Migliore et al. 1999). In this way Kv4 can affect all calcium-dependent processes, such as long-term potentiation, Synapses between parallel fibers and DCN pyramidal cells are strengthened when post-synaptic depolarization is coupled with high frequency stimulation of parallel fibers and this response is attenuated with calcium block (Fujino and Oertel 2003). Kv4 channels expressed in pyramidal cells could determine what kinds of synaptic input will lead to LTP and under what conditions LTP will occur.

Further, a specific kind of synaptic strengthening that depends upon the precise timing of both the EPSP and the post-synaptic action potential (spike timing dependent plasticity) is directly affected by changing the voltage sensitivity of Kv4 channels by phosphorylation (Watanabe et al. 2002). Spike timing dependent plasticity also occurs at synapses between parallel fibers and pyramidal cell apical dendrites (Tzounopoulos et al. 2004). The timing between EPSP and action potential must be under 10 msec for this strengthening to develop. It is therefore possible that Kv4 channels regulate the development of this type of synaptic potentiation. The timing of EPSP to action potential might also depend upon post-translational modifications of Kv4 channels such as phosphorylation. By controlling the voltage sensitivity of Kv4 channels, the cell could set what patterns and strengths of synaptic input would potentiate and depress synapses. Because pyramidal cells

are integrating multi-sensory information, some synapses could be potentiated so that their effect on the pyramidal cell is stronger than other synapses that represent other types of sensory information. Such a mechanism would be necessary for pyramidal differentially adapt to certain types of incoming information.

## **Chapter 4: Expression Patterns of Kv4.2 and Kv4.3 in the DCN**

### **4.1 Introduction**

The Dorsal Cochlear Nucleus, a laminated structure located on the lateral side of brainstem, is thought to be essential for localizing sound sources in elevation. Functional studies have shown that when the DCN is lesioned, animals have trouble fixating on a sound source that is located above or below the head (May 2000; Sutherland et al. 1998). The ability to localize sound in this plane is the result of sensory input from not only the auditory nerve, but also other sensory nuclei, which converge in the DCN thereby enabling the animal to determine the position of the sound source in relation to the position of the pinna and head (for review see (Oertel and Young 2004)). Integration of multiple sensory input is accomplished, in part, by the organization of the DCN into layers. The outermost layer, called the molecular layer, contains axons of the granule cell system that carry information from multiple sensory systems (Osen 1969a; b). The fusiform cell layer contains the cell bodies of the principle cells of the nucleus, known as the pyramidal cells. Pyramidal cells have 2 branches of dendrites; the apical branch projects into the molecular layer to receive input from the granule cell axons, and the basal branch extends into the third layer, or deep layer, of the DCN and receives information from the terminating auditory nerve fibers (Osen 1970). Other cells found in the DCN include glycinergic inhibitory interneurons named cartwheel, and vertical cells, and glutamatergic granule cells. Cartwheel cells are located in the fusiform and molecular layer while vertical cells are found in the deep layer (Wouterlood

and Mugnaini 1984; Zhang and Oertel 1993a; b). The granule cells, characterized by smaller cell bodies than pyramidal cells, are distributed throughout the nucleus in clusters, and receive non-auditory input from somatosensory nuclei and descending auditory input from the auditory cortex and inferior colliculus (Babalian 2005; Coomes and Schofield 2004; Mugnaini et al. 1980a; Mugnaini et al. 1980b; Schofield and Coomes 2005; Shore 2005; Young et al. 1995). Axons from all three of these cells types synapse on the pyramidal cells, which then process and relay the integrated information to the inferior colliculus (Roth et al. 1978).

While the pattern and position of synaptic inputs are certainly essential in shaping the output of the DCN principal cells, intrinsic conductances also play an important role in processing information and generating response patterns of pyramidal cells (Hancock and Voigt 2002; Kanold and Manis 2001; 1999; Manis 1990). One conductance in particular, a subthreshold, rapidly-inactivating potassium channel, is essential for the build-up response pattern in pyramidal cells (Evans and Nelson 1973), which is characterized by a long latency to the first spike. When the channel is opened by depolarizing voltages, the resulting current ( $I_A$ ) can shape many aspects of neuronal output such as action potential width, action potential frequency, strength of post-synaptic depolarization, spread and intensity of back-propagating action potentials, and action potential repolarization (Cai et al. 2004; Hoffman et al. 1997; Kim et al. 2005; Liss et al. 2001; Mitterdorfer and Bean 2002; Molineux et al. 2005). Work in our lab has revealed that  $I_A$  is important in encoding the timing of inhibitory inputs of pyramidal cells (Kanold and Manis 2005a). Since inhibition is an essential component of DCN function (Reiss and Young 2005),  $I_A$  may play an important role in information processing and sound localization by the DCN.

Potassium channels that give rise to  $I_A$  are found in the Kv1, Kv3 and Kv4 families of potassium channels. *In situ* hybridization (ISH) studies have shown that Kv4 family members Kv4.2 and Kv4.3 are expressed in the DCN (Fitzakerley et al. 2000; Serodio and Rudy 1998). In addition, our lab has demonstrated that a toxin rHpTx-2) specific for Kv4 channels blocks the  $I_A$  current in pyramidal cells (Chapter 3). When this toxin is applied to DCN in a rat brain slice preparation, the build-up response pattern is obliterated. Further, the kinetics and pharmacology of  $I_A$  in pyramidal cells closely resembles the kinetics and pharmacology reported for Kv4.2 and Kv4.3 (Kanold and Manis 1999). However, the precise cellular expression profiles of Kv4.2 and Kv4.3 has yet to be determined.

In this study we used ISH and immunohistochemistry to determine which *shal* potassium channel pyramidal cells express. Kv4.2 and Kv4.3 were both present in the DCN at the mRNA level and at the protein level. Kv4.3 mRNA staining was confined to the fusiform cell layer while Kv4.2 mRNA staining was found throughout the fusiform and deep layers of the DCN. Pyramidal cells, which were identified with a retrograde tracer, did not stain for Kv4.2 protein or Kv3.4 protein. However pyramidal cells did stain for Kv4.3 protein. These results suggest that Kv4.3 is responsible for  $I_A$  in DCN pyramidal cells.

## **4.2 Materials and Methods**

***Tissue preparation for in situ hybridization.*** Two Sprague-Dawley rats, aged post-natal day 14, were deeply anesthetized with ketamine (100 mg/kg)-xylazine (10 mg/kg), decapitated, and the brains removed. The brains were fixed in 4% paraformaldehyde in PBS for 72 hours then cryo-protected in 30% sucrose in PBS until saturation. 20  $\mu$ M frozen serial sections were cut in the coronal plane and placed on poly-lysine coated slides and stored at  $-80^\circ\text{C}$  until the ISH procedure was performed.

***Preparation of in situ hybridization probes.*** A vector containing the full coding sequence for Kv4.2 was kindly donated by Lyanne C. Schlichter (Toronto Western Research Institute) (Wong and Schlichter 2004). This vector was digested with BamHI and HindIII, yielding a fragment of the coding sequence that included 992 bases starting with base pair 861 and ending at base pair 1852 (Blast search, gi|76881821|ref|NM\_031730.2|). This DNA fragment was ligated into the multiple cloning site of pBluescript II (Stratagene, La Jolla, CA) after the vector was digested with Hind III and BamH I. Successful cloning was verified by T7 sequencing of the DNA. The vector that included the probe was then linearized with either Xba I or Apa I in order to synthesize either the sense or the anti-sense probes. The probes were then synthesized by incubating the DNA template, DIG NTP labeling mix, reaction buffer, DEPC treated water, RNase inhibitor and RNA polymerase (Roche) for 2 hours at 37°C. The probe was purified by adding 2.5 µl 4M LiCl and 75 µl cold 100% EtOH and storing at -80°C overnight followed by centrifugation and re-suspension of the RNA pellet.

The Kv4.3 probe was prepared in a similar manner except that the DNA fragment used for the probe was amplified from cDNA using PCR, from a rat brain cDNA library (Invitrogen, Carlsbad, CA). The primers were created with Xba I sites to enable cloning into the pBluescript II vector. The forward primer sequence was gcgtctagagcggttaacctgaggacact and the reverse primer sequence was gcgtctagattggtctccagaagaacgtg. The resulting amplicon was 902 basepairs long, which included bases 3244-4144 of Kv4.3 (BLAST search, gi|1050331|gb|L48619.1|RATKV43R). Both the pBluescript II vector and the PCR product were digested using the restriction enzyme Xba I. The Kv4.3 probe was then ligated into the vector and successful cloning was verified by sequencing the DNA using a probe for the T7 promoter. The vector was then linearized with Hind III or Not I in order to synthesize sense

and anti-sense probes. All restriction enzymes were obtained from New England Biolabs (Ipswich, MA).

***In situ hybridization.*** Rat brain sections were warmed to room temperature and dried at 50°C for 10 minutes. Following fixation in 4% paraformaldehyde in DEPC-PBS at room temperature for 15 minutes, sections were washed three times in DEPC-PBS at room temperature for 5 minutes each. The slides were then treated with 1 µg/ml proteinase K in PBS at room temperature for 15 minutes and then washed 3 times in DEPC-PBS for 5 minutes each. Following the washes the sections were incubated with triethanolamine-HCL with acetic anhydride for 10 minutes at room temperature and then washed again 3 times in DEPC-PBS for 5 minutes each. Finally, the sections were prehybridized for 4 hours at 60°C in hybridization buffer (Roche), which was then replaced with 1-2 µg/ml of probe in hybridization buffer and incubated for 12-16 additional hours. The slides were then washed with saline-sodium citrate in a series of washes for 15 and 20 minutes at 60°C followed by two washes with PBS for 20 minutes each at room temperature. To visualize Digoxigenin (DIG), the slides were blocked with 10% blocking buffer consisting of heat-inactivated sheep serum and 1% Roche Blocking Reagent in maleic acid buffer at room temperature for 1 hour. Following blocking, sections were incubated for 2 hours at room temperature with anti-digoxigenin Fab-AP (Roche) diluted 1:2000 in blocking buffer. The sections were then washed four times in DIG washing buffer for 10 minutes each and were then developed overnight in the dark in NBT/BCIP solution, and rinsed several times in PBS at room temperature. Finally, the slides were fixed again in 4% paraformaldehyde to inactivate the alkaline phosphatases and mounted in Aquatex (Merck).

The slides were visualized on a Leica M420 dissecting microscope equipped with a Leica DFC 480 color camera and digitized using Leica Firecam (v1.8) software on a Mac computer. Photoshop (Adobe) and Image J were used to adjust the brightness and contrast and the image size. Image J was used to measure the total diameter of the DCN and the distance of cells from the lateral edge of the DCN.

***Retrograde labeling and tissue preparation-*** Rat pups, 20-30 days of age and of either sex, were anesthetized using IP injections of sodium pentobarbital (45 mg/kg). When the rat was areflexic to corneal stimulation, it was administered 0.02 cc atropine to control secretions and placed in a stereotaxic headholder (DKI, Tujunga, CA). The surgical suite was heated to 30° C to assist in the maintenance of the subject's body temperature. A midline incision was made in the skin and the soft tissue pushed laterally. A hole (3 mm in diameter) was drilled 2 mm lateral to the midline and 7 mm posterior to Bregma. A 5 microliter syringe filled with 10% dextran fluorescein (10,000 MW, Molecular Probes, Eugene, OR) in 0.1 M Tris buffer, pH 7.4, was lowered into the hole at a 10° angle to target the inferior colliculus (IC) calculated to be AP -8.3, ML 2, and DV -4 in accordance to rat stereotaxic coordinates (Paxinos and Watson, 1998). One microliter of dextran fluorescein was injected at insertion depths of 2, 3, and 4 mm. Each injection was made over a period of 30 seconds, and at the end of the last injection, the syringe was left for 5 minutes. The syringe was then withdrawn, the hole in the skull filled with bone wax, and the skin sutured. The rat was given 0.02 cc Dopram and 0.02 cc bupinorphine (IM), 1 cc sterile saline (SC), and placed in a heated box for recovery. When the animal was up and moving about, it was returned to its home cage in the animal facility. Each rat was allowed a 7-10 day post-injection survival period.

At the end of the survival period, rats were administered a lethal dose of sodium pentobarbital (75 mg/kg, IP). When they were areflexic to corneal stimulation, they were transcardially perfused with a solution of 4% paraformaldehyde in 0.1 M phosphate buffer. After passing 250 ml of fixative through the animal, the heads were removed and the skull opened to allow fixative access to the brain. Brains were postfixed (5° C) overnight in the same fixative. The next morning, the brainstem at the level of the pons was separated from the rest of the brain and placed in 30% sucrose in 0.1 M phosphate buffer. The brain was blocked through the thalamus, embedded in bovine serum albumin hardened with formaldehyde, and cut on a Vibratome from caudal to rostral at a thickness of 100 µm. Sections through the inferior colliculus were examined under a fluorescent microscope to verify placement of the injection site. When injections were localized to the IC, corresponding sections through the dorsal cochlear nucleus were collected on a cryostat. 10 µm frozen sections of the DCN in the trans-strial plane (Blackstad et al. 1984) were collected on slides and used for immunohistochemistry.

***Immunostaining and confocal microscopy.*** The sections were blocked and permeabilized in a solution containing 0.5% Triton X-100, 20% normal goat serum, 0.8% bovine serum albumin, and 1% cold water fish gelatin in PBS for 1 hour at room temperature. The Kv4.3 polyclonal antibody (Sigma) or the Kv4.2 monoclonal antibody (An et al. 2000), were diluted in a solution containing 5% normal goat serum, 0.2% bovine serum albumin and 1% cold water fish gelatin in PBS. The Kv4.3 antibody was diluted 1:200 (1 µg/mL) and the Kv4.2 antibody was diluted 1:1000. The sections were then incubated with the antibody overnight at 4°C. After incubation with the primary antibody, the sections were washed three times in PBS at room temperature for 15 minutes each. Secondary antibodies were obtained from

Molecular Probes (Invitrogen). A goat anti-mouse antibody that fluoresced at 568 nm for the Kv4.2 monoclonal antibody and a goat anti-rabbit antibody that fluoresced at 633 nm for the Kv4.3 polyclonal antibody were used. The secondary antibody was diluted 1:1000 in a solution containing 1% cold water fish gelatin, 0.2% bovine serum albumin and 1% horse serum in PBS and the slices were incubated with the secondary antibody for 1 hour at room temperature. Finally, the sections were washed three times in room temperature PBS for 15 minutes and mounted using Fluoromount-GT (Electron Microscopy Sciences). Rabbit IgG (1 $\mu$ g/mL) was used as a negative control for the Kv4.3 antibody. All reagents were obtained from Sigma-Aldrich (St. Louis, MO) unless otherwise noted.

Digital images were collected using a Leica confocal microscope with either a 10x, 0.6 NA objective or a 40x 1.25 NA objective and the Leica TCS-NT software system. The 10 $\mu$ m sections were optically sectioned with 1 $\mu$ m steps. Photoshop (Adobe) and Image J were used to adjust the images for brightness and contrast and size.

***Nissl Staining.*** Nissl staining was carried out to identify cell types in the same sections used for the ISH experiments. The sections were hydrated in 5 minute intervals each, in the following solutions: Xylene (twice), 100% EtOH (two times), 95% EtOH, 70% EtOH. The slides were then dipped in water and then stained in 0.5% Cresyl Violet for 30 minutes. The sections were then differentiated in water for 5 minutes and then dehydrated by incubating in the following solutions for 5 minutes: 70% EtOH, 95%EtOH, 100%EtOH (twice) and xylene (twice). The slides were then mounted using Permount (Biomedica) and visualized with the same microscope used in the ISH experiments.

## **4.3 Results**

### **4.3.1 Kv4.2 *In situ* hybridization**

The Kv4.2 antisense probe labeled many cells in the DCN (Figure 1). This labeling was significantly greater than the background labeling observed in tissue labeled with the Kv4.2 sense probe (Figure 1D). The Kv4.2 antisense probe labeled cell somata that were widely distributed in nearly all layers of the DCN (Figure 1B,C). Labeled cells in the molecular layer were observed rarely. Labeled cell bodies were both large and small. It is likely that many of these cells are granule cells since they can be found in many layers of the DCN. Some of the larger cells are likely giant cells or pyramidal cells; however, the exact cell type cannot be determined by the staining patterns alone. Staining of granule cell layers in the cerebellum served as a positive control (Figure 1A). The Kv4.2 antisense probe did not label cells heavily in the VCN. This absence of labeling is seen in Figure 1A where the VCN is denoted by a red arrow. The staining in the VCN is not greater than the background staining observed with the Kv4.2 sense probe (Figure 1 A,D).

### **4.3.2 Kv4.3 *In situ* hybridization**

The Kv4.3 antisense probe did not label as many cells in the DCN as the Kv4.2 probe. In fact, the overall staining in all parts of the brain was less for Kv4.3 than it was for Kv4.2. Despite the decrease in the level of intensity, Kv4.3 labeled cells were still detected in the DCN (Figure 2). Labeling for Kv4.3 was also detected in the cerebellar granule cell layer. Stained Kv4.3 cells in the DCN were confined to the fusiform cell layer with only a few cells detected in the deep layer (Figure 2B,C). The labeling of cells in the DCN was also greater than the background labeling of the sense probe in the DCN, which showed no labeled cells (Figure 2D).

When the staining pattern of the two probes are compared in a magnified image, it is obvious that many more cells are stained for Kv4.2 than for Kv4.3 (Figure 3). The Kv4.2 staining also seems to be found in cell somata scattered throughout the nucleus, whereas the Kv4.3 staining is found in cells in the fusiform cell layer (Figure 3B, black arrows) and a few cells in the deep layer (Figure 3B, red arrows). To determine if the Kv4.2 probe and the Kv4.3 probe labeled different populations of cells, we compared the number of cells labeled with the two probes and the distance of the labeled cells from the DCN lateral edge. Three unbiased investigators counted the number of labeled cells in two DCN sections from two different rat brains. There were more than twice the number (Kv4.2 mean number of cells=111 cells versus mean of Kv4.3 cells counted=53.3 cells) of cells stained for Kv4.2 than were stained for Kv4.3. The investigators then measured the distance of each labeled cell body from the lateral edge of the DCN and the total thickness of the DCN at the level of the cell body. We calculated the relative position of the cell by dividing the distance of the cell body from the lateral edge of the DCN by the total thickness of the DCN. Using the normalized distance, we plotted a histogram binned in 0.05  $\mu\text{m}$  increments, that displayed the number of cells that were found in each bin (Figure 3C). The cells labeled for Kv4.2 were found throughout all layers of the DCN. The cells labeled with Kv4.3 were found most highly concentrated at the center of the nucleus. These histograms represent two different populations of cells ( $P < 0.05$ , using a Kolmogorov-Smirnov statistic). While Kv4.3 likely labels a subset of cells labeled with Kv4.2, there was clearly more Kv4.2 label observed in the DCN. The Kv4.3 labeling is confined to layer 2 of the DCN. The population of cells labeled with Kv4.3 most likely reflects pyramidal cells. Kv4.2 labeling is found in many cells throughout the DCN but it is not clear exactly what kinds of cells are labeled. However,

it is likely that granule cells express Kv4.2 since the labeled cells are spread throughout the DCN and granule cells are also found spread throughout this nucleus.

**Figure 4.1**

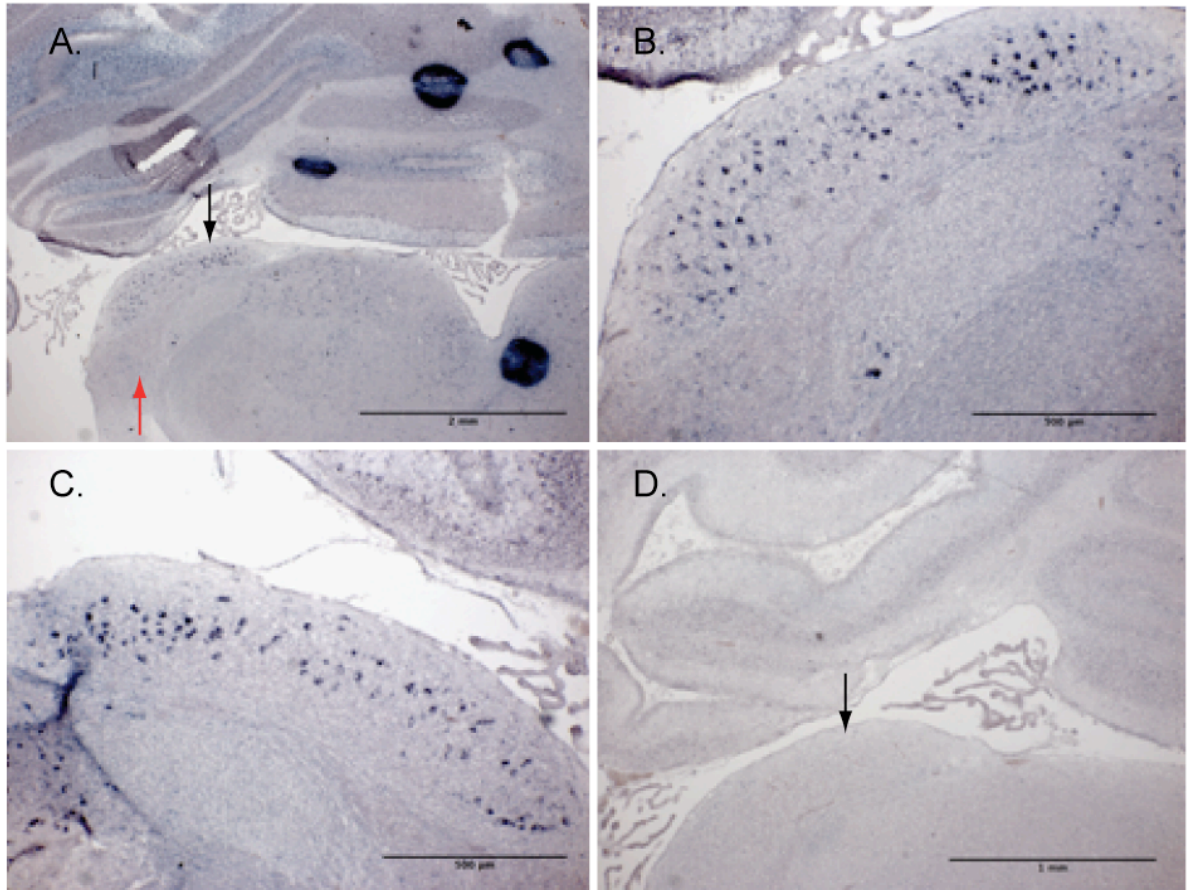


**Figure 4.1** Kv4.2 was detected in many cells in the DCN using *in situ* hybridization of Kv4.2 mRNA

**A** Low magnification of a brain section labeled with anti-sense Kv4.2 probe. The arrow denotes the DCN.

**B-C** High magnification of Kv4.2 anti-sense mRNA labeling in the DCN in two rat brain coronal sections.

**D** High magnification of Kv4.2 sense probe control showing background labeling in the DCN. There is no labeling of any cells.

**Figure 4.2**

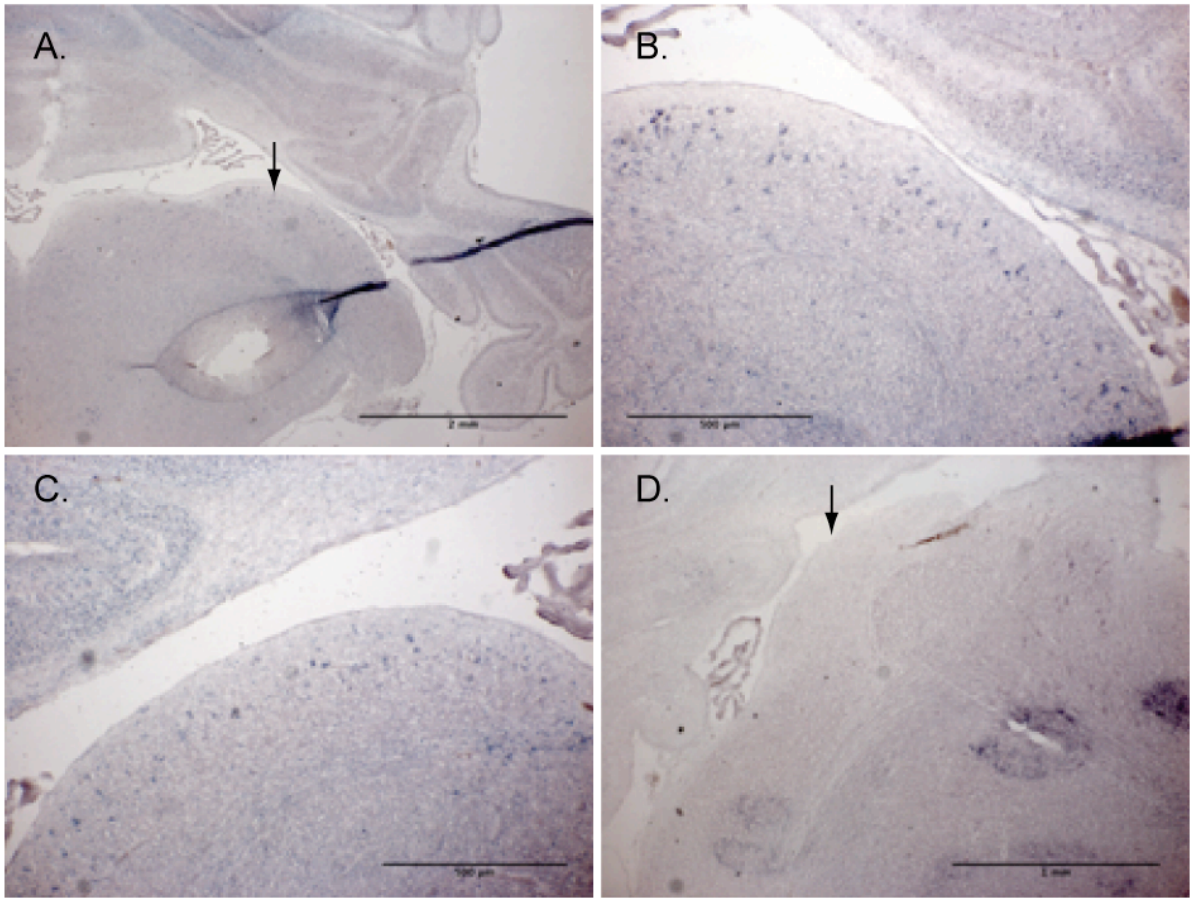


**Figure 4.2** Kv4.3 mRNA was detected in cells in rat DCN by in situ hybridization.

**A** Low magnification of a brain section labeled with anti-sense Kv4.3 probe. The arrow denotes the DCN.

**B-C** High magnification of Kv4.3 anti-sense mRNA labeling in the DCN in two different rat brain coronal sections.

**D** High magnification of Kv4.3 sense probe control showing background labeling in the DCN. There is no labeling of any cells.

**Figure 4.3**

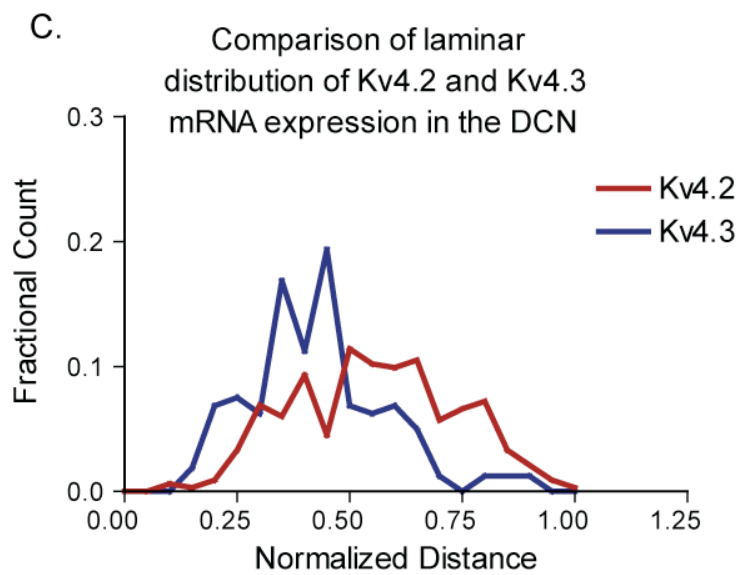
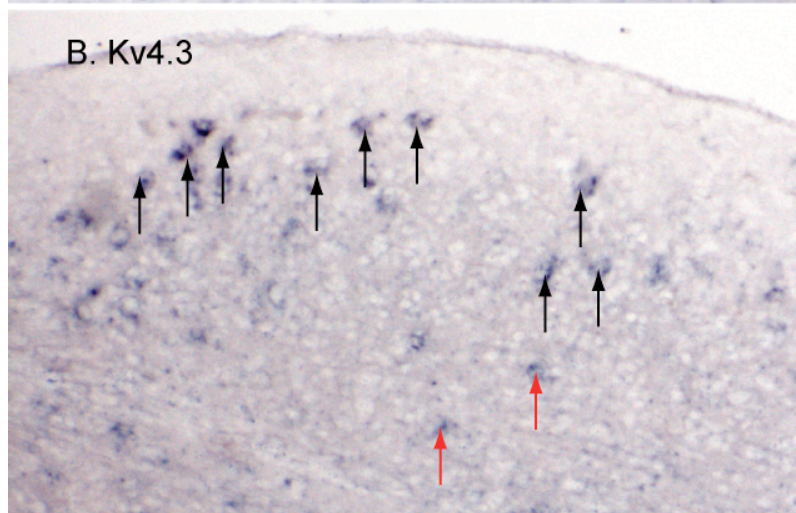
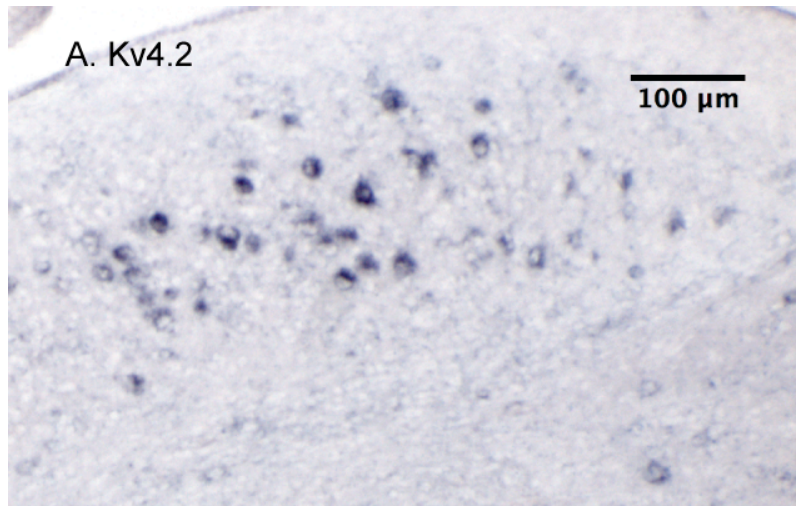


**Figure 4.3** Comparison of labeling pattern of Kv4.2 and Kv4.3 probes in the DCN.

**A** Magnified image showing Kv4.2 expression in cells throughout all layers of the DCN.

**B** Magnified image showing Kv4.3 is confined to cells in the fusiform cell layer (black arrows) and a few cells in the deep layer (red arrows).

**C** Histogram showing the fraction of total labeled cells in 0.05  $\mu\text{m}$  bins denoting the normalized depth of the cell body in the DCN. The two histograms denote significantly different populations of cells.

### 4.3.3 Kv4.2 and Kv4.3 Immunocytochemistry

Since it was difficult to determine the exact cellular expression pattern of Kv4.2 and Kv4.3 using ISH, we used antibodies against Kv4.2 and Kv4.3 to ascertain if pyramidal cells express either of these potassium channels at the protein level. To date there are no known cellular markers for pyramidal cells. Therefore, to label pyramidal cells, we injected the inferior colliculi of rats with a retrograde tracer. Since pyramidal cells are the dominant projection neurons of the DCN, and all of the axons of pyramidal cells project to the inferior colliculus, we were able to label pyramidal cells with dextran fluorescein. Cells labeled with dextran fluorescein were easily visualized by confocal microscopy because of the punctate appearance of the dye (Figures 4.5-4.8).

A monoclonal antibody against Kv4.2, created in the lab of James Trimmer (UC Davis), labels the cell membranes of granule cells of the cerebellum, which are known to express Kv4.2 (Figure 4.4). This antibody has been used in other studies to determine the cellular and subcellular expression pattern of Kv4.2 (An et al. 2000). The Kv4.2 antibody labeled cells in the DCN (Figure 4.5A). Cell membranes were most heavily labeled by the antibody; however, it was hard to determine if dendrites were also stained. The cells that were stained were small compared to the retrogradely-labeled pyramidal cells (Figure 4.5A-C)). While cells that were stained with the anti-Kv4.2 antibody were found throughout the nucleus in pockets of cells, the labeled pyramidal cells did not show any Kv4.2 staining. At high magnification, it is clear that Kv4.2 is absent in retrogradely-labeled pyramidal cells (Figure 4.6). Smaller cells that surround pyramidal cells do express Kv4.2 (Figure 4.6A,D). These cells are likely to be granule cells since they are found throughout the nucleus in clusters and they are less than 10  $\mu\text{m}$  in diameter. However, we did not find any pyramidal

cells that were labeled both with the tracer and with Kv4.2 (10/10 cells unlabeled) (Figure 4.6C,F). The population of pyramidal cells that were labeled with the retrograde dye in these experiments do not express Kv4.2. However, there might be another population of pyramidal cells not labeled with the retrograde tracer that do express Kv4.2

To determine whether Kv4.3 is expressed in pyramidal cells, we stained sections of DCN that also contained retrogradely-labeled pyramidal cells with a polyclonal antibody against Kv4.3. Kv4.3 staining was robust in the DCN. Many dendrites contained Kv4.3, especially dendrites that projected into the molecular layer (Figure 4.7A,D). In addition, Kv4.3 labeled cell bodies and proximal dendrites of retrogradely-labeled pyramidal cells. As seen in Figure 4.7, Kv4.3 staining is observed in all cells labeled with dextran fluorescein (14/14 cells positive). Kv4.3 also labeled cells that were not labeled by the retrograde tracer. These cells might also be pyramidal cells because the shape of the soma and the location of the cell body are similar to the shape and location of other labeled pyramidal cells. In addition, while the fusiform and molecular layers show dense staining by the Kv4.3 antibody, the deep layer of the DCN is much more lightly labeled by this antibody.

We used rabbit-IgG at the same concentration of the Kv4.3 antibody as a negative control since the peptide used to make the antibody was not available. The rabbit IgG did not stain cells in the DCN showing the Kv4.3 antibody staining pattern was due to the interaction of the antibody and the potassium channel and not due to non-specific interactions (Figure 4.8).

**Figure 4.4**

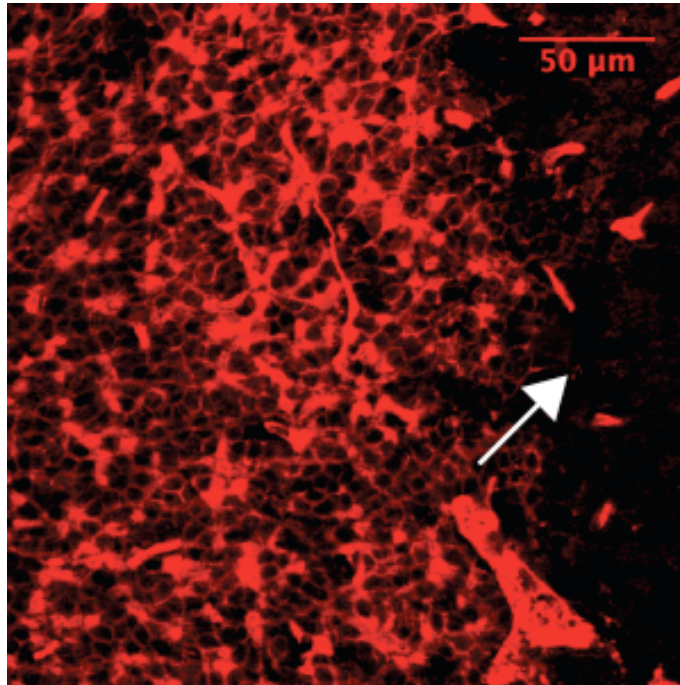


**Figure 4.4** The monoclonal Kv4.2 antibody labels granule cells in the cerebellum. It is absent in other cerebellar layers that do not have granule cells (white arrow).

Figure 4.5

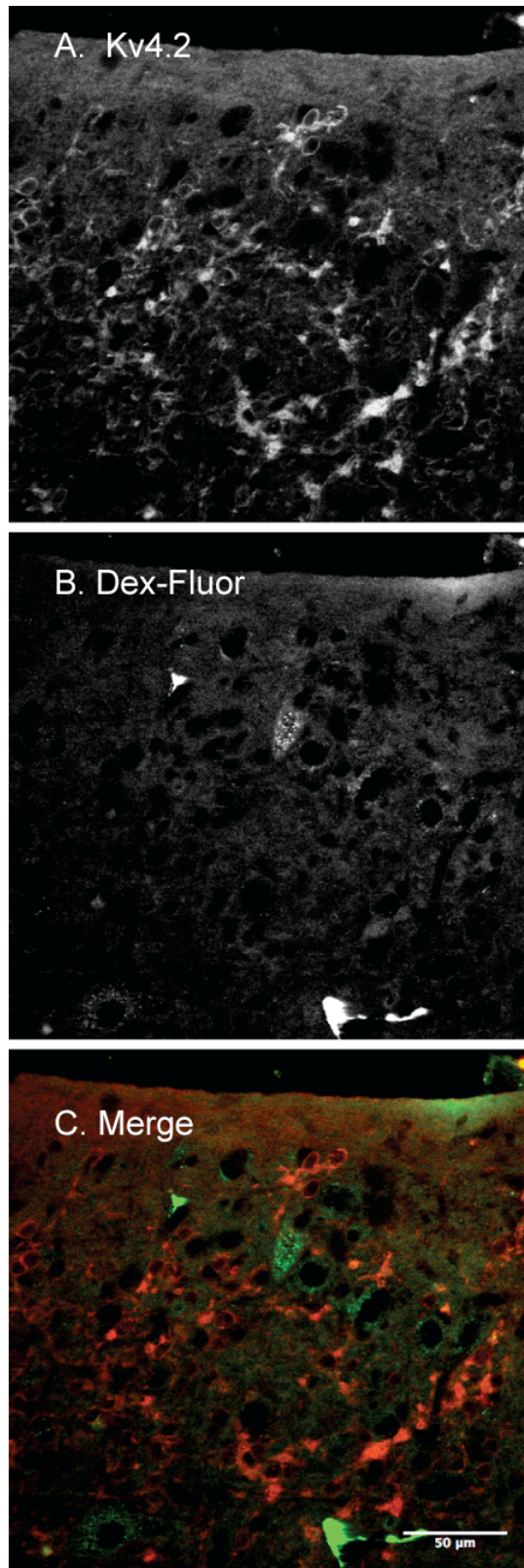


**Figure 4.5** A Kv4.2 monoclonal antibody labels smaller cells in the DCN but is absent in retrogradely labeled pyramidal cells.

**A** The monoclonal Kv4.2 antibody labels the cell membranes of small round cells in the DCN.

**B** Pyramidal cells retrogradely labeled with dextran fluorescein.

**C** Merged image of both labels. The Kv4.2 is not labeled in the retrogradely-labeled pyramidal cells.

Figure 4.6

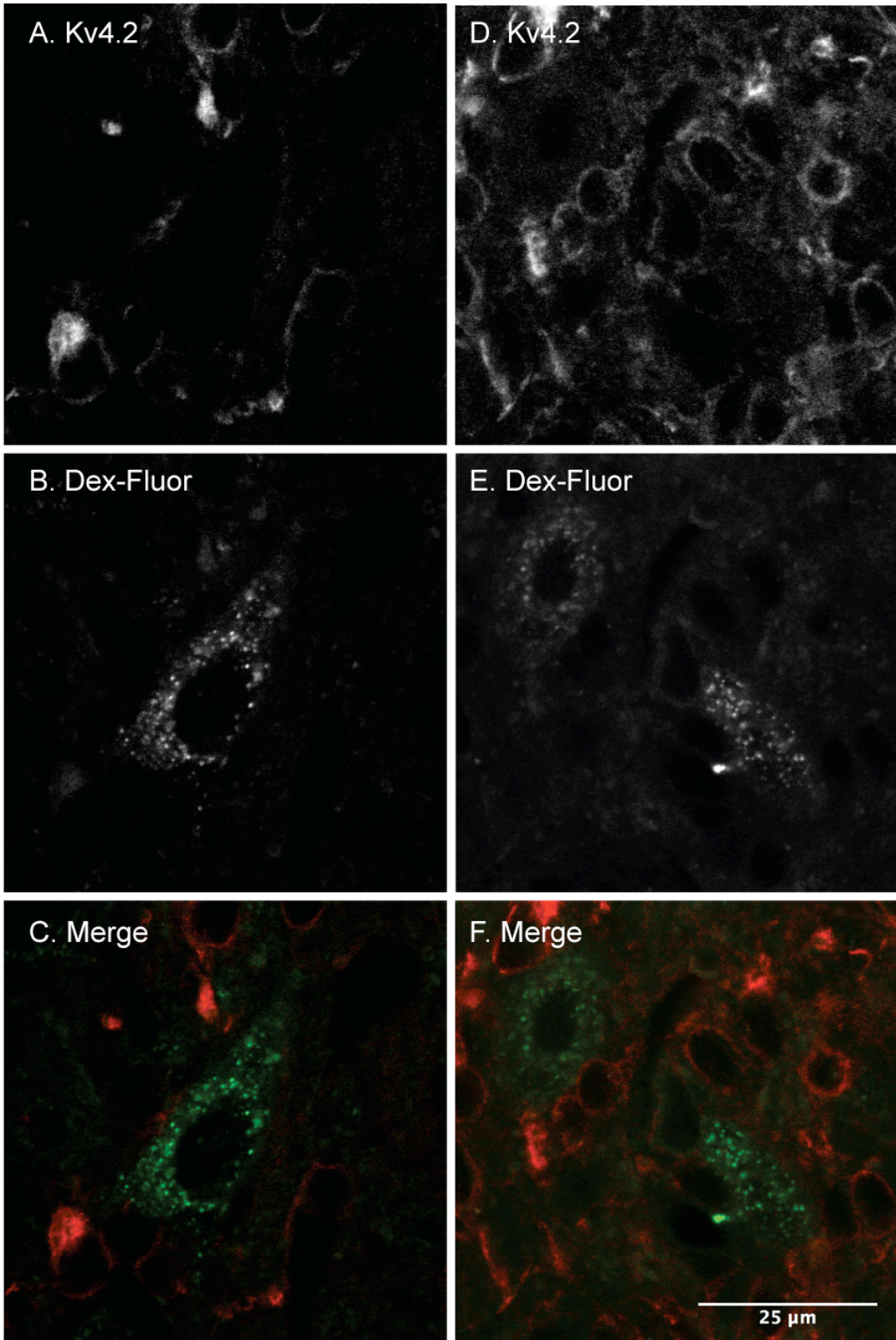


**Figure 4.6** A higher magnification of the DCN reveals that labeled pyramidal cells do not contain labeling for Kv4.2.

**A,D** Anti-Kv4.2 monoclonal antibody labeling in smaller cells in the DCN.

**B,E** Pyramidal cells retrogradely-labeled with fluorescein-dextran.

**C,F** Merged image of both labels. Even at a higher magnification, no Kv4.2 labeling is found in fluorescein labeled pyramidal cells. The Kv4.2 labeling is found in smaller cells that surround the larger pyramidal cells.

Figure 4.7

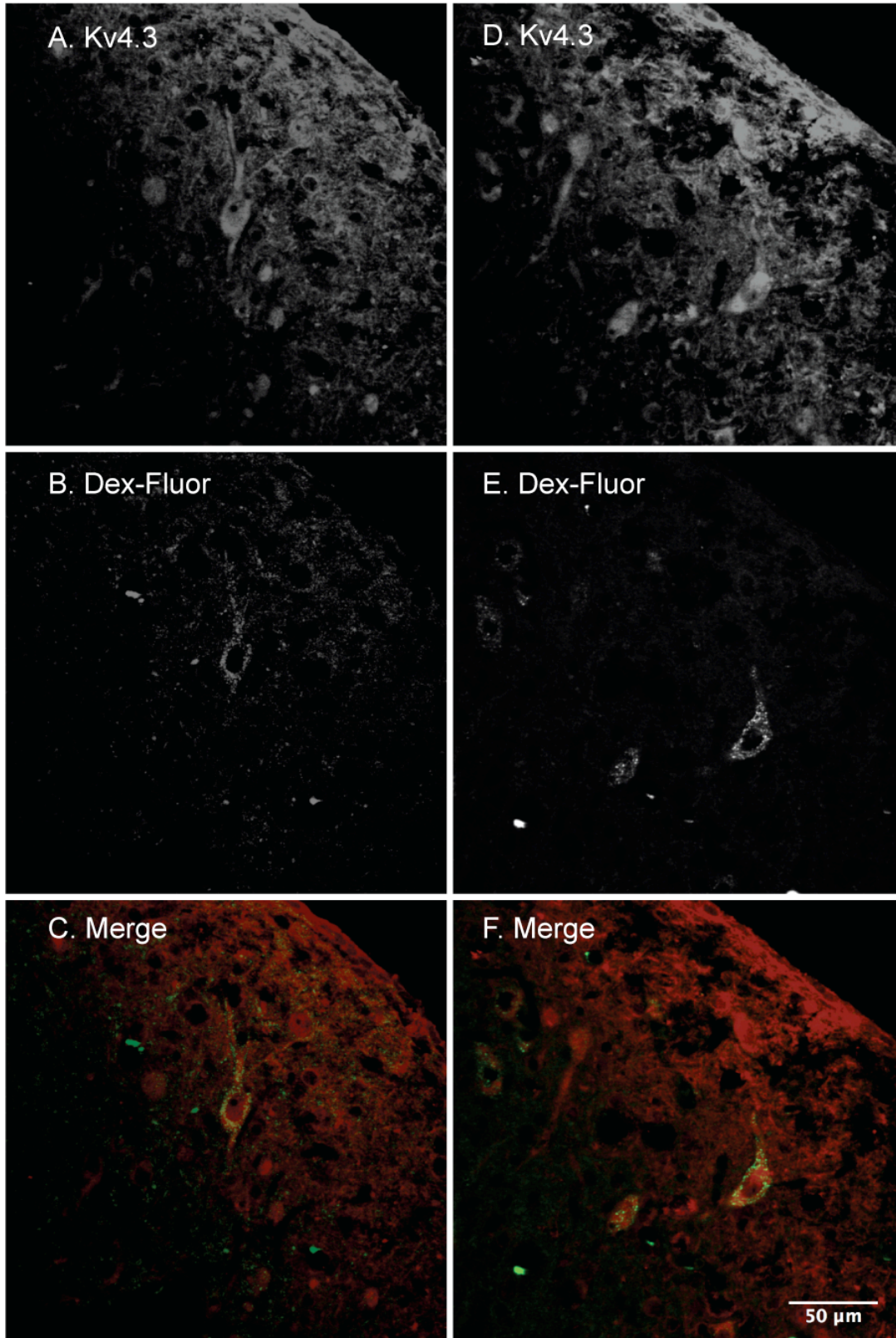


**Figure 4.7** Kv4.3 polyclonal antibody labeling is found in pyramidal cells of the DCN.

**A,D** DCN labeling with the Kv4.3 polyclonal antibody. Cell bodies and dendrites are labeled. The molecular and fusiform layers are heavily labeled for Kv4.3 whereas the deep layer shows less labeling.

**B,E** Pyramidal cell bodies retrogradely-labeled with fluorescein-dextran.

**C,F** Merged image containing both of the labels. Pyramidal cells that are labeled with fluorescein-dextran are also labeled with Kv4.3.

Figure 4.8

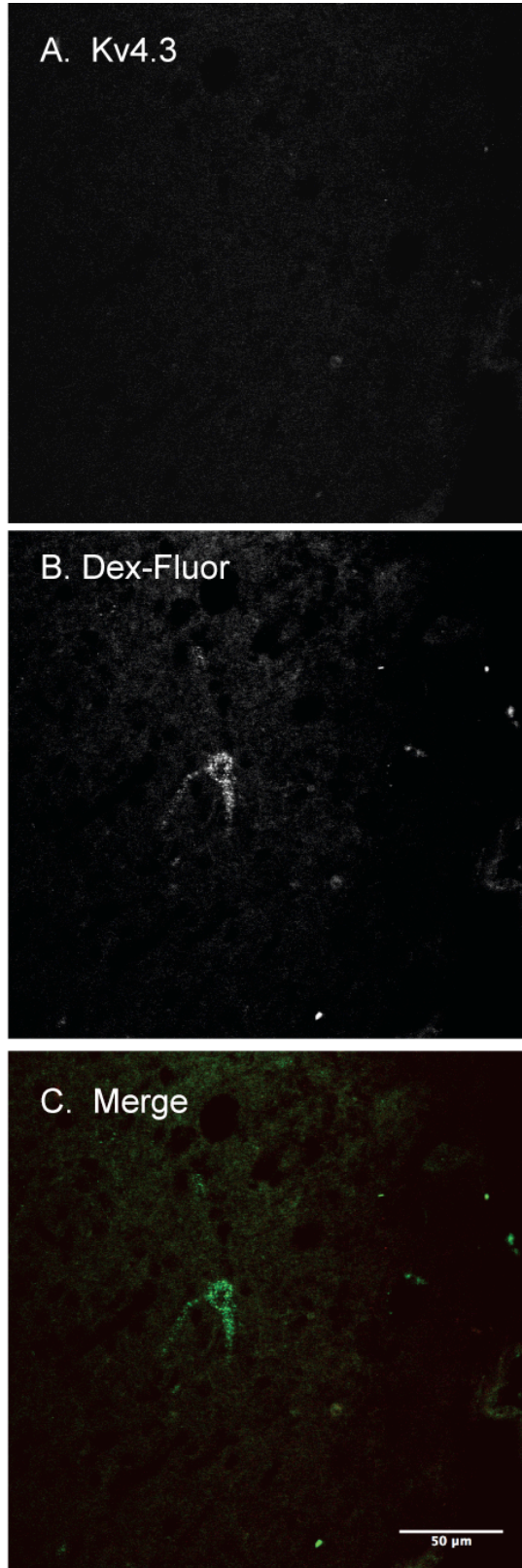


**Figure 4.8** Rabbit IgG does not label any cells in the DCN.

**A** Rabbit IgG (1 $\mu$ g/mL) was used as a negative control to show background labeling.

**B** Dex-Fluor labeled pyramidal cell.

**C** Merged image of A and B. No cells were labeled when rabbit IgG was used instead of anti Kv4.3 antibody showing that the labeling observed in sections labeled with anti Kv4.3 antibody is specific.

#### **4.3.4 Kv3.4 immunocytochemistry**

Another channel known to give rise to A currents is Kv3.4. In previous studies we have shown that toxins that specifically block Kv3.4 are ineffective at reducing A currents in outside-out patches pulled from pyramidal cell somata. However, to confirm that Kv3.4 is not expressed in pyramidal cells, we stained DCN sections with a poly-clonal Kv3.4 antibody. As seen in figure 9, Kv3.4 does label some cells in the DCN (Figure 9 A). However, pyramidal cells do not show any labeling for Kv3.4 (figure 9 B-C). It is unlikely that Kv3.4 is expressed by pyramidal cells in the DCN.

Figure 4.9

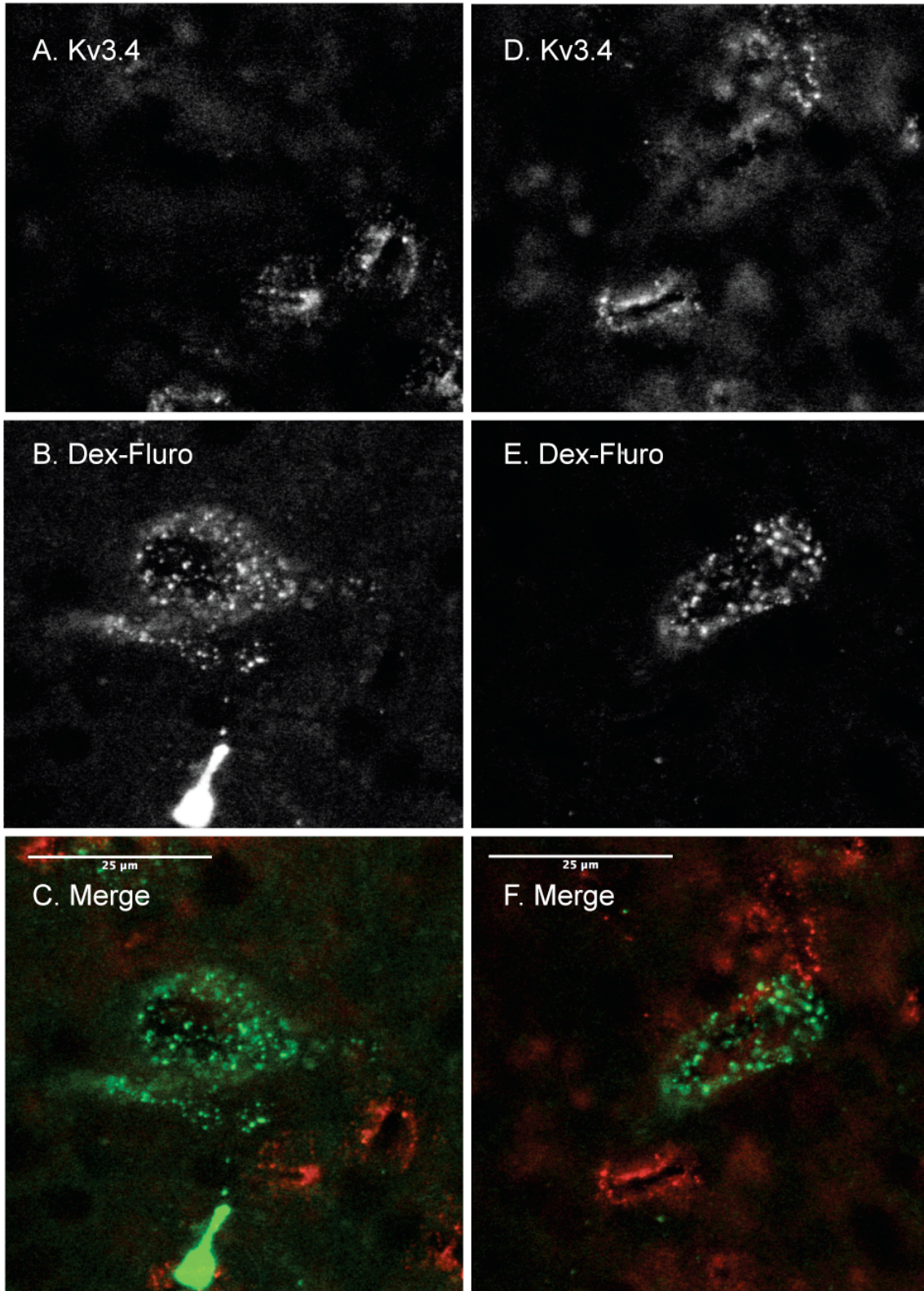


**Figure 4.9** Pyramidal cells do not express Kv3.4 protein.

**A** Staining pattern for a Kv3.4 polyclonal antibody in the DCN.

**B** Retrogradely labeled pyramidal cells **C.** Merged image of A and B.

## 4.4 Discussion

In this study we have used ISH and immunocytochemistry to determine which Kv4 potassium channel is expressed by DCN pyramidal cells. Kv4.2 mRNA is expressed at high levels in the DCN in cells that are found in both the fusiform and deep layers. Kv4.2 protein is found in small cells that are clustered in the fusiform and deep layers but absent in neurons that project to the inferior colliculus. Kv4.3 mRNA is expressed in fewer cells than Kv4.2 and cell bodies labeled for Kv4.3 mRNA are usually found in the fusiform cell layer. In conjunction with Kv4.3 mRNA expression patterns, the anti-Kv4.3 antibody labeled pyramidal cell bodies and dendrites. From these results we conclude that Kv4.3, and not Kv4.2 is responsible for at least a portion  $I_A$  in pyramidal cells.

### 4.4.1 *In Situ* Hybridization Experiments

The data presented in this paper are consistent with results described by others. Serodio and Rudy first showed by ISH that Kv4.2 was expressed at higher levels than Kv4.3 in the DCN (Serodio and Rudy 1998). However, the authors of this study did not make any attempt to define which cells in particular expressed of Kv4.2 and Kv4.3. Later, Fitzakerley and colleagues carried out an ISH study more specific to cells in the cochlear nucleus. Their data, collected in mice, corroborated much of the Serodio and Rudy findings. These authors also reported Kv4.2 mRNA was expressed at high levels in the DCN with Kv4.3 expressed at low levels (Fitzakerley et al. 2000). They also reported that Kv4.2 was found in large projection neurons of the cochlear nucleus including pyramidal cells of the DCN. Our ISH data are consistent in every aspect with these findings and we also show that the cells labeled with Kv4.2 probes represent a different population of cells than those cells that express Kv4.3 mRNA.

In addition, our ISH results in rat brain mirror those found in the Allen Brain Atlas (<http://www.brainatlas.org/aba/>) (Lein et al. 2006). DCN Kv4.2 labeling in these images is also found in smaller cell bodies that are located throughout the nucleus. Kv4.3, on the other hand, clearly labels cells that are found only in the fusiform cell layer. The images in the Allen Brain atlas distinctly show labeling in large cell bodies in the fusiform layer. Our results confirm that Kv4 expression patterns are similar in the rat as they are in the mouse.

#### **4.4.2 Immunocytochemistry**

By specifically labeling pyramidal cells with a retrograde tracer dye, we were able to determine which Kv4 channel protein was expressed by pyramidal cells. While Kv4.2 mRNA was found in the fusiform cell layer in our ISH experiments, Kv4.2 protein was not found in pyramidal cells, rather it was found in small cells throughout the nucleus. We suggest that these cells are predominantly granule cells. The DCN is derived from a similar area of embryological tissue as the cerebellum and the anatomy and circuitry of these two brain regions is comparable. Granule cells of the cerebellum express Kv4.2 ion channels (Shibata et al. 1999), so it is not surprising that DCN granule cells also express Kv4.2. On the other hand, we were somewhat surprised to find that no back labeled pyramidal cells showed labeling for Kv4.2. In light of the ISH results of Fitzakerley and colleagues and our own ISH results, we expected to see at least some pyramidal cells that stained for the Kv4.2 channel. However, it is entirely possible that the cell expresses Kv4.2 mRNA, but the channel is either not trafficked to the membrane or the mRNA is not translated. In addition, there could be developmental effects that we did not study. The animals used in the immunocytochemistry studies were 3 weeks older than those used in the ISH experiments.

There have been developmental changes in ion channel expression reported for the DCN (Fitzakerley et al. 2000).

Kv4.3 is likely the channel responsible for  $I_A$ . Kv4.3 mRNA is expressed in the fusiform cell layer and Kv4.3 protein is found in pyramidal cells bodies and dendrites. These data support our other findings that the channel that gives rise to  $I_A$  in pyramidal cells is a member of the Kv4 family of potassium channels since the kinetic and pharmacological characteristics of this current match those reported for Kv4 channels (Kanold and Manis 2001; 1999).

It is predictable that staining for Kv4.3 is found throughout the fusiform and molecular layer. Kv4 channels are targeted to the somatodendritic compartments of neurons by a dileucine-containing motif (Hsu et al. 2003; Rivera et al. 2003; Sheng et al. 1992). The cell bodies of pyramidal cells are found in the fusiform cell layer, while the apical dendrites project into the molecular layer. Pyramidal cells also have basal dendrites that extend into the deep layer, however there are fewer dendritic branches. Perhaps the smaller numbers of dendrites made it difficult to see Kv4.3 staining in the deep layer of the nucleus. Although an alternate explanation is Kv4.3 is selectively targeted to the apical branch of dendrites. Selective dendritic targeting of glutamate receptors has been described previously in DCN pyramidal cells (Rubio and Wenthold 1997). In addition, differential subcellular localization has been reported for the Kv4 channels. For instance, Kv4 channels are localized to the post-synaptic membranes in rat supraoptic neurons (Alonso and Widmer 1997). Further, in visual cortical pyramidal cells and interneurons, Kv4.2 and Kv4.3 are targeted to the post-synaptic membrane of GABAergic synapses, but they are found just outside the synaptic region of excitatory synapses (Burkhalter et al. 2006). In cerebellar granule cells, Kv4.2 is targeted to

excitatory synapses, while in hippocampus it is located extrasynaptically at inhibitory synapses (Jinno et al. 2005; Shibasaki et al. 2004). Since subcellular targeting of Kv4 channels is thought to be activity dependent, it is possible that differential subcellular targeting of Kv4 channels takes place in pyramidal cells. We were not able to detect which synapses on which dendritic branch contain clusters of Kv4.3 channels with the resolution of our images. In the future it will be important to understand which synapses contain Kv4.3 so that we can gain a greater understanding of the role Kv4.3 plays in synaptic integration and information processing in DCN pyramidal cells.

## **Chapter 5: Discussion**

### **5.1 Spike Timing and Potassium Channels in DCN Pyramidal Cells**

A neuron must be able to differentiate spatiotemporal patterns of input, and then process, encode and relay that information as a train of action potentials to target neurons. This ability is paramount to proper neuronal function. To this end, neurons can encode information by a rate code or by the precise timing of action potentials in relation to one another. Pyramidal cells, previous to this work, have either been thought of as neurons that utilize a rate code to encode information or, if they display any timing specific information, they encode timing information that only represents the sound waveform envelope, such as amplitude modulation. Here we show that these cells are capable of firing precisely timed trains of action potentials to time varying input presented at the cell body. The events that elicit precisely timed spikes in pyramidal cells are very short in duration, leading us to conclude that at least in some circumstances, these neurons can behave as coincidence detectors for spatiotemporal patterns of input on short time scales.

In addition to synaptic input, intrinsic conductances also shape pyramidal cells response patterns. Sound evoked response patterns of pyramidal cells are dominated by inhibition. In addition, there is temporally related inhibitory input to pyramidal cells from at least three types of inhibitory interneurons. Therefore, any conductance that is sensitive to inhibition would play an important role in pyramidal cell output patterns. The work presented

here reveals that one of the conductances that shapes pyramidal cell response patterns is the Kv4.3 channel. Hyperpolarizing voltages with short latencies disinhibit Kv4.3. Furthermore, this channel activates at sub-threshold voltages. These characteristics of Kv4.3 confer additional timing sensitivity to pyramidal cells and affect the spike generating mechanism. The new understanding of pyramidal cells brought to us by the work presented here lead to new insights into the exact function of pyramidal cells within the auditory system. These possibilities will be discussed in this chapter.

## **5.2 Comparison of DCN Pyramidal Cells to Other Brainstem Neurons**

There is no doubt that the auditory system is the quintessential example of spike time coding by neurons in the CNS. As discussed previously, neurons in the auditory nerve phase lock to sound frequency information up to 4000 Hz in mammals while neurons in the medial superior olive (MSO) utilize interaural time differences on a microsecond scale to localize a sound source (Oertel 1999). Other auditory brainstem neurons like the bushy cells in the VCN, and the glycinergic cells in the medial nucleus of the trapezoid body (MNTB) must preserve the timing code relayed to them through large calyceal synapses. In light of the importance of timing in the auditory brainstem, it is not surprising that DCN pyramidal cells also can utilize spike timing to encode information. However, the cellular machinery used to encode timing are quite different in DCN pyramidal cells when compared to other auditory brainstem neurons.

First, principal cells of the anterior VCN (bushy cells), posterior VCN (octopus cells), MNTB and MSO all respond to stimuli with either primary-like or onset response patterns. Both of these response patterns show one or two short latency spikes and then a sharp decrease in the probability of firing (see Figure 1.4). Usually, these cells will only fire one

action potential in response to a depolarization. Bushy cells, and MNTB neurons are sharply tuned to frequency information while octopus cells are tuned to broadband transients and sound wave periodicity (Oertel 1999). MSO neurons receive input from both ipsilateral and contralateral bushy cells along with inhibitory input from the MNTB, and act as coincidence detectors in order to decode sound location in the azimuth (Grothe and Sanes 1994). On the other hand, DCN pyramidal cells respond with multiple spikes when presented with tonal stimuli. In addition, DCN cells show little tuning to frequency information but are instead strongly excited by broadband stimuli and phase lock only to envelope modulation. Therefore, DCN neurons are most likely performing computations that differ remarkably from the other brainstem neurons, which are responsible for conveying frequency information and azimuthal sound localization information.

The intrinsic conductances expressed in pyramidal cells also differ from those in other auditory neurons. In order to fire precisely timed spikes to very high frequency input, VCN, MNTB and MSO neurons are equipped with low threshold and high threshold potassium channels that provide strong outward rectification. In general, such currents are provided by Kv1.1, Kv1.2 and Kv3.1 channels. All brainstem neurons that fire only one or two action potentials in response to sustained depolarization express these channels (Klug and Trussell 2006; Manis and Marx 1991; Rothman and Manis 2003; Svirskis et al. 2003; Trussell 1999). Kv1.1 and Kv1.2 channels open at subthreshold voltages slowly, but remain open as long as the cell membrane remains depolarized and act in concert with high voltage activated potassium channels (like Kv3.1) to quickly repolarize the membrane during an action potential. This behavior is essential if a neuron is to follow high frequency input, like that of the auditory nerve (Manis 2007).

Since Kv1.1 and Kv1.2 channels open slowly at sub-threshold voltages, they endow the neuron with a mechanism to generate a spike only in response to large and rapid depolarizations. If a large depolarization occurs either because of transmitter release at endbulb synapses (in the case of bushy cells and MNTB neurons) or two coincident EPSPs (in the case of MSO neurons), the membrane will depolarize quickly before these potassium channels have time to open and an action potential will be fired (Trussell 1999). In contrast, if only small depolarizations or non-coincident EPSPs arrive at the neurons, the membrane depolarization will not be fast enough to reach threshold before the potassium channels activate and lead to a dampened depolarization and a slow rise in membrane potential (Ferragamo and Oertel 2002). These characteristics enable neurons to only respond to precisely-timed coincident input or large depolarizations from the endbulbs of Held. These channels also lead to brief synaptic events by shortening the membrane time constant. This feature is particularly important for neurons of the MSO to act as coincidence detectors (Svirskis et al. 2003). If synaptic events are not brief, they can integrate over longer periods of time and elicit spikes that do not represent information relevant to interaural time differences. Blocking these channels results in wide action potentials and poorly timed spikes (Klug and Trussell 2006).

The channel profile of the aforementioned auditory neurons contrasts starkly with DCN pyramidal cells. Pyramidal cells do not heavily express Kv1.1, 1.2 and 3.1 channels. This difference explains, at least in part, the difference in response patterns observed in pyramidal cells when compared to other auditory brainstem neurons. Pyramidal cells fire repeated spikes to depolarizing current. In addition, the latencies to spikes are often delayed when the depolarizations are preceded by hyperpolarizations as demonstrated in this work

and in other work done by our lab (Kanold and Manis 2001; 2005a; 1999; Manis 1990). As established in this work, this response pattern is due to the Kv4.3 channel. Since Kv4.3 rapidly inactivates, the outward rectification in pyramidal cells is transient, and repetitive spikes can be fired to a sustained depolarizing current. The lack of lasting outward rectification by Kv1 and Kv3 channels also explains why pyramidal cells do not phase lock to frequency information contained in the auditory nerve. They express different potassium channels than those found in neurons that do phase lock to sound wave frequency.

On the other hand, Kv4.3 channels confer other properties to pyramidal cells that could be useful in encoding other kinds of timing and auditory information. Pyramidal cells respond to different types of sensory information than the other brainstem auditory neurons in that they must integrate multiple types of sensory information with auditory information. The MSO, VCN and MNTB do not integrate multiple sensory inputs. The contrasting expression profiles of these types of cells might reflect these differing functions.

In addition to the multi-sensory integration function of pyramidal cells, it has recently been demonstrated that pyramidal cells respond to the rising phase of spectral notches in order to enable sound localization in the vertical plane (Reiss and Young 2005). Modeling studies have shown that this sensitivity is, in part, due to the inhibitory inputs associated with sound information onto pyramidal cells. However, it is thought that part of the sound localization function of the DCN also involves comparing sound information with the position of the head or pinna in order to adequately interpret spectral notch position. It is possible that the different expression patterns of Kv4.3 potassium channels and other intrinsic conductances in pyramidal cells are specialized for this function.

For instance, Kv4.3 confers to pyramidal cells a mechanism by which inhibitory inputs are encoded. When a pyramidal cell receives inhibitory input, Kv4.3 channel inactivation is removed and the channel will be in the closed state and available to open to any depolarizing input onto the cell. If an EPSP occurs in a certain time window after an IPSP, the EPSP will be dampened due to the transient outward rectification provided by Kv4.3. Perhaps patterns of inhibition from both vertical cells, and wideband inhibitors associated with sound information, and cartwheel cells and stellate cells associated with somatosensory information deinactivate Kv4.3 and thereby prime the spike generating mechanism with the proper configuration to fire a spike exactly when the rising phase of the spectral notch and head position are in the proper spatiotemporal input pattern. This mechanism would encode the location of the sound source in relation to the position of the head. A straightforward experiment to test this hypothesis would be to block Kv4.3 channels (or knock them out) in the DCN and determine if this perturbation affects an animal's ability to orient to a sound source.

What we know after many years of research is pyramidal cells are not simple auditory neurons like other brainstem auditory neurons. They are modulated by somatosensory and other input on the apical dendrites (Kanold and Young 2001; Shore 2005; Shore and Zhou 2006). Therefore, attempts to study them as other brainstem auditory neurons will likely fail to reveal the true function of these neurons. As more parameters of the DCN are elucidated, we can apply them to physiological models of the DCN to ascertain how and under what circumstances the two converging inputs (auditory and non-auditory) are integrated into one signal by pyramidal cells.

### 5.3 Comparison of DCN Pyramidal Cells with Other CNS Neurons

DCN pyramidal cells are more aptly compared with other CNS neurons such as deep cerebellar nuclei neurons, hippocampal CA1 pyramidal cells, and other cortical neurons. To date, all of these neurons' timing properties have been investigated to some extent, and more complicated and subtle mechanisms exist within these cells to control spike timing when compared with auditory brainstem neurons. DCN pyramidal cells are more like these neurons in that they process multiple types of sensory input and express A-currents. In the past, these CNS neurons, just like pyramidal cells, have been thought of primarily as integrators rather than coincidence detectors, because they exhibit slow membrane time constants that allow for summation of excitatory inputs. However, new insights into these neurons have argued that under the correct circumstances, even these neurons can behave as coincidence detectors and utilize spike timing to encode information (Grande et al. 2004). Some of these conditions include strong synchronous inhibition, faster decaying EPSPs, adaptive spike thresholds, and noisy background activity (Azouz and Gray 2000; Grande et al. 2004; Hausser and Clark 1997). These characteristics can decrease the membrane time constant and attenuate integration properties in these neurons, leading the neuron to fire precisely timed action potentials in response to synchronous input. The environment of DCN pyramidal cells provides these conditions in that there is strong inhibitory inputs and spontaneous background activity from the auditory nerve. The work presented in Chapter Two also reveals that pyramidal cells are more likely to fire spikes when large depolarizing currents lower spike threshold so that a spike is more likely to be fired on synchronous input.

Another similarity of DCN pyramidal cells with non-auditory neurons is the potential ability of inhibition to control spike timing. DCN response patterns are dominated by

inhibition and the timing of inhibition in the DCN is tightly linked to the timing of excitation. Inhibition has been shown to be essential for neurons to use a spike timing code in higher cortical neurons and in cerebellar neurons. For instance, in neurons of the deep cerebellar nuclei, the timing precision of spike times was affected only by changing the strength of synchronous inhibitory input. Even when the inhibitory inputs were slightly jittered, the timing precision remained high (Gauck and Jaeger 2000) . Strong synchronous excitatory inputs could overcome the preference for inhibition to determine the precision of spike times in these cells; however, it is only when the inhibitory inputs are completely randomized that excitation determines the output pattern and timing of spikes (Gauck and Jaeger 2003).

Since DCN and other CNS neurons also possess characteristics that favor synaptic integration, these neurons can switch what scheme of information encoding they are using, depending on the kind of information they are receiving. For instance, if the information they are processing requires that they encode the information as a timing code, then there will be more inhibition and membrane dynamics will be set to shorten EPSP decay time constants. If the information needs to be sent as a rate code, the neurons will switch to the integration state. Hauser and Clark demonstrated this state dependence in cerebellar Purkinje cells (1997) and the same idea has been demonstrated recently in hippocampal CA1 pyramidal neurons (Gasparini and Magee 2006).

DCN pyramidal cells, like these higher cortical neurons, receive and encode multiple kinds of information. They can encode the envelope waveform in addition to encoding sound localization information. It is certainly possible that other information is processed and encoded in the DCN. Therefore, we postulate that DCN pyramidal cells are also state

dependent--sometimes using a rate code, and at other times encoding their inputs with spike timing.

Kv4.3 would play a part in determining the state of the neuron. For example, in environments where inhibition dominates and Kv4.3 is deinactivated, Kv4.3 might enable pyramidal cells to become strong coincidence detectors for short periods by only allowing very large and rapid synchronized depolarizations to elicit precisely timed spikes. It is possible that the dominance of inhibition in this nucleus is present to enable pyramidal cells to be better coincidence detectors by deinactivation of Kv4.3 and decreasing the membrane time constant as reported in other neurons (Grande et al. 2004). Since these effects are transient, pyramidal cells could switch rapidly between a state where inhibition is dominant and timing is utilized to a state where inhibition is minimal and EPSP integration drives the spike generator.

When DCN neurons are in a state that is encoding information by integration of synaptic input over time, Kv4.3 could also play an important role in this regime by allowing the cell to encode timing of excitatory input. Kv4.3 rapidly inactivates when activated and because it is capable of closed-state inactivation, a percentage of this channel is always inactivated at rest. Therefore, unless the cell is briefly hyperpolarized, the availability of channels to open and oppose inward current is lessened. Further, if even more channels are inactivated by subthreshold EPSPs, enough of the channels could become inactivated so that usual subthreshold EPSPs are able to elicit spikes since there is little to no opposing current. This mechanism would also allow different patterns of spatiotemporal input to force the cell into different coding states, depending on the kinds of information that was being relayed to the pyramidal cell. With Kv4.3 inactivated, on the other hand, the pyramidal cells would act

more as integrators and weaker depolarizations could elicit spikes. This would result in potentially more ways in which the pyramidal cells could encode information.

Finally, DCN pyramidal cells are more similar to hippocampal, cortical and cerebellar neurons because their synapses can be strengthened and weakened by certain patterns of input. Kv4 channels play an important role by enabling the cells to potentiate synapses based on the patterns of input and output. In hippocampal pyramidal cells, Hebbian plasticity is altered when Kv4.2 channel voltage sensitivity is shifted (Watanabe et al. 2002). This is due to Kv4.2 ability to attenuate back propagating action potentials that allow  $Ca^{2+}$  to enter dendrites, and initiate signaling cascades that result in altered synaptic strength. When preceding depolarizing input inactivates Kv4.2, it will not be available to oppose inward current resulting from back propagating action potentials, and more  $Ca^{2+}$  will enter the dendrites. If the depolarizing input is too far removed in time from the back propagating action potential, Kv4.2 can activate and open to attenuate  $Ca^{2+}$  entry. Parallel fiber synapses on apical dendrites of pyramidal cells potentiate according to Hebbian rules like hippocampal pyramidal cells (Tzounopoulos et al. 2004). So far, this same type of synaptic plasticity has not been reported for other auditory brainstem neurons. Therefore, Kv4.3 is more than likely an important component of spike-timing dependent plasticity in pyramidal neurons. Since this channel can be modulated, pyramidal cells could alter the conditions under which synapses are potentiated or depressed. This ability would be very useful to neurons that integrate multiple types of sensory information.

In sum, while pyramidal cells do not perform the same kinds of information encoding as other brainstem auditory neurons, Kv4.3 channels could confer sensitivity to different patterns of spatiotemporal input. This mechanism would enable them to encode these

patterns of input in a state-dependent way, by the precise timing of action potentials based on the particulars of the neuronal environment and the type of information being relayed to the cell. This type of information encoding resembles that thought to be used by hippocampal pyramidal neurons and neurons of the cerebellum.

#### **5.4 Kv4.3 Effects on Dendritic Integration**

Since Kv4.3 channels are targeted to the somatodendritic compartment of neurons and are expressed in and around synapses (see introduction), these channels may alter dendritic integration at pyramidal cell synapses. It is now well accepted that dendrites do not function as simple passive cables as previously suggested (Rall 1967). If they did behave in this manner, the cable properties of dendrites would cause synaptic potentials to attenuate as a function of the distance from the soma. In addition, there would be different time integration windows for proximal and distal synapses (Magee 2000). With these properties, the neuron is only responsive to the *quantity* of excitatory input, and it would be difficult for a neuron to predictably fire a precisely timed action potential in response to recognizable *patterns* of input.

However, dendritic specializations are now thought to produce dendritic potentials that defy cable properties (Yuste and Tank 1996). For example, dendrites can elicit spikes in response to excitatory input if they express either Ca<sup>2+</sup> or Na<sup>+</sup> channels and the input is temporally or spatially coincident (Gasparini et al. 2004; Losonczy and Magee 2006; Stuart and Sakmann 1994). In addition, these same studies demonstrated that dendritic potassium channels, like Kv4.2 and Kv4.3 or HCN channels, could attenuate excitatory input. Such conductances change the behavior of dendrites from a linear, integrative cable, to one that exhibits nonlinear output based on the spatiotemporal pattern of input (Magee 2000). For

example, if EPSPs converge on a neuron close in space and time, the actual change in membrane potential at the soma is greater than would be predicted with a linear integration. Such supra-linearities could lead to short latency, well timed spikes by increasing the rising slope of the membrane potential (Azouz and Gray 2000; Gasparini et al. 2004). In contrast, Kv4.2 and HCN channels attenuate excitatory potentials. These dynamic properties benefit the neuron by conferring upon them a mechanism by which they can recognize and respond to patterns of input with precisely timed spikes and reduce ill-timed spikes fired in response to noisy or jittery input. Thus, it is the *qualities*, and not just the *quantity* of synaptic input that is encoded in the output.

Further, these dendritic conductances allow for modulation in the behavior of the neuron. This modulation could result from second messenger systems being activated by neuromodulators such as acetylcholine or norepinephrine (Hoffman and Johnston 1999) or by patterns of input, which engage different configurations of dendritic conductances (Berman and Maler 1998; Llinas and Sugimori 1980; Llinas 1988). Therefore, the neuron represents not just the synaptic input in to the cell, but also the condition of the neuron itself, which can be altered by both history of activity and neuromodulation. With these intrinsic properties, the neuron can respond to very specific changes in the information it must process and encode.

How could such mechanisms be useful in DCN pyramidal cells? We have already shown both in this work and previous work, that Kv4.3 confers a mechanism by which inhibitory inputs are encoded by the timing of spikes. After a period of inhibition, the same excitatory input will result in a delay in spike time compared to the timing without the previous inhibition. There is no doubt that inhibitory inputs play an essential role in

information encoding in the DCN. It is possible that Kv4.3 is responsible for the output patterns of pyramidal cells in response to patterns of inhibitory input.

In addition, Kv4.3 could provide a mechanism by which certain patterns of input lead to supra-linear behavior, while other patterns of input lead to sub-linear behavior. The state of the neuron would depend upon the patterns of input and neuromodulation. When there is strong inhibitory input, Kv4.3 would be available to activate. In this scenario Kv4.3 would attenuate any weak or spatiotemporally distant input further by opening its outward conductance (sub-linear state). However, if there was very coincident input, it could overcome this opposition and lead to a well-timed spike (supra-linear state). The threshold for how spatiotemporally succinct these inputs would need to be could be set by history the history of activity or neuromodulation of the channel through phosphorylation. One possible mechanism for such neuromodulation is acetylcholine. It is known that the DCN receives cholinergic inputs (Chen et al. 1994; 1995). In addition, it is known that muscarinic stimulation leads to changes in Kv4 channel voltage sensitivity (Hoffman and Johnston 1999). Therefore, these cholinergic inputs in the DCN might supply some of the neuromodulation necessary for the neurons to switch between these two states.

By allowing the cell to be tuned to history of input and neuromodulation, Kv4.3 could provide the link between auditory and non-auditory inputs. Information about head position would push a pyramidal cell into a certain regime. When the pyramidal cells sense subsequent auditory information, it is processed in terms of the sensory input that has placed certain constraints on the pyramidal cell. In this way, spectral notch information would be interpreted based on the head position. This mechanism would allow pyramidal cells to encode the auditory information along with non-auditory information.

Channels other than Kv4.3 would certainly play a role in this type of information encoding. Apical dendrites also express  $\text{Ca}^{2+}$  channels that, when activated, could boost any excitatory input from auditory nerve fibers resulting in action potentials that would not have been elicited without the  $\text{Ca}^{2+}$  spikes. It is not known if apical or basal dendrites express  $\text{Na}^+$  channels but they could also perform the same role only faster. Pyramidal cells do express a low-threshold persistent  $\text{Na}^+$  current that, when activated, could boost synaptic excitation (Manis et al. 2003). Work in this area will prove very helpful in further understanding the role of spatiotemporal patterns of input and the auditory and non-auditory convergence onto pyramidal cells.

## **5.5 Potential Pathologies**

Kv4.2 channels have been implicated in temporal lobe epilepsy. In this disorder, it is thought that there are fewer Kv4.2 channels expressed and those that are expressed are phosphorylated and therefore have higher activation voltages. This higher activation voltage profile essentially reduces the number of channels that open in response to depolarization (Bernard et al. 2004). This change in Kv4.2 current results in increased dendritic excitability, which leads to epileptic behavior of neurons.

The DCN has also been implicated in a hearing disorder that might be caused by increased activity of neurons. Tinnitus is the perception of a phantom sound and has been associated with increased activity of the DCN (Zhang and Kaltenbach 1998). While the exact cell type associated with this increase in spontaneous activity is debated (Brozoski et al. 2002; Chang et al. 2002), it is possible that dysregulation of Kv4.2 or Kv4.3 is responsible since these channels play a major role in determining neuronal excitability. In addition, since these channels set the conditions under which LTP and LTD occur, changes in their voltage

sensitivity could result in aberrant synaptic plasticity. More research in this area is needed to determine what role, if any, Kv4 channels and the DCN play in this disorder.

## **5.6 Summary**

The work presented in this thesis has demonstrated that pyramidal cells in the DCN can fire well-timed action potentials in response to time-varying input. Small IPSP-like currents augment this timing precision. Intrinsic conductances can play an important role in determining what kind of input leads to spiking, so we tested whether HCN channels or potassium channels affect pyramidal cells spike timing. A rapidly-inactivating potassium current altered the timing of spikes after periods of inhibition. The channel responsible for this current in pyramidal cells was also determined to arise from Kv4.3. Kv4 channels have important functions in other neurons known to integrate complex information and alter synaptic efficacy in response to synaptic input. Therefore, it is probably that Kv4.3 plays an essential role in pyramidal cell information encoding and in the proper function of the DCN.

## Bibliography

- Abeles M, Bergman H, Margalit E, and Vaadia E.** Spatiotemporal firing patterns in the frontal cortex of behaving monkeys. *J Neurophysiol* 70: 1629-1638, 1993.
- Adams JC.** Single unit studies on the dorsal and intermediate acoustic striae. *J Comp Neurol* 170: 97-106, 1976.
- Adams JP, Anderson AE, Varga AW, Dineley KT, Cook RG, Pfaffinger PJ, and Sweatt JD.** The A-type potassium channel Kv4.2 is a substrate for the mitogen-activated protein kinase ERK. *J Neurochem* 75: 2277-2287, 2000.
- Alonso G, and Widmer H.** Clustering of KV4.2 potassium channels in postsynaptic membrane of rat supraoptic neurons: an ultrastructural study. *Neuroscience* 77: 617-621, 1997.
- An WF, Bowlby MR, Betty M, Cao J, Ling HP, Mendoza G, Hinson JW, Mattsson KI, Strassle BW, Trimmer JS, and Rhodes KJ.** Modulation of A-type potassium channels by a family of calcium sensors. *Nature* 403: 553-556, 2000.
- Anderson AE, Adams JP, Qian Y, Cook RG, Pfaffinger PJ, and Sweatt JD.** Kv4.2 phosphorylation by cyclic AMP-dependent protein kinase. *J Biol Chem* 275: 5337-5346, 2000.
- Azouz R, and Gray CM.** Dynamic spike threshold reveals a mechanism for synaptic coincidence detection in cortical neurons in vivo. *Proc Natl Acad Sci U S A* 97: 8110-8115, 2000.
- Babalian AL.** Synaptic influences of pontine nuclei on cochlear nucleus cells. *Exp Brain Res* 167: 451-457, 2005.
- Babalian AL, Ryugo DK, and Rouiller EM.** Discharge properties of identified cochlear nucleus neurons and auditory nerve fibers in response to repetitive electrical stimulation of the auditory nerve. *Exp Brain Res* 153: 452-460, 2003.
- Bahring R, Boland LM, Varghese A, Gebauer M, and Pongs O.** Kinetic analysis of open- and closed-state inactivation transitions in human Kv4.2 A-type potassium channels. *J Physiol* 535: 65-81, 2001.
- Bair W, and Koch C.** Temporal precision of spike trains in extrastriate cortex of the behaving macaque monkey. *Neural computation* 8: 1185-1202, 1996.
- Baldwin TJ, Tsaour ML, Lopez GA, Jan YN, and Jan LY.** Characterization of a mammalian cDNA for an inactivating voltage-sensitive K<sup>+</sup> channel. *Neuron* 7: 471-483, 1991.

**Bardoni R, and Belluzzi O.** Kinetic study and numerical reconstruction of A-type current in granule cells of rat cerebellar slices. *J Neurophysiol* 69: 2222-2231, 1993.

**Beierholm U, Nielsen CD, Ryge J, Alstrom P, and Kiehn O.** Characterization of reliability of spike timing in spinal interneurons during oscillating inputs. *Journal of neurophysiology* 86: 1858-1868, 2001.

**Berman NJ, and Maler L.** Interaction of GABAB-mediated inhibition with voltage-gated currents of pyramidal cells: computational mechanism of a sensory searchlight. *J Neurophysiol* 80: 3197-3213, 1998.

**Bernard C, Anderson A, Becker A, Poolos NP, Beck H, and Johnston D.** Acquired dendritic channelopathy in temporal lobe epilepsy. *Science* 305: 532-535, 2004.

**Berrebi AS, and Mugnaini E.** Distribution and targets of the cartwheel cell axon in the dorsal cochlear nucleus of the guinea pig. *Anat Embryol (Berl)* 183: 427-454, 1991.

**Berry MJ, Warland DK, and Meister M.** The structure and precision of retinal spike trains. *Proceedings of the National Academy of Sciences of the United States of America* 94: 5411-5416, 1997.

**Birnbaum SG, Varga AW, Yuan LL, Anderson AE, Sweatt JD, and Schrader LA.** Structure and function of Kv4-family transient potassium channels. *Physiol Rev* 84: 803-833, 2004.

**Blackstad TW, Osen KK, and Mugnaini E.** Pyramidal neurones of the dorsal cochlear nucleus: a Golgi and computer reconstruction study in cat. *Neuroscience* 13: 827-854, 1984.

**BoSmith RE, Briggs I, and Sturgess NC.** Inhibitory actions of ZENECA ZD7288 on whole-cell hyperpolarization activated inward current (I<sub>h</sub>) in guinea-pig dissociated sinoatrial node cells. *Br J Pharmacol* 110: 343-349, 1993.

**Brawer JR, Morest DK, and Kane EC.** The neuronal architecture of the cochlear nucleus of the cat. *J Comp Neurol* 155: 251-300, 1974.

**Brown MC, and Ledwith JV, 3rd.** Projections of thin (type-II) and thick (type-I) auditory-nerve fibers into the cochlear nucleus of the mouse. *Hearing research* 49: 105-118, 1990.

**Brozoski TJ, Bauer CA, and Caspary DM.** Elevated fusiform cell activity in the dorsal cochlear nucleus of chinchillas with psychophysical evidence of tinnitus. *J Neurosci* 22: 2383-2390, 2002.

**Buonomano DV.** Timing of neural responses in cortical organotypic slices. *Proc Natl Acad Sci U S A* 100: 4897-4902, 2003.

- Buracas GT, Zador AM, DeWeese MR, and Albright TD.** Efficient discrimination of temporal patterns by motion-sensitive neurons in primate visual cortex. *Neuron* 20: 959-969, 1998.
- Burkhalter A, Gonchar Y, Mellor RL, and Nerbonne JM.** Differential expression of I(A) channel subunits Kv4.2 and Kv4.3 in mouse visual cortical neurons and synapses. *J Neurosci* 26: 12274-12282, 2006.
- Cai X, Liang CW, Muralidharan S, Kao JP, Tang CM, and Thompson SM.** Unique roles of SK and Kv4.2 potassium channels in dendritic integration. *Neuron* 44: 351-364, 2004.
- Carr CE, Soares D, Parameshwaran S, and Perney T.** Evolution and development of time coding systems. *Curr Opin Neurobiol* 11: 727-733, 2001.
- Chang H, Chen K, Kaltenbach JA, Zhang J, and Godfrey DA.** Effects of acoustic trauma on dorsal cochlear nucleus neuron activity in slices. *Hearing research* 164: 59-68, 2002.
- Chen K, Waller HJ, and Godfrey DA.** Cholinergic modulation of spontaneous activity in rat dorsal cochlear nucleus. *Hearing research* 77: 168-176, 1994.
- Chen K, Waller HJ, and Godfrey DA.** Muscarinic receptor subtypes in rat dorsal cochlear nucleus. *Hearing research* 89: 137-145, 1995.
- Chen X, and Johnston D.** Properties of single voltage-dependent K<sup>+</sup> channels in dendrites of CA1 pyramidal neurones of rat hippocampus. *J Physiol* 559: 187-203, 2004.
- Coomes DL, and Schofield BR.** Separate projections from the inferior colliculus to the cochlear nucleus and thalamus in guinea pigs. *Hearing research* 191: 67-78, 2004.
- Davis KA, Miller RL, and Young ED.** Effects of somatosensory and parallel-fiber stimulation on neurons in dorsal cochlear nucleus. *J Neurophysiol* 76: 3012-3024, 1996.
- de Ruyter van Steveninck RR, Lewen GD, Strong SP, Koberle R, and Bialek W.** Reproducibility and variability in neural spike trains. *Science* 275: 1805-1808, 1997.
- Diesmann M, Gewaltig MO, and Aertsen A.** Stable propagation of synchronous spiking in cortical neural networks. *Nature* 402: 529-533, 1999.
- Dodla R, Svirskis G, and Rinzel J.** Well-timed, brief inhibition can promote spiking: postinhibitory facilitation. *J Neurophysiol* 95: 2664-2677, 2006.
- Dorval AD, Christini DJ, and White JA.** Real-Time linux dynamic clamp: a fast and flexible way to construct virtual ion channels in living cells. *Ann Biomed Eng* 29: 897-907, 2001.

**Dorval AD, Jr., and White JA.** Channel noise is essential for perithreshold oscillations in entorhinal stellate neurons. *J Neurosci* 25: 10025-10028, 2005.

**Doyle DA, Morais Cabral J, Pfuetzner RA, Kuo A, Gulbis JM, Cohen SL, Chait BT, and MacKinnon R.** The structure of the potassium channel: molecular basis of K<sup>+</sup> conduction and selectivity. *Science* 280: 69-77, 1998.

**Evans EF, and Nelson PG.** The responses of single neurones in the cochlear nucleus of the cat as a function of their location and the anaesthetic state. *Exp Brain Res* 17: 402-427, 1973.

**Farago AF, Awatramani RB, and Dymecki SM.** Assembly of the brainstem cochlear nuclear complex is revealed by intersectional and subtractive genetic fate maps. *Neuron* 50: 205-218, 2006.

**Fellous JM, Houweling AR, Modi RH, Rao RP, Tiesinga PH, and Sejnowski TJ.** Frequency dependence of spike timing reliability in cortical pyramidal cells and interneurons. *J Neurophysiol* 85: 1782-1787, 2001.

**Fellous JM, Tiesinga PH, Thomas PJ, and Sejnowski TJ.** Discovering spike patterns in neuronal responses. *J Neurosci* 24: 2989-3001, 2004.

**Ferragamo MJ, and Oertel D.** Octopus cells of the mammalian ventral cochlear nucleus sense the rate of depolarization. *J Neurophysiol* 87: 2262-2270, 2002.

**Fitzakerley JL, Star KV, Rinn JL, and Elmquist BJ.** Expression of Shal potassium channel subunits in the adult and developing cochlear nucleus of the mouse. *Hear Res* 147: 31-45, 2000.

**Francis HW, Scott JC, and Manis PB.** Protein kinase C mediates potentiation of synaptic transmission by phorbol ester at parallel fibers in the dorsal cochlear nucleus. *Brain research* 951: 9-22, 2002.

**Frick A, Magee J, and Johnston D.** LTP is accompanied by an enhanced local excitability of pyramidal neuron dendrites. *Nat Neurosci* 7: 126-135, 2004.

**Fricker D, and Miles R.** EPSP amplification and the precision of spike timing in hippocampal neurons. *Neuron* 28: 559-569, 2000.

**Frisina RD.** Subcortical neural coding mechanisms for auditory temporal processing. *Hearing research* 158: 1-27, 2001.

**Frisina RD, Walton JP, and Karcich KJ.** Dorsal cochlear nucleus single neurons can enhance temporal processing capabilities in background noise. *Exp Brain Res* 102: 160-164, 1994.

**Froemke RC, and Dan Y.** Spike-timing-dependent synaptic modification induced by natural spike trains. *Nature* 416: 433-438, 2002.

**Fujino K, and Oertel D.** Bidirectional synaptic plasticity in the cerebellum-like mammalian dorsal cochlear nucleus. *Proceedings of the National Academy of Sciences of the United States of America* 100: 265-270, 2003.

**Gardner SM, Trussell LO, and Oertel D.** Correlation of AMPA receptor subunit composition with synaptic input in the mammalian cochlear nuclei. *J Neurosci* 21: 7428-7437, 2001.

**Gardner SM, Trussell LO, and Oertel D.** Time course and permeation of synaptic AMPA receptors in cochlear nuclear neurons correlate with input. *J Neurosci* 19: 8721-8729, 1999.

**Gasparini S, and Magee JC.** State-dependent dendritic computation in hippocampal CA1 pyramidal neurons. *J Neurosci* 26: 2088-2100, 2006.

**Gasparini S, Migliore M, and Magee JC.** On the initiation and propagation of dendritic spikes in CA1 pyramidal neurons. *J Neurosci* 24: 11046-11056, 2004.

**Gauck V, and Jaeger D.** The contribution of NMDA and AMPA conductances to the control of spiking in neurons of the deep cerebellar nuclei. *J Neurosci* 23: 8109-8118, 2003.

**Gauck V, and Jaeger D.** The control of rate and timing of spikes in the deep cerebellar nuclei by inhibition. *J Neurosci* 20: 3006-3016, 2000.

**Godfrey DA, Kiang NY, and Norris BE.** Single unit activity in the dorsal cochlear nucleus of the cat. *The Journal of comparative neurology* 162: 269-284, 1975.

**Goldberg JM, and Brownell WE.** Discharge characteristics of neurons in anteroventral and dorsal cochlear nuclei of cat. *Brain Res* 64: 35-54, 1973.

**Golding NL, and Oertel D.** Context-dependent synaptic action of glycinergic and GABAergic inputs in the dorsal cochlear nucleus. *J Neurosci* 16: 2208-2219, 1996.

**Golding NL, and Oertel D.** Physiological identification of the targets of cartwheel cells in the dorsal cochlear nucleus. *J Neurophysiol* 78: 248-260, 1997.

**Grande LA, Kinney GA, Miracle GL, and Spain WJ.** Dynamic influences on coincidence detection in neocortical pyramidal neurons. *J Neurosci* 24: 1839-1851, 2004.

**Grothe B, and Sanes DH.** Synaptic inhibition influences the temporal coding properties of medial superior olivary neurons: an in vitro study. *J Neurosci* 14: 1701-1709, 1994.

**Haas JS, and White JA.** Frequency selectivity of layer II stellate cells in the medial entorhinal cortex. *Journal of neurophysiology* 88: 2422-2429, 2002.

- Hackney CM, Osen KK, and Kolston J.** Anatomy of the cochlear nuclear complex of guinea pig. *Anat Embryol (Berl)* 182: 123-149, 1990.
- Hancock KE, and Voigt HF.** Intracellularly labeled fusiform cells in dorsal cochlear nucleus of the gerbil. II. Comparison of physiology and anatomy. *J Neurophysiol* 87: 2520-2530, 2002.
- Hausser M, and Clark BA.** Tonic synaptic inhibition modulates neuronal output pattern and spatiotemporal synaptic integration. *Neuron* 19: 665-678, 1997.
- Heller AJ.** Classification and epidemiology of tinnitus. *Otolaryngol Clin North Am* 36: 239-248, 2003.
- Hewitt MJ, and Meddis R.** A computer model of dorsal cochlear nucleus pyramidal cells: intrinsic membrane properties. *The Journal of the Acoustical Society of America* 97: 2405-2413, 1995.
- Hirsch JA, and Oertel D.** Intrinsic properties of neurones in the dorsal cochlear nucleus of mice, in vitro. *J Physiol* 396: 535-548, 1988a.
- Hirsch JA, and Oertel D.** Synaptic connections in the dorsal cochlear nucleus of mice, in vitro. *J Physiol* 396: 549-562, 1988b.
- Hoffman DA, and Johnston D.** Downregulation of transient K<sup>+</sup> channels in dendrites of hippocampal CA1 pyramidal neurons by activation of PKA and PKC. *J Neurosci* 18: 3521-3528, 1998.
- Hoffman DA, and Johnston D.** Neuromodulation of dendritic action potentials. *J Neurophysiol* 81: 408-411, 1999.
- Hoffman DA, Magee JC, Colbert CM, and Johnston D.** K<sup>+</sup> channel regulation of signal propagation in dendrites of hippocampal pyramidal neurons. *Nature* 387: 869-875, 1997.
- Holmqvist MH, Cao J, Hernandez-Pineda R, Jacobson MD, Carroll KI, Sung MA, Betty M, Ge P, Gilbride KJ, Brown ME, Jurman ME, Lawson D, Silos-Santiago I, Xie Y, Covarrubias M, Rhodes KJ, Distefano PS, and An WF.** Elimination of fast inactivation in Kv4 A-type potassium channels by an auxiliary subunit domain. *Proceedings of the National Academy of Sciences of the United States of America* 99: 1035-1040, 2002.
- Holmqvist MH, Cao J, Knoppers MH, Jurman ME, Distefano PS, Rhodes KJ, Xie Y, and An WF.** Kinetic modulation of Kv4-mediated A-current by arachidonic acid is dependent on potassium channel interacting proteins. *J Neurosci* 21: 4154-4161, 2001.

- Hsu YH, Huang HY, and Tsaor ML.** Contrasting expression of Kv4.3, an A-type K<sup>+</sup> channel, in migrating Purkinje cells and other post-migratory cerebellar neurons. *The European journal of neuroscience* 18: 601-612, 2003.
- Hunter JD, and Milton JG.** Amplitude and frequency dependence of spike timing: implications for dynamic regulation. *Journal of neurophysiology* 90: 387-394, 2003.
- Hunter JD, Milton JG, Thomas PJ, and Cowan JD.** Resonance effect for neural spike time reliability. *Journal of neurophysiology* 80: 1427-1438, 1998.
- Jaeger D, and Bower JM.** Synaptic control of spiking in cerebellar Purkinje cells: dynamic current clamp based on model conductances. *J Neurosci* 19: 6090-6101, 1999.
- Jerng HH, Pfaffinger PJ, and Covarrubias M.** Molecular physiology and modulation of somatodendritic A-type potassium channels. *Mol Cell Neurosci* 27: 343-369, 2004.
- Jinno S, Jeromin A, and Kosaka T.** Postsynaptic and extrasynaptic localization of Kv4.2 channels in the mouse hippocampal region, with special reference to targeted clustering at gabaergic synapses. *Neuroscience* 134: 483-494, 2005.
- Johnston D, Christie BR, Frick A, Gray R, Hoffman DA, Schexnayder LK, Watanabe S, and Yuan LL.** Active dendrites, potassium channels and synaptic plasticity. *Philos Trans R Soc Lond B Biol Sci* 358: 667-674, 2003.
- Johnston D, Hoffman DA, Colbert CM, and Magee JC.** Regulation of back-propagating action potentials in hippocampal neurons. *Curr Opin Neurobiol* 9: 288-292, 1999.
- Joris PX.** Interaural time sensitivity dominated by cochlea-induced envelope patterns. *J Neurosci* 23: 6345-6350, 2003.
- Joris PX, Louage DH, Cardoen L, and van der Heijden M.** Correlation index: a new metric to quantify temporal coding. *Hearing research* 216-217: 19-30, 2006.
- Joris PX, and Smith PH.** Temporal and binaural properties in dorsal cochlear nucleus and its output tract. *J Neurosci* 18: 10157-10170, 1998.
- Kaltenbach JA, and Afman CE.** Hyperactivity in the dorsal cochlear nucleus after intense sound exposure and its resemblance to tone-evoked activity: a physiological model for tinnitus. *Hearing research* 140: 165-172, 2000.
- Kaltenbach JA, Rachel JD, Mathog TA, Zhang J, Falzarano PR, and Lewandowski M.** Cisplatin-induced hyperactivity in the dorsal cochlear nucleus and its relation to outer hair cell loss: relevance to tinnitus. *J Neurophysiol* 88: 699-714, 2002.

**Kaltenbach JA, Zacharek MA, Zhang J, and Frederick S.** Activity in the dorsal cochlear nucleus of hamsters previously tested for tinnitus following intense tone exposure. *Neurosci Lett* 355: 121-125, 2004.

**Kaltenbach JA, Zhang J, and Finlayson P.** Tinnitus as a plastic phenomenon and its possible neural underpinnings in the dorsal cochlear nucleus. *Hearing research* 206: 200-226, 2005.

**Kane ES.** Descending inputs to the cat dorsal cochlear nucleus: an electron microscopic study. *J Neurocytol* 6: 583-605, 1977.

**Kanold PO, and Manis PB.** A physiologically based model of discharge pattern regulation by transient K<sup>+</sup> currents in cochlear nucleus pyramidal cells. *J Neurophysiol* 85: 523-538, 2001.

**Kanold PO, and Manis PB.** Encoding the timing of inhibitory inputs. *J Neurophysiol* 93: 2887-2897, 2005a.

**Kanold PO, and Manis PB.** Encoding the timing of inhibitory inputs. *J Neurophysiol* 93: 2887-2897, 2005b.

**Kanold PO, and Manis PB.** Transient potassium currents regulate the discharge patterns of dorsal cochlear nucleus pyramidal cells. *J Neurosci* 19: 2195-2208, 1999.

**Kanold PO, and Young ED.** Proprioceptive information from the pinna provides somatosensory input to cat dorsal cochlear nucleus. *J Neurosci* 21: 7848-7858, 2001.

**Kiang NY-s.** *Discharge patterns of single fibers in the cat's auditory nerve.* Cambridge, Mass.: M.I.T. Press, 1965, p. xvii, 154 p.

**Kim DO, Ghoshal S, Khant SL, and Parham K.** A computational model with ionic conductances for the fusiform cell of the dorsal cochlear nucleus. *The Journal of the Acoustical Society of America* 96: 1501-1514, 1994.

**Kim DO, Sirianni JG, and Chang SO.** Responses of DCN-PVCN neurons and auditory nerve fibers in unanesthetized decerebrate cats to AM and pure tones: analysis with autocorrelation/power-spectrum. *Hear Res* 45: 95-113, 1990.

**Kim J, Wei DS, and Hoffman DA.** Kv4 potassium channel subunits control action potential repolarization and frequency-dependent broadening in rat hippocampal CA1 pyramidal neurones. *J Physiol* 569: 41-57, 2005.

**Klee R, Ficker E, and Heinemann U.** Comparison of voltage-dependent potassium currents in rat pyramidal neurons acutely isolated from hippocampal regions CA1 and CA3. *J Neurophysiol* 74: 1982-1995, 1995.

**Klug A, and Trussell LO.** Activation and deactivation of voltage-dependent K<sup>+</sup> channels during synaptically driven action potentials in the MNTB. *J Neurophysiol* 96: 1547-1555, 2006.

**Kollo M, Holderith NB, and Nusser Z.** Novel subcellular distribution pattern of A-type K<sup>+</sup> channels on neuronal surface. *J Neurosci* 26: 2684-2691, 2006.

**Konig P, Engel AK, and Singer W.** Integrator or coincidence detector? The role of the cortical neuron revisited. *Trends Neurosci* 19: 130-137, 1996.

**Lein ES, Hawrylycz MJ, Ao N, Ayres M, Bensinger A, Bernard A, Boe AF, Boguski MS, Brockway KS, Byrnes EJ, Chen L, Chen L, Chen TM, Chi Chin M, Chong J, Crook BE, Czaplinska A, Dang CN, Datta S, Dee NR, Desaki AL, Desta T, Diep E, Dolbeare TA, Donelan MJ, Dong HW, Dougherty JG, Duncan BJ, Ebbert AJ, Eichele G, Estin LK, Faber C, Facer BA, Fields R, Fischer SR, Fliss TP, Frensley C, Gates SN, Glattfelder KJ, Halverson KR, Hart MR, Hohmann JG, Howell MP, Jeung DP, Johnson RA, Karr PT, Kawal R, Kidney JM, Knapik RH, Kuan CL, Lake JH, Laramée AR, Larsen KD, Lau C, Lemon TA, Liang AJ, Liu Y, Luong LT, Michaels J, Morgan JJ, Morgan RJ, Mortrud MT, Mosqueda NF, Ng LL, Ng R, Orta GJ, Overly CC, Pak TH, Parry SE, Pathak SD, Pearson OC, Puchalski RB, Riley ZL, Rockett HR, Rowland SA, Royall JJ, Ruiz MJ, Sarno NR, Schaffnit K, Shapovalova NV, Sivisay T, Slaughterbeck CR, Smith SC, Smith KA, Smith BI, Sotdt AJ, Stewart NN, Stumpf KR, Sunkin SM, Sutram M, Tam A, Teemer CD, Thaller C, Thompson CL, Varnam LR, Visel A, Whitlock RM, Wohnoutka PE, Wolkey CK, Wong VY, Wood M, Yaylaoglu MB, Young RC, Youngstrom BL, Feng Yuan X, Zhang B, Zwingman TA, and Jones AR.** Genome-wide atlas of gene expression in the adult mouse brain. *Nature* 2006.

**Levine RA, Abel M, and Cheng H.** CNS somatosensory-auditory interactions elicit or modulate tinnitus. *Exp Brain Res* 153: 643-648, 2003.

**Liberman MC.** Auditory-nerve response from cats raised in a low-noise chamber. *The Journal of the Acoustical Society of America* 63: 442-455, 1978.

**Liberman MC.** Efferent synapses in the inner hair cell area of the cat cochlea: an electron microscopic study of serial sections. *Hearing research* 3: 189-204, 1980.

**Liss B, Franz O, Sewing S, Bruns R, Neuhoff H, and Roeper J.** Tuning pacemaker frequency of individual dopaminergic neurons by Kv4.3L and KChip3.1 transcription. *Embo J* 20: 5715-5724, 2001.

**Llinas R, and Sugimori M.** Electrophysiological properties of in vitro Purkinje cell somata in mammalian cerebellar slices. *J Physiol* 305: 171-195, 1980.

**Llinas RR.** The intrinsic electrophysiological properties of mammalian neurons: insights into central nervous system function. *Science* 242: 1654-1664, 1988.

**Lorente de Nó R.** *The primary acoustic nuclei*. New York: Raven Press, 1981, p. xii, 177.

**Losonczy A, and Magee JC.** Integrative properties of radial oblique dendrites in hippocampal CA1 pyramidal neurons. *Neuron* 50: 291-307, 2006.

**Louage DH, van der Heijden M, and Joris PX.** Temporal properties of responses to broadband noise in the auditory nerve. *J Neurophysiol* 91: 2051-2065, 2004.

**Magee JC.** Dendritic integration of excitatory synaptic input. *Nat Rev Neurosci* 1: 181-190, 2000.

**Mainen ZF, and Sejnowski TJ.** Influence of dendritic structure on firing pattern in model neocortical neurons. *Nature* 382: 363-366, 1996.

**Mainen ZF, and Sejnowski TJ.** Reliability of spike timing in neocortical neurons. *Science* 268: 1503-1506, 1995.

**Malmierca MS, Le Beau FE, and Rees A.** The topographical organization of descending projections from the central nucleus of the inferior colliculus in guinea pig. *Hearing research* 93: 167-180, 1996.

**Manis PB.** Handbook of the Senses. 2007.

**Manis PB.** Membrane properties and discharge characteristics of guinea pig dorsal cochlear nucleus neurons studied in vitro. *J Neurosci* 10: 2338-2351, 1990.

**Manis PB.** Responses to parallel fiber stimulation in the guinea pig dorsal cochlear nucleus in vitro. *J Neurophysiol* 61: 149-161, 1989.

**Manis PB, and Brownell WE.** Synaptic organization of eighth nerve afferents to cat dorsal cochlear nucleus. *J Neurophysiol* 50: 1156-1181, 1983.

**Manis PB, and Marx SO.** Outward currents in isolated ventral cochlear nucleus neurons. *J Neurosci* 11: 2865-2880, 1991.

**Manis PB, and Molitor SC.** N-methyl-D-aspartate receptors at parallel fiber synapses in the dorsal cochlear nucleus. *J Neurophysiol* 76: 1639-1656, 1996.

**Manis PB, Molitor SC, and Wu H.** Subthreshold oscillations generated by TTX-sensitive sodium currents in dorsal cochlear nucleus pyramidal cells. *Exp Brain Res* 153: 443-451, 2003.

**Manis PB, Spirou GA, Wright DD, Paydar S, and Ryugo DK.** Physiology and morphology of complex spiking neurons in the guinea pig dorsal cochlear nucleus. *The Journal of comparative neurology* 348: 261-276, 1994.

**May BJ.** Role of the dorsal cochlear nucleus in the sound localization behavior of cats. *Hear Res* 148: 74-87, 2000.

**Middlebrooks JC, and Green DM.** Sound localization by human listeners. *Annu Rev Psychol* 42: 135-159, 1991.

**Migliore M, Hoffman DA, Magee JC, and Johnston D.** Role of an A-type K<sup>+</sup> conductance in the back-propagation of action potentials in the dendrites of hippocampal pyramidal neurons. *J Comput Neurosci* 7: 5-15, 1999.

**Mitterdorfer J, and Bean BP.** Potassium currents during the action potential of hippocampal CA3 neurons. *J Neurosci* 22: 10106-10115, 2002.

**Molineux ML, Fernandez FR, Mehaffey WH, and Turner RW.** A-type and T-type currents interact to produce a novel spike latency-voltage relationship in cerebellar stellate cells. *J Neurosci* 25: 10863-10873, 2005.

**Molitor SC, and Manis PB.** Dendritic Ca<sup>2+</sup> transients evoked by action potentials in rat dorsal cochlear nucleus pyramidal and cartwheel neurons. *J Neurophysiol* 89: 2225-2237, 2003.

**Molitor SC, and Manis PB.** Evidence for functional metabotropic glutamate receptors in the dorsal cochlear nucleus. *J Neurophysiol* 77: 1889-1905, 1997.

**Molitor SC, and Manis PB.** Voltage-gated Ca<sup>2+</sup> conductances in acutely isolated guinea pig dorsal cochlear nucleus neurons. *J Neurophysiol* 81: 985-998, 1999.

**Mugnaini E.** GABA neurons in the superficial layers of the rat dorsal cochlear nucleus: light and electron microscopic immunocytochemistry. *J Comp Neurol* 235: 61-81, 1985.

**Mugnaini E, Osen KK, Dahl AL, Friedrich VL, Jr., and Korte G.** Fine structure of granule cells and related interneurons (termed Golgi cells) in the cochlear nuclear complex of cat, rat and mouse. *J Neurocytol* 9: 537-570, 1980a.

**Mugnaini E, Warr WB, and Osen KK.** Distribution and light microscopic features of granule cells in the cochlear nuclei of cat, rat, and mouse. *J Comp Neurol* 191: 581-606, 1980b.

**Nadal MS, Amarillo Y, Vega-Saenz de Miera E, and Rudy B.** Evidence for the presence of a novel Kv4-mediated A-type K(+) channel-modifying factor. *J Physiol* 537: 801-809, 2001.

**Nadal MS, Ozaita A, Amarillo Y, Vega-Saenz de Miera E, Ma Y, Mo W, Goldberg EM, Misumi Y, Ikehara Y, Neubert TA, and Rudy B.** The CD26-related dipeptidyl aminopeptidase-like protein DPPX is a critical component of neuronal A-type K<sup>+</sup> channels. *Neuron* 37: 449-461, 2003.

**Nelken I, Kim PJ, and Young ED.** Linear and nonlinear spectral integration in type IV neurons of the dorsal cochlear nucleus. II. Predicting responses with the use of nonlinear models. *J Neurophysiol* 78: 800-811, 1997.

**Nelken I, and Young ED.** Linear and nonlinear spectral integration in type IV neurons of the dorsal cochlear nucleus. I. Regions of linear interaction. *J Neurophysiol* 78: 790-799, 1997.

**Nelken I, and Young ED.** Two separate inhibitory mechanisms shape the responses of dorsal cochlear nucleus type IV units to narrowband and wideband stimuli. *J Neurophysiol* 71: 2446-2462, 1994.

**Neuert V, Verhey JL, and Winter IM.** Responses of dorsal cochlear nucleus neurons to signals in the presence of modulated maskers. *J Neurosci* 24: 5789-5797, 2004.

**Neuert V, Verhey JL, and Winter IM.** Temporal representation of the delay of iterated rippled noise in the dorsal cochlear nucleus. *Journal of neurophysiology* 93: 2766-2776, 2005.

**Nowak LG, Sanchez-Vives MV, and McCormick DA.** Influence of low and high frequency inputs on spike timing in visual cortical neurons. *Cereb Cortex* 7: 487-501, 1997.

**Oertel D.** The role of timing in the brain stem auditory nuclei of vertebrates. *Annu Rev Physiol* 61: 497-519, 1999.

**Oertel D, and Wu SH.** Morphology and physiology of cells in slice preparations of the dorsal cochlear nucleus of mice. *J Comp Neurol* 283: 228-247, 1989.

**Oertel D, and Young ED.** What's a cerebellar circuit doing in the auditory system? *Trends Neurosci* 27: 104-110, 2004.

**Ohya S, Tanaka M, Oku T, Asai Y, Watanabe M, Giles WR, and Imaizumi Y.** Molecular cloning and tissue distribution of an alternatively spliced variant of an A-type K<sup>+</sup> channel alpha-subunit, Kv4.3 in the rat. *FEBS Lett* 420: 47-53, 1997.

**Oliver DL, Ostapoff EM, and Beckius GE.** Direct innervation of identified tectothalamic neurons in the inferior colliculus by axons from the cochlear nucleus. *Neuroscience* 93: 643-658, 1999.

**Osen KK.** Course and termination of the primary afferents in the cochlear nuclei of the cat. An experimental anatomical study. *Arch Ital Biol* 108: 21-51, 1970.

**Osen KK.** Cytoarchitecture of the cochlear nuclei in the cat. *J Comp Neurol* 136: 453-484, 1969a.

- Osen KK.** Projection of the cochlear nuclei on the inferior colliculus in the cat. *J Comp Neurol* 144: 355-372, 1972.
- Osen KK.** The intrinsic organization of the cochlear nuclei. *Acta Otolaryngol* 67: 352-359, 1969b.
- Pal B, Por A, Szucs G, Kovacs I, and Rusznak Z.** HCN channels contribute to the intrinsic activity of cochlear pyramidal cells. *Cell Mol Life Sci* 60: 2189-2199, 2003.
- Petralia RS, Rubio ME, Wang YX, and Wenthold RJ.** Differential distribution of glutamate receptors in the cochlear nuclei. *Hearing research* 147: 59-69, 2000.
- Petrecca K, Miller DM, and Shrier A.** Localization and enhanced current density of the Kv4.2 potassium channel by interaction with the actin-binding protein filamin. *J Neurosci* 20: 8736-8744, 2000.
- Pfeiffer RR.** Classification of response patterns of spike discharges for units in the cochlear nucleus: tone-burst stimulation. *Exp Brain Res* 1: 220-235, 1966.
- Popper AN, and Fay RR.** *The Mammalian auditory pathway : neurophysiology*. New York: Springer-Verlag, 1992, p. xi, 431 p.
- Rall W.** Distinguishing theoretical synaptic potentials computed for different soma-dendritic distributions of synaptic input. *J Neurophysiol* 30: 1138-1168, 1967.
- Ramakers GM, and Storm JF.** A postsynaptic transient K(+) current modulated by arachidonic acid regulates synaptic integration and threshold for LTP induction in hippocampal pyramidal cells. *Proceedings of the National Academy of Sciences of the United States of America* 99: 10144-10149, 2002.
- Reich DS, Victor JD, Knight BW, Ozaki T, and Kaplan E.** Response variability and timing precision of neuronal spike trains in vivo. *J Neurophysiol* 77: 2836-2841, 1997.
- Reinagel P, and Reid RC.** Precise firing events are conserved across neurons. *J Neurosci* 22: 6837-6841, 2002.
- Reiss LA, and Young ED.** Spectral edge sensitivity in neural circuits of the dorsal cochlear nucleus. *J Neurosci* 25: 3680-3691, 2005.
- Rhode WS.** Vertical cell responses to sound in cat dorsal cochlear nucleus. *J Neurophysiol* 82: 1019-1032, 1999.
- Rhode WS, and Greenberg S.** Encoding of amplitude modulation in the cochlear nucleus of the cat. *J Neurophysiol* 71: 1797-1825, 1994.

**Rhode WS, Oertel D, and Smith PH.** Physiological response properties of cells labeled intracellularly with horseradish peroxidase in cat ventral cochlear nucleus. *J Comp Neurol* 213: 448-463, 1983a.

**Rhode WS, and Smith PH.** Physiological studies on neurons in the dorsal cochlear nucleus of cat. *J Neurophysiol* 56: 287-307, 1986.

**Rhode WS, Smith PH, and Oertel D.** Physiological response properties of cells labeled intracellularly with horseradish peroxidase in cat dorsal cochlear nucleus. *The Journal of comparative neurology* 213: 426-447, 1983b.

**Rhodes KJ, Carroll KI, Sung MA, Doliveira LC, Monaghan MM, Burke SL, Strassle BW, Buchwalder L, Menegola M, Cao J, An WF, and Trimmer JS.** KChIPs and Kv4 alpha subunits as integral components of A-type potassium channels in mammalian brain. *J Neurosci* 24: 7903-7915, 2004.

**Rice JJ, May BJ, Spirou GA, and Young ED.** Pinna-based spectral cues for sound localization in cat. *Hearing research* 58: 132-152, 1992.

**Rivera JF, Ahmad S, Quick MW, Liman ER, and Arnold DB.** An evolutionarily conserved dileucine motif in Shal K<sup>+</sup> channels mediates dendritic targeting. *Nat Neurosci* 6: 243-250, 2003.

**Rose JE, Brugge JF, Anderson DJ, and Hind JE.** Phase-locked response to low-frequency tones in single auditory nerve fibers of the squirrel monkey. *J Neurophysiol* 30: 769-793, 1967.

**Roth GL, Aitkin LM, Andersen RA, and Merzenich MM.** Some features of the spatial organization of the central nucleus of the inferior colliculus of the cat. *J Comp Neurol* 182: 661-680, 1978.

**Rothman JS, and Manis PB.** Differential expression of three distinct potassium currents in the ventral cochlear nucleus. *J Neurophysiol* 89: 3070-3082, 2003.

**Rubio ME, and Wenthold RJ.** Glutamate receptors are selectively targeted to postsynaptic sites in neurons. *Neuron* 18: 939-950, 1997.

**Rusznak Z, Forsythe ID, Brew HM, and Stanfield PR.** Membrane currents influencing action potential latency in granule neurons of the rat cochlear nucleus. *The European journal of neuroscience* 9: 2348-2358, 1997.

**Ryan AF, Woolf NK, and Sharp FR.** Tonotopic organization in the central auditory pathway of the Mongolian gerbil: a 2-deoxyglucose study. *J Comp Neurol* 207: 369-380, 1982.

**Ryugo DK, and May SK.** The projections of intracellularly labeled auditory nerve fibers to the dorsal cochlear nucleus of cats. *J Comp Neurol* 329: 20-35, 1993.

**Ryugo DK, and Willard FH.** The dorsal cochlear nucleus of the mouse: a light microscopic analysis of neurons that project to the inferior colliculus. *J Comp Neurol* 242: 381-396, 1985.

**Salinas E, and Sejnowski TJ.** Correlated neuronal activity and the flow of neural information. *Nat Rev Neurosci* 2: 539-550, 2001.

**Salvinelli F, Casale M, Paparo F, Persico AM, and Zini C.** Subjective tinnitus, temporomandibular joint dysfunction, and serotonin modulation of neural plasticity: causal or casual triad? *Med Hypotheses* 61: 446-448, 2003.

**Sanes DH, McGee J, and Walsh EJ.** Metabotropic glutamate receptor activation modulates sound level processing in the cochlear nucleus. *J Neurophysiol* 80: 209-217, 1998.

**Sanguinetti MC, Johnson JH, Hammerland LG, Kelbaugh PR, Volkmann RA, Saccomano NA, and Mueller AL.** Heteropodatoxins: peptides isolated from spider venom that block Kv4.2 potassium channels. *Mol Pharmacol* 51: 491-498, 1997.

**Scannevin RH, Wang K, Jow F, Megules J, Kopsco DC, Edris W, Carroll KC, Lu Q, Xu W, Xu Z, Katz AH, Olland S, Lin L, Taylor M, Stahl M, Malakian K, Somers W, Mosyak L, Bowlby MR, Chanda P, and Rhodes KJ.** Two N-terminal domains of Kv4 K(+) channels regulate binding to and modulation by KChIP1. *Neuron* 41: 587-598, 2004.

**Schofield BR, and Coomes DL.** Projections from auditory cortex contact cells in the cochlear nucleus that project to the inferior colliculus. *Hearing research* 206: 3-11, 2005.

**Schrader LA, Anderson AE, Mayne A, Pfaffinger PJ, and Sweatt JD.** PKA modulation of Kv4.2-encoded A-type potassium channels requires formation of a supramolecular complex. *J Neurosci* 22: 10123-10133, 2002.

**Schrader LA, Birnbaum SG, Nadin BM, Ren Y, Bui D, Anderson AE, and Sweatt JD.** ERK/MAPK regulates the Kv4.2 potassium channel by direct phosphorylation of the pore-forming subunit. *Am J Physiol Cell Physiol* 290: C852-861, 2006.

**Schreiber S, Fellous JM, Tiesinga P, and Sejnowski TJ.** Influence of ionic conductances on spike timing reliability of cortical neurons for suprathreshold rhythmic inputs. *Journal of neurophysiology* 91: 194-205, 2004.

**Seidemann E, Zohary E, and Newsome WT.** Temporal gating of neural signals during performance of a visual discrimination task. *Nature* 394: 72-75, 1998.

**Serodio P, Kentros C, and Rudy B.** Identification of molecular components of A-type channels activating at subthreshold potentials. *J Neurophysiol* 72: 1516-1529, 1994.

- Serodio P, and Rudy B.** Differential expression of Kv4 K<sup>+</sup> channel subunits mediating subthreshold transient K<sup>+</sup> (A-type) currents in rat brain. *J Neurophysiol* 79: 1081-1091, 1998.
- Shadlen MN, and Newsome WT.** The variable discharge of cortical neurons: implications for connectivity, computation, and information coding. *J Neurosci* 18: 3870-3896, 1998.
- Shen NV, and Pfaffinger PJ.** Molecular recognition and assembly sequences involved in the subfamily-specific assembly of voltage-gated K<sup>+</sup> channel subunit proteins. *Neuron* 14: 625-633, 1995.
- Sheng M, Tsaur ML, Jan YN, and Jan LY.** Subcellular segregation of two A-type K<sup>+</sup> channel proteins in rat central neurons. *Neuron* 9: 271-284, 1992.
- Shibasaki K, Nakahira K, Trimmer JS, Shibata R, Akita M, Watanabe S, and Ikenaka K.** Mossy fibre contact triggers the targeting of Kv4.2 potassium channels to dendrites and synapses in developing cerebellar granule neurons. *J Neurochem* 89: 897-907, 2004.
- Shibata R, Misonou H, Campomanes CR, Anderson AE, Schrader LA, Doliveira LC, Carroll KI, Sweatt JD, Rhodes KJ, and Trimmer JS.** A fundamental role for KChIPs in determining the molecular properties and trafficking of Kv4.2 potassium channels. *J Biol Chem* 278: 36445-36454, 2003.
- Shibata R, Wakazono Y, Nakahira K, Trimmer JS, and Ikenaka K.** Expression of Kv3.1 and Kv4.2 genes in developing cerebellar granule cells. *Dev Neurosci* 21: 87-93, 1999.
- Shofner WP, and Young ED.** Excitatory/inhibitory response types in the cochlear nucleus: relationships to discharge patterns and responses to electrical stimulation of the auditory nerve. *J Neurophysiol* 54: 917-939, 1985.
- Shore SE.** Multisensory integration in the dorsal cochlear nucleus: unit responses to acoustic and trigeminal ganglion stimulation. *The European journal of neuroscience* 21: 3334-3348, 2005.
- Shore SE, and Moore JK.** Sources of input to the cochlear granule cell region in the guinea pig. *Hearing research* 116: 33-42, 1998.
- Shore SE, and Zhou J.** Somatosensory influence on the cochlear nucleus and beyond. *Hearing research* 216-217: 90-99, 2006.
- Smith PH, Massie A, and Joris PX.** Acoustic stria: anatomy of physiologically characterized cells and their axonal projection patterns. *J Comp Neurol* 482: 349-371, 2005.
- Softky WR.** Simple codes versus efficient codes. *Curr Opin Neurobiol* 5: 239-247, 1995.

**Softky WR, and Koch C.** The highly irregular firing of cortical cells is inconsistent with temporal integration of random EPSPs. *J Neurosci* 13: 334-350, 1993.

**Song WJ, Tkatch T, Baranauskas G, Ichinohe N, Kitai ST, and Surmeier DJ.** Somatodendritic depolarization-activated potassium currents in rat neostriatal cholinergic interneurons are predominantly of the A type and attributable to coexpression of Kv4.2 and Kv4.1 subunits. *J Neurosci* 18: 3124-3137, 1998.

**Sourdet V, Russier M, Daoudal G, Ankri N, and Debanne D.** Long-term enhancement of neuronal excitability and temporal fidelity mediated by metabotropic glutamate receptor subtype 5. *J Neurosci* 23: 10238-10248, 2003.

**Spiro GA, and Young ED.** Organization of dorsal cochlear nucleus type IV unit response maps and their relationship to activation by bandlimited noise. *Journal of neurophysiology* 66: 1750-1768, 1991.

**Stevens CF, and Zador AM.** Input synchrony and the irregular firing of cortical neurons. *Nat Neurosci* 1: 210-217, 1998.

**Strassle BW, Menegola M, Rhodes KJ, and Trimmer JS.** Light and electron microscopic analysis of KChIP and Kv4 localization in rat cerebellar granule cells. *J Comp Neurol* 484: 144-155, 2005.

**Stuart GJ, and Sakmann B.** Active propagation of somatic action potentials into neocortical pyramidal cell dendrites. *Nature* 367: 69-72, 1994.

**Sutherland DP, Masterton RB, and Glendenning KK.** Role of acoustic striae in hearing: reflexive responses to elevated sound-sources. *Behav Brain Res* 97: 1-12, 1998.

**Svirskis G, Dodla R, and Rinzel J.** Subthreshold outward currents enhance temporal integration in auditory neurons. *Biol Cybern* 89: 333-340, 2003.

**Svirskis G, Kotak V, Sanes DH, and Rinzel J.** Enhancement of signal-to-noise ratio and phase locking for small inputs by a low-threshold outward current in auditory neurons. *J Neurosci* 22: 11019-11025, 2002.

**Svirskis G, Kotak V, Sanes DH, and Rinzel J.** Sodium along with low-threshold potassium currents enhance coincidence detection of subthreshold noisy signals in MSO neurons. *Journal of neurophysiology* 91: 2465-2473, 2004.

**Tiesinga PH, and Sejnowski TJ.** Rapid temporal modulation of synchrony by competition in cortical interneuron networks. *Neural computation* 16: 251-275, 2004.

**Trussell LO.** Synaptic mechanisms for coding timing in auditory neurons. *Annu Rev Physiol* 61: 477-496, 1999.

**Tsaur ML, Chou CC, Shih YH, and Wang HL.** Cloning, expression and CNS distribution of Kv4.3, an A-type K<sup>+</sup> channel alpha subunit. *FEBS Lett* 400: 215-220, 1997.

**Tzounopoulos T, Kim Y, Oertel D, and Trussell LO.** Cell-specific, spike timing-dependent plasticities in the dorsal cochlear nucleus. *Nat Neurosci* 7: 719-725, 2004.

**Varga AW, Yuan LL, Anderson AE, Schrader LA, Wu GY, Gatchel JR, Johnston D, and Sweatt JD.** Calcium-calmodulin-dependent kinase II modulates Kv4.2 channel expression and upregulates neuronal A-type potassium currents. *J Neurosci* 24: 3643-3654, 2004.

**Voigt HF, and Young ED.** Cross-correlation analysis of inhibitory interactions in dorsal cochlear nucleus. *J Neurophysiol* 64: 1590-1610, 1990.

**Voigt HF, and Young ED.** Evidence of inhibitory interactions between neurons in dorsal cochlear nucleus. *J Neurophysiol* 44: 76-96, 1980.

**Voigt HF, and Young ED.** Neural correlations in the dorsal cochlear nucleus: pairs of units with similar response properties. *J Neurophysiol* 59: 1014-1032, 1988.

**Wang D, and Schreurs BG.** Characteristics of IA currents in adult rabbit cerebellar Purkinje cells. *Brain research* 1096: 85-96, 2006.

**Wang H, Yan Y, Liu Q, Huang Y, Shen Y, Chen L, Chen Y, Yang Q, Hao Q, Wang K, and Chai J.** Structural basis for modulation of Kv4 K(+) channels by auxiliary KChIP subunits. *Nat Neurosci* 10: 32-39, 2007.

**Wang K, Ash JF, and Singer SJ.** Filamin, a new high-molecular-weight protein found in smooth muscle and non-muscle cells. *Proceedings of the National Academy of Sciences of the United States of America* 72: 4483-4486, 1975.

**Watanabe S, Hoffman DA, Migliore M, and Johnston D.** Dendritic K<sup>+</sup> channels contribute to spike-timing dependent long-term potentiation in hippocampal pyramidal neurons. *Proceedings of the National Academy of Sciences of the United States of America* 99: 8366-8371, 2002.

**Weedman DL, and Ryugo DK.** Projections from auditory cortex to the cochlear nucleus in rats: synapses on granule cell dendrites. *J Comp Neurol* 371: 311-324, 1996.

**Weinberg RJ, and Rustioni A.** A cuneocochlear pathway in the rat. *Neuroscience* 20: 209-219, 1987.

**Wong W, Newell EW, Jugloff DG, Jones OT, and Schlichter LC.** Cell surface targeting and clustering interactions between heterologously expressed PSD-95 and the Shal voltage-gated potassium channel, Kv4.2. *J Biol Chem* 277: 20423-20430, 2002.

**Wong W, and Schlichter LC.** Differential recruitment of Kv1.4 and Kv4.2 to lipid rafts by PSD-95. *J Biol Chem* 279: 444-452, 2004.

**Wouterlood FG, and Mugnaini E.** Cartwheel neurons of the dorsal cochlear nucleus: a Golgi-electron microscopic study in rat. *J Comp Neurol* 227: 136-157, 1984.

**Wouterlood FG, Mugnaini E, Osen KK, and Dahl AL.** Stellate neurons in rat dorsal cochlear nucleus studies with combined Golgi impregnation and electron microscopy: synaptic connections and mutual coupling by gap junctions. *J Neurocytol* 13: 639-664, 1984.

**Wright DD, and Ryugo DK.** Mossy fiber projections from the cuneate nucleus to the cochlear nucleus in the rat. *J Comp Neurol* 365: 159-172, 1996.

**Yang EK, Alvira MR, Levitan ES, and Takimoto K.** Kvbeta subunits increase expression of Kv4.3 channels by interacting with their C termini. *J Biol Chem* 276: 4839-4844, 2001.

**Young ED.** Identification of response properties of ascending axons from dorsal cochlear nucleus. *Brain Res* 200: 23-37, 1980.

**Young ED, and Brownell WE.** Responses to tones and noise of single cells in dorsal cochlear nucleus of unanesthetized cats. *J Neurophysiol* 39: 282-300, 1976.

**Young ED, Nelken I, and Conley RA.** Somatosensory effects on neurons in dorsal cochlear nucleus. *J Neurophysiol* 73: 743-765, 1995.

**Yuan LL, Adams JP, Swank M, Sweatt JD, and Johnston D.** Protein kinase modulation of dendritic K<sup>+</sup> channels in hippocampus involves a mitogen-activated protein kinase pathway. *J Neurosci* 22: 4860-4868, 2002.

**Yuan LL, Chen X, Kunjilwar K, Pfaffinger P, and Johnston D.** Acceleration of K<sup>+</sup> channel inactivation by MEK inhibitor U0126. *Am J Physiol Cell Physiol* 290: C165-171, 2006.

**Yuste R, and Tank DW.** Dendritic integration in mammalian neurons, a century after Cajal. *Neuron* 16: 701-716, 1996.

**Zarayskiy VV, Balasubramanian G, Bondarenko VE, and Morales MJ.** Heteropoda toxin 2 is a gating modifier toxin specific for voltage-gated K<sup>+</sup> channels of the Kv4 family. *Toxicon* 45: 431-442, 2005.

**Zhan X, Pongstaporn T, and Ryugo DK.** Projections of the second cervical dorsal root ganglion to the cochlear nucleus in rats. *J Comp Neurol* 496: 335-348, 2006.

**Zhang JS, and Kaltenbach JA.** Increases in spontaneous activity in the dorsal cochlear nucleus of the rat following exposure to high-intensity sound. *Neurosci Lett* 250: 197-200, 1998.

**Zhang S, and Oertel D.** Cartwheel and superficial stellate cells of the dorsal cochlear nucleus of mice: intracellular recordings in slices. *Journal of neurophysiology* 69: 1384-1397, 1993a.

**Zhang S, and Oertel D.** Neuronal circuits associated with the output of the dorsal cochlear nucleus through fusiform cells. *Journal of neurophysiology* 71: 914-930, 1994.

**Zhang S, and Oertel D.** Tuberculoventral cells of the dorsal cochlear nucleus of mice: intracellular recordings in slices. *J Neurophysiol* 69: 1409-1421, 1993b.

**Zhao HB, and Liang ZA.** Processing of modulation frequency in the dorsal cochlear nucleus of the guinea pig: amplitude modulated tones. *Hearing research* 82: 244-256, 1995.

**Zheng X, and Voigt HF.** A modeling study of notch noise responses of type III units in the gerbil dorsal cochlear nucleus. *Ann Biomed Eng* 34: 697-708, 2006.

**Zhou J, and Shore S.** Projections from the trigeminal nuclear complex to the cochlear nuclei: a retrograde and anterograde tracing study in the guinea pig. *J Neurosci Res* 78: 901-907, 2004.

**Zhou W, Qian Y, Kunjilwar K, Pfaffinger PJ, and Choe S.** Structural insights into the functional interaction of KChIP1 with Shal-type K(+) channels. *Neuron* 41: 573-586, 2004.